Summer 2021

Partitioning of Volatile Organic Compounds Into the Multiple Environmental Compartments

Jeonghyeon Ahn

PARTITIONING OF VOLATILE ORGANIC COMPOUNDS INTO THE MULTIPLE ENVIRONMENTAL COMPARTMENTS

by

Jeonghyeon Ahn

Bachelor of Science
Sejong University, 2013

Master of Science in Engineering
Hanyang University, 2015

Submitted in Partial Fulfillment of the Requirements

For the Degree of Doctor of Philosophy in

Environmental Health Sciences

Arnold School of Public Health

University of South Carolina

2021

Accepted by:

Eric Vejerano, Major Professor

Jamie Lead, Committee Member

Geoff Scott, Committee Member

Byung-Mu Lee, Committee Member

Tracey L. Weldon, Interim Vice Provost and Dean of the Graduate School

DEDICATION

This dissertation is dedicated to my beloved family and everyone who has supported me to pursue my doctoral degree. A special feeling of gratitude to my husband Sewoon and my wonderful son Jio for being there for me. I am truly thankful for having you in my life.

ACKNOWLEDGEMENTS

I would like to express my deepest appreciation to my academic adviser Dr. Eric Vejerano for his consistent support and guidance during this research. I also wish to say thank you to my supportive dissertation committee members who kept me on track. The author thanks the SmartState Center for Environmental Nanoscience and Risk (CENR). This work was supported by the US Army Research Office.

ABSTRACT

Volatile organic compounds (VOCs) dominate the class of pollutants that accumulate in the atmosphere and indoors. Partitioning coefficient is a measure of a compound's ability to distribute between two phases. Assessing the partitioning of VOCs is essential to determine their transport, fate, behavior, and adverse environmental and health impacts across multiple environmental compartments. Studies on VOC partitioning have been limited because discriminating the small mass fraction of VOCs in aerosol particles is difficult to quantify. The partitioning of VOCs into soil, air, and aerosol particle phases was investigated under dynamic laboratory conditions. A bench-scale system that precisely controlled the relative humidity (RH), temperature, and composition of aerosol particles was developed to investigate the partitioning of surrogate VOCs into inorganic (ammonium sulfate) and organic (succinic acid) aerosol particles. The gas-particle partitioning coefficients (K_p) were experimentally derived at different RH levels and temperatures. The soil-to-air partitioning (K_{SA}) was investigated as a function of the soil water and organic matter contents. Partitioning of non-polar substituted aromatics was sensitive to the organic matter content in water-saturated soil. K_{SA} decreased with high water content only for non-polar substituted aromatic VOCs. K_{SA} of VOCs on soil with high organic matter content correlated strongly with the saturated vapor pressure and octanol-air partitioning constant, but not on clay soil. K_p of VOCs decreased as RH levels increased. The amount of VOC that partitioned onto inorganic aerosol particles was significant only at low RH levels, whereas RH levels exceeding 50% have a negligible

effect on partitioning. The enthalpy of desorption for trichloroethylene and 1,2-dichlorobenzene partitioning into both aerosol particles was constant over the temperature range of 278.15K to 308.15K, whereas *n*-butanol exhibited nonlinear temperature dependence. K_{SA} values were used to calculate the VOC concentrations released from a simulated chemical spill under a worst-case scenario, and K_p values were used to calculate the regional deposition of particles into the respiratory tract. Accumulated VOC concentrations in the atmosphere from the soil were below the threshold limits set by regulatory agencies. The mass of deposited aerosol-particle phase VOCs was below 200 pg during a 24 h inhalation.

TABLE OF CONTENTS

LIST OF TABLES

LIST OF FIGURES

CHAPTER 1

INTRODUCTION AND MOTIVATION

Predicting the environmental and human health impact of accidental chemical spills and emissions of contaminants moving across different environmental compartments (soil, air, and airborne particles) hinges on acquiring partitioning data that closely mimic environmental conditions. Volatile organic compounds (VOCs) emitted from biological and anthropogenic sources have dominated the class of organic contaminants present in the atmosphere (Breus & Mishchenko, 2006; Dumanoglu et al., 2014; Rao & Vejerano, 2018). Despite several decades of decreasing emissions of VOCs from mobile sources, a recent study has shown that emissions from volatile chemical products (VCPs) have been increasing. VOCs emitted from VCPs are twice as large as those emitted from transportation, with VCPs emitted by the petrochemical industry as one of the largest sources (Vijayaraghavan et al., 2014; McDonald et al., 2018). Approximately, 50-90 million tons of VOCs have contaminated soil annually worldwide from accidental spills and leaks (Breus & Mishchenko, 2006). In addition, 1,150 Tg C/year of VOCs are emitted from natural sources, which are ~ 10× higher (142 TgC/year) than anthropogenic emission of VOC (Goldstein and Galbally 2007). The hundreds of VOCs detected in indoor and outdoor air span a wide class of VOCs such as alkanes and aromatic compounds containing multifunctional groups (Jang et al., 2004; Arp et al., 2008a; Salthammer, 2016). Many VOCs have been linked to dysfunctions of internal organs (US EPA, 2014a) and even with

some type of cancer (*e.g.,* leukemia) in humans (Seitz & Stickel, 2010; St.Helen et al., 2014). In the U.S. alone, of the 479 contaminated sites, 84% of the soil contaminants were VOCs (Breus & Mishchenko, 2006). VOCs in soil will eventually partition into the atmosphere since they preferentially distribute into the air (Hwang et al., 2018; Rao & Vejerano, 2018). In 2016, approximately 16 million tons of VOCs were emitted into the atmosphere in the U.S. alone (Statista, 2018).

VOC emission from the soil depends on the soil moisture dynamics, soil temperature, solar irradiance, and carbon availability (*i.e.*, organic matter content) (Rossabi et al., 2018). Previous studies that investigated the soil-to-air partitioning of VOCs were mainly performed on unsaturated soil that contained extremely low water (oven-dried and air-dried soil, which are in equilibrium at a relative humidity (RH) of < 90%) and low organic matter content (Kim et al., 2003; Goss, 2004; Shih & Wu, 2005; Asensio et al., 2007; Sanscartier et al., 2009). These soil were mainly composed of minerals that contained minimal organic matter (*e.g.*, < 3% by weight for most mineral soil (Chiou, 2003). Results from such studies may have limited applicability in assessing the emission of VOCs since most soil in diverse environments will likely contain a high amount of water and organic matter. What is lacking is a comprehensive investigation of the partitioning for a broader class of VOCs of varying polarities into water-saturated soil (in equilibrium with an RH of nearly 100%) (Hoff et al., 1993). Entrainment and transport of VOCs as they move through soil column will depend on the soil properties, physicochemical properties of the VOCs, and the condition at which these interactions are occurring. Soil moisture dynamics strongly affects the emission of VOCs in the soil (Rossabi et al., 2018). The behavior of VOCs partitioning into water-saturated soil (*i.e.,* surface and internal pores are coated/filled

by water vapors) (Seneviratne et al., 2010; SU et al., 2014) will substantially differ from unsaturated soil (Ong & Lion, 1991a). A small amount of water easily saturates soil (*e.g.*, < 1% by mass for sand-dominated soil) (Hoff et al., 1993; Batterman et al., 1995). Soil/air partition coefficient (K_{SA}) decreases significantly with increasing water content because water competes strongly with VOCs to occupy the available sorption site in soil (Kim et al., 2005; Shih & Wu, 2005). Some VOCs are highly soluble in water; a large mass fraction of these VOCs in the water-saturated soil migrates to groundwater while those that interact poorly will partition preferentially into the air or interact actively with components in soil (Rivett et al., 2011). For some VOCs, their concentrations in groundwater have exceeded the United States Environmental Protection Agency drinking water standards (Moran et al., 2007; Fram & Belitz, 2011). Additionally, soil may contain considerable amounts of organic matter. Studies on the partitioning of VOCs into unsaturated soil are dominated by adsorption onto the mineral surface, while the organic matter content of the soil is deemed not important on partitioning (Shih & Wu, 2005; Rivett et al., 2011). But different functional groups that are present on the VOCs will interact to a varying extent with water, as well as with the hydrophobic and hydrophilic domains in the organic matter fraction of the soil affecting the emission of VOCs into the air.

VOCs preferentially partition in the gas phase because of their high vapor pressure and low boiling point (< 240°C at standard atmospheric pressure) (US EPA, 2014b). Because of these properties, it is assumed that the mass fraction of VOCs that will sorb onto ambient aerosol particles is insignificant compared to those of semi-volatile organic compounds (SVOCs). Studies have measured that sufficient VOC concentration can exist in ambient particulate matter at a concentration level comparable to very low abundance

SVOCs (Hamilton et al., 2004; Khanal & Shooter, 2004; Odabasi et al., 2005). Matsumoto and colleagues detected VOC concentration in ambient aerosols sampled from the urban atmosphere, with benzene as the dominant compound (Matsumoto et al., 2010). For this reason, few studies have investigated the mechanism and extent of partitioning onto aerosol particles for VOCs (Rao & Vejerano, 2018). The numerous studies on the partitioning mechanism and the models developed to predict the gas-particle partitioning (K_p) coefficients of organic compounds have focused on semivolatile organic compounds (SVOCs) (Pankow, 1987; Pankow & Bidleman, 1991; Goss & Eisenreich, 1997; Goss & Schwarzenbach, 1998; Pankow, 1998). Although the extent of aerosol particle partitioning for VOCs is less than SVOCs, VOCs dominate the class of atmospheric pollutants emitted from biogenic and anthropogenic sources. No systematic studies have investigated if this assumption is correct, partly because discriminating the mass fraction of VOCs in aerosol from the high concentration in the gas is an experimental challenge. One study in the extant literature demonstrated that VOCs could modify the biological impact of ambient aerosols. A laboratory-scale chamber study has shown that aerosol that had been passed over vapors of acrolein, induce significant damage and inflammation on lung cells compared with the pure aerosol (Ebersviller et al., 2012a, 2012b). Considering that acrolein is extremely volatile, even a small mass fraction of it modified the aerosol's biological response (Ebersviller et al., 2012a, 2012b). Other studies have established that most VOCs also reversibly or irreversibly partition into ambient atmospheric aerosol particles (Volkamer et al., 2007; Ebersviller et al., 2012a) with mass fractions similar to those of SVOCs (Odabasi et al., 2005; Arp et al., 2008a; Matsumoto et al., 2010).

The gas-particle partitioning coefficient, K_p, is a measure of the distribution of a compound between gas and particle phase (Pankow, 1987) described by equation (1.1):

$$K_p = \frac{C_p}{C_g \times \mathrm{TSP}}, \quad \mathrm{m^3\ \mu g^{-1}} \tag{1.1}$$

where C_p and C_g are the concentration of the organic compound *i* in the particle and gas phases, respectively (μg m^{-3}), and total suspended particulate matter (TSP) is the mass concentration of the aerosols (μg m^{-3}). It predicts the mobility and fate in the environment. Discriminating the low mass fraction of VOCs in aerosol particle to the high gas-phase concentration is an experimental challenge. To date, measurement of the gas-particle partitioning of VOCs has been derived from field studies (Matsumoto et al., 2010). However, determining K_p *via* field sampling is more likely semiquantitative because it is susceptible to inaccuracies from multiple factors inherent during sampling. For compounds with low K_p, such as VOCs, partitioning between the gas and particle phases is controlled by equilibrium (Ansari & Pandis, 2000; Mai et al., 2015). Equilibrium is affected by temperature and modulated by the VOC's nature, such as its solubility and polarity. Within the narrow range of temperature in the lower troposphere, the sorption of compounds with varying polarities on aerosol particles is sensitive to temperature fluctuations. Only scant reports have investigated the mechanism and extent of partitioning for VOCs (Rao & Vejerano, 2018). Studies on the partitioning mechanism of organic compounds into aerosols and the models developed to predict the K_p of gas-aerosol partitioning date back to 1980s (Pankow, 1987; Pankow & Bidleman, 1991; Goss & Eisenreich, 1997; Pankow, 1998; Goss & Schwarzenbach, 1998) but were heavily focused on SVOCs rather than on

VOCs. The partitioning was primarily attributed to absorption into the water-insoluble organic matters (WIOM) of aerosols because of the high hydrophobicity of the SVOCs.

The extent of the partitioning of VOCs will depend on the nature of the VOCs and aerosols, and the environmental condition (more importantly relative humidity (RH) and temperature) at which partitioning occurs (Liu et al., 2015; Rao & Vejerano, 2018; Thevenet et al., 2018). This interaction will alter the dosimetry in both phases, but little is known so far on the direct interactions between VOCs and aerosols (Ebersviller et al., 2012a, 2012b). A small increase in RH could substantially increase the total organic aerosol mass, in which water provides a large absorbing matrix for organics (Jathar et al., 2016).

We also focus on RH and aerosol composition. The interaction of aerosol components with their surroundings is complex; changes in one property influence other physicochemical behavior (Choi & Chan, 2002; Krieger et al., 2012; Martin, 2000). Uptake of water by the aerosols at different RH is a critical factor (Ding et al., 2021; Hennigan et al., 2008, 2009; Sun et al., 2013; Zhang et al., 2012). RH affects aerosol properties such as mass, size distribution, and composition (Hennigan et al., 2008; Zhang et al., 2012). For instance, modeling studies on SOA formation predicted a small increase in RH (0.1%) could increase the total organic aerosol by 3% (Jathar et al., 2016). Organic-phase water can increase the aerosol mass and provides a larger absorbing matrix for organics (Jathar et al., 2016). Uptake of water can cover active sites on aerosol, which decreases the amount of organics that will partition onto the aerosol via adsorption. Once covered, the VOCs' mass fraction will depend on the VOCs' nature (*i.e.*, solubility, polarity, and hydrophobic/hydrophilic properties) (Arp et al., 2008b; Matsumoto et al., 2010; Wei et al., 2016) and other physicochemical properties.

Aerosol composition varies widely from its source (Pöschl, 2005). In dry aerosol particles, the major components include inorganics (*e.g.*, ammonium nitrate, ammonium sulfate, ammonium chloride), organic matter (*e.g.*, succinic acid, *n*-alkanes, polycyclic aromatic hydrocarbons), and elemental carbon (Donahue et al., 2009). Organic matter in aerosol is a mixture of thousands of organic compounds from numerous sources with more than half of the organic matter being water-soluble (Rao & Vejerano, 2018). The majority of the mass fraction of water-soluble organic matter (WSOM) are dicarboxylic acids (C2–C6), dicarbonyls (*e.g.*, glyoxal), ketoacids (C2–C5), polyols (C2–C7), hydroxylamines, amino acids (C2–C6), and nitrophenols (Donaldson & Valsaraj, 2010). VOCs are much less hydrophobic than SVOCs (*e.g.*, pesticides, polycyclic aromatic hydrocarbons, polychlorinated biphenyls), with some being hydrophilic. The partitioning of VOCs into the WSOM of aerosol particles may dominate overall partitioning. The organic fraction of atmospheric aerosol contains a large amount of water-soluble organic compounds (Saxena & Hildemann, 1996; Gysel et al., 2004; Decesari et al., 2005). Among the most abundant is succinic acid (Kawamura & Bikkina, 2016). Ammonium sulfate and succinic acid coexist in atmospheric aerosol (Lightstone et al., 2000; Q. Liu et al., 2016). The presence of water-soluble organic acid (*e.g.*, succinic acid) can modify the phase behavior or inorganic constituent, particularly those exhibiting distinct phase transition such as ammonium sulfate (Jing et al., 2018). Although aerosols composed of a higher amount of inorganic component dictates water uptake, an equal concentration (organic: inorganic), organic acids will influence water uptake behavior (Prenni et al., 2003). For predicting water uptake on aerosol with mixed composition, data from pure components can be used, assuming that each component contributes independently (Prenni et al., 2003).

Exposure to VOCs via multiple routes induces short-term and long-term adverse health effects (Cakmak et al., 2014; Gao et al., 2014; D. R. Brown et al., 2015). Prenatal exposure to gas-phase VOCs negatively affects postnatal growth (Chang et al., 2017). The detection of a substantial fraction of VOCs in aerosol particles has an important impact on human health (Dockery et al., 1993; Pope et al., 1995) because VOCs in submicron aerosol particles can reach regions of the respiratory system that are typically inaccessible to those in the gas phase. Most gas-phase VOCs are poorly absorbed by cells, therefore, immediately exhaled (Ebersviller et al., 2012a). Aerosols passed over vapors of acrolein, an extremely volatile compound, induce significant damage and inflammation on lung cells compared to the pure aerosol particles (Ebersviller et al., 2012a, 2012b). Hence, the impact of the gas-particle partitioning of VOCs should not be ignored.

CHAPTER 2

OBJECTIVES AND SCOPE

Assessing environmental and human health impacts of chemical spills relies on information about how chemicals move across multiple environments. Here, we report a part of our investigation on the partitioning of VOCs as they move across the soil, air, and airborne particles. The traditional process to measure the VOC partitioning involves collecting the samples in the field in which soil or aerosol consisting of various components was already formed. The field sampling method has been known to result in large variability in partitioning coefficient because of thermodynamic and non-thermodynamic factors such as the dynamic environmental conditions over the sampling period, non-equilibrium conditions, and sampling artifacts (Wang et al., 2014; Kristensen et al., 2016). In addition, scant research was conducted on VOC partitioning onto airborne aerosol at different RH conditions. Many gas-particle partitioning studies have focused on SVOCs (Weschler and Nazaroff, 2010); however, SVOCs cannot accurately describe the VOC partitioning behavior because of the substantial differences in their physicochemical properties. Therefore, the K_p of laboratory-generated aerosols composed of only pure aerosols was measured in a bench-scale system under precisely controlled experimental conditions. Therefore, four objectives were set to this study as follow:

The first objective is the development of a laboratory-scale bench system to characterize K_p to understand the partitioning behavior between VOCs in air and aerosol

particles. By maintaining a stable experimental condition in each test, the specific K_p can be measured accurately. The detailed but uncomplicated system setup may contribute to other researchers' work on investigating the global fate and transport of VOCs as well as their health effects.

The second objective was to determine the physicochemical properties of the VOCs that can be used to predict their partitioning coefficient. Results will inform the prediction of the K_{SA}, that can be used as proxies for measuring emissions of VOCs from the soil into the air when air measurement is not readily available or difficult to obtain.

The third objective was to investigate the partitioning of VOCs into aerosol particles depending on dynamic environmental conditions and physicochemical properties. Results from this study will increase our understanding of the partitioning of VOCs in a different aerosol component and help future studies on the model development to predict K_p of the VOC-to-aerosol partitioning process.

The fourth objective was to estimate the transportation and fate of VOC in the environment, such as after chemical spills because of natural disasters. In addition, the accumulation of VOCs was calculated due to the deposition of VOC-containing aerosols in the respiratory system as a surrogate of exposure to VOCs. This study will help to understand the impacts of VOC partitioning on multiple environmental compartment and human health.

Intellectual merit and major outcome. The proposed research was assessed the partitioning of VOCs into soil and aerosol particles under different conditions to estimate the K_{SA} and K_p for these VOCs. This research will contribute to create models for VOCs'

partitioning into the multiple environmental compartments. Determination of the partitioning coefficient at different conditions allows prediction of the fate and transport of VOCs in the environment and the impacts on health. The overall research scopes are outlined in Figure 2.1.

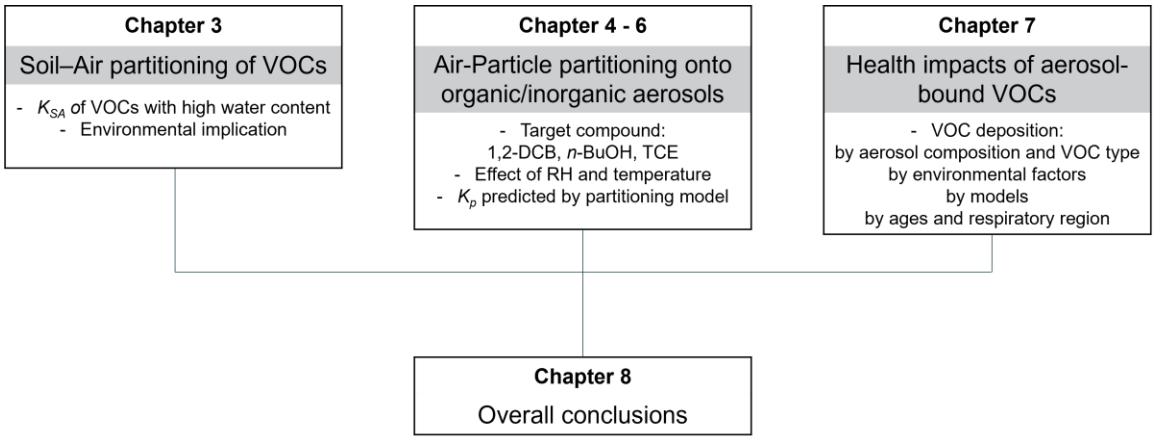

Figure 2.1 The diagram presenting dissertation outline.

CHAPTER 3

SOIL-TO-AIR PARTITIONING OF VOLATILE ORGANIC COMPOUNDS INTO SOILS WITH HIGH WATER CONTENT[1]

3.1 Types of VOCs

All standards and solvents used in this study were analytical grade reagents. Chemicals were purchased from Sigma-Aldrich, unless otherwise noted, and were used as received. Six VOCs were purchased. Nonpolar VOCs include the aromatic VOCs (benzene (99.8%), 1,2-dichlorobenzene (1,2-DCB, 99%,), and toluene (≥ 99.8%, BeanTown Chemical) and the chlorinated alkane VOC (trichloroethylene (TCE, ≥ 99.5%)). 1-Butanol (≥ 99.4%) and methyl tert-butyl ether (MTBE, 99.9%) were used as representatives of polar and weakly polar VOCs, respectively. The deuterated VOCs, benzene-*d*6, 1,2-DCB-*d*4, toluene-*d*8, 1-butanol-*d*10, MTBE-*d*3, and TCE-*d* were used as the internal standards to quantify the VOCs. All deuterated chemicals were purchased from AccuStandard except for 1-butanol-*d*10 (99%, Sigma-Aldrich) and TCE-*d* (98%, Sigma-Aldrich). Methanol (> 99.99%, Fisher Chemical) was used as a solvent for the calibration standards. The physicochemical properties of VOCs are listed in Table 3.1. The VOCs in this study

[1] Reprinted here with permission of publisher: Jeonghyeon Ahn *et al.*, Soil-to-air partitioning of volatile organic compounds into soils with high water content. Environmental Chemistry 17(8) (2020) 545-557.

Table 3.1. Physicochemical properties of the VOCs

	CAS	Molecular weight (g/mol)	Vapor pressure (mm Hg)	Solubility (g/L)	*Log K_{ow}* (log L/kg)	*log K_{oc}* (log L/kg)	Dimension-less Henry's law constant	*logK_{oa}* (log L/kg)	Diffusion coefficient in water (cm^2/sec), $\times10^{-6}$	Diffusion coefficient in air (cm^2/sec), $\times10^{-2}$
Benzene	71-43-2	78.114	94.8	1.79	2.13	1.82	0.227	2.77	9.8	8.8
1,2-DCB	95-50-1	147	1.36	0.156	3.43	2.58	0.078	4.54	7.9	6.9
Toluene	108-88-3	92.141	28.4	0.526	2.73	2.15	0.276	3.29	8.6	8.7
TCE	79-01-6	131.38	69	1.28	2.42	1.97	0.428	2.79	9.1	7.9
MTBE	1634-04-4	88.15	250	51.0	1.06	1.15	0.024	2.67	94.1	7.92
1-Butanol	71-36-3	74.123	7.0	63.2	0.505	0.77	3.55E-4	4.33	9.3	8.0

Note: data were taken from the PubChem Database (https://pubchem.ncbi.nlm.nih.gov/) except for the organic carbon-water partition coefficient (K_{oc}) and dimensionless Henry's law constant, which were taken from the GSI Chemical Database (https://www.gsi-net.com/en/publications/gsi-chemical-database.html). The octanol-air partition coefficient (K_{oa}) data were calculated by dividing the octanol-water partition coefficient (K_{ow}) by the dimensionless Henry's law constant.

included a wide range of each parameter, thus were good representatives in the best correlate with K_{SA}.

3.2 Soil and soil characterization

In our initial experiment, we found that the soil collected from the environment contained significant concentration levels of 1,2-DCB; therefore, we purchased soil to lessen the presence of organic contaminants contained in the soil. Two types of soil were purchased and used without further treatment to compare K_{SA} of VOCs according to the soil water content and physicochemical properties of VOCs: clay (470025–200, VWR), which we refer to as *S-clay*, and silt with high organic matter content (470025–202, VWR), which we refer to as *S-om*. The Brunauer–Emmett–Teller (BET) test was used to determine the specific surface area and porosity of the soil through nitrogen adsorption at 77K using a surface area and porosity analyzer (Micromeritics ASAP 2020). The BET surface area and the total pore volume of each soil were determined by a multipoint BET method using the adsorption data at the relative pressure (p/p_0) within 0.5. The percent of the adsorbed water and organic matter of each soil were characterized by simultaneously performing thermogravimetric analysis (TGA) and differential scanning calorimetry (DSC) thermal analyses from 25 to 700°C (298 to 973K) with a heating rate of 10 °C min^{-1} (0.167 K s^{-1}) in air. The results are shown in Figure 3.1. Weight loss from 25 to 150°C (298 to 423K) was taken as a measure of the adsorbed water content in the soil, and the weight loss from 250 to 370°C (523 to 643K) for the amount of the organic matter (Post & Henderson, 2012). The soil particle density was measured to calculate the partition coefficient, which was estimated by dividing the mass of the soil by the volume of the particles measured using a graduated cylinder. The maximum water holding capacity (WHC) of each soil was

determined by first adding water into the soil sample to form a mixture and then centrifuging the mixture at 5600 × g for 3 min to separate the unabsorbed water. The difference in mass of the water added into the soil and the water extracted from it after centrifuging was the maximum amount of water the soil could hold (water holding capacity (WHC)).

The results of the soil characterization are summarized in Table 3.2. The clay mineral (*S-clay*) contained negligible amounts, ~ 0.5 wt%, of organic matter. *S-clay* also had a much larger surface area (~ 2×) than that of *S-om*, which was similar to silt. In contrast, *S-om* contained a large amount of organic matter (~ 10.7 wt%). Organic matter in the soil can absorb water efficiently, which enhances the WHC of the soil (Brown & Wherrett, 2018). The amount of adsorbed water in the original soil (4% and 6% of the soil mass) without any treatment generated nearly an RH level of 100% in the sealed glass bottle during the partitioning experiment. Therefore, both of the as-received soils from the vendor were already saturated with water before the test. The RH level inside the bottle containing the soil was measured after inserting a temperature and humidity probe (USBQTENKI-T-RH-CC2, Dracal Technologies, Inc.), then sealing it, and equilibrating it at 25°C (298K) in a temperature-controlled chamber for 20 min.

3.3 Measurement of soil/air equilibrium partitioning coefficient

The K_{SA} was determined using equation (3.1):

$$K_{SA} = \frac{C_{is}}{C_{ia}}\, d_s \tag{3.1}$$

where C_{is} and C_{ia} are the concentrations of VOCs, i, in soil (μg g^{-1}) and air (μg m^{-3})

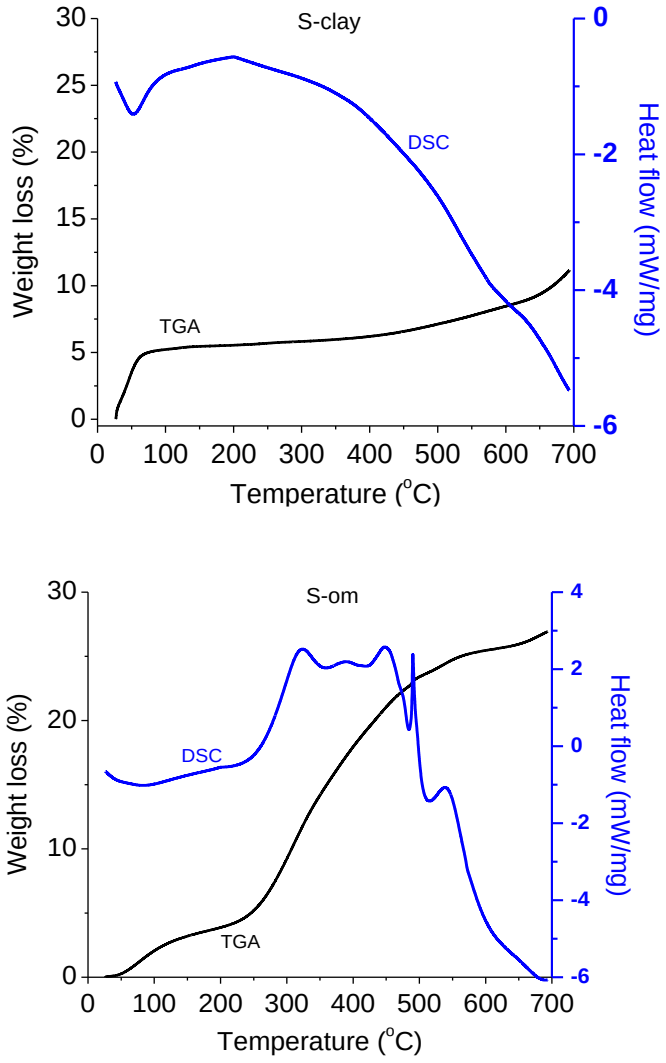

Figure 3.1. TGA-SDC test results for characterizing the adsorbed water and organic matter contents in clay and silt soil.

Table 3.2. Physicochemical properties of the soils.

Soil	Surface area (m^2/g)	Organic matter (% of soil mass)	Particle density (g/cm^3)	Adsorbed water (% of soil mass)	Water holding capacity (%)
S-clay	23	~0	2.20	6	64
S-om	10.8	10.7	1.82	4	67

respectively, and d_s is the density of the soil particle (g m^{-3}). The batch sorption experiments were carried out in 10-mL borosilicate glass bottles; each contained 1 g of soil (*S-clay* or *S-om*) and different amounts of de-ionized water to achieve 5, 20, 40, 60 and 80% of the WHC of the soil. The glass bottles were shaken on a mini orbital shaker (VWR International) at 0.54 × *g* for 6 h to mix the water with the soil thoroughly. The temperature was kept at 25 ± 0.2°C (298 ± 273.4K) by installing the mini shaker in a temperature-controlled chamber (CEO932, Lunaire Environmental, New Columbia, PA). After that, the pure liquid VOC (0.4 µL for 1-butanol, benzene, toluene and 1,2-DCB; 1 µL for MTBE and TCE) was injected into the glass bottle through the Teflon-lined rubber septum and immediately sealed with an aluminum crimp cap. The glass bottle that contained the water and liquid VOC was agitated for 24 h at 25 ± 0.2°C. While temperature affects partitioning (Ranjan et al., 2012; Wei et al., 2016), we conducted the experiment only at this temperature because the mass transfer of VOCs from the soil into the air depends primarily on the subsurface temperature, which fluctuates sinusoidally with depth but has a maximum temperature close to 25°C (Nofziger, 2003). Steady-state was established in less than 24 h for the VOC with the lowest vapor pressure (1,2-DCB) (Figure 3.2) thus we deemed that 24 h was sufficient for other VOCs to reach steady-state, which is consistent with the times that are frequently observed and reported in the literature (Rogers et al. 1980; Shimizu et al. 1992; Tekrony and Ahlert 2001).

The volumes of the pure VOCs injected into the glass bottles were set at 0.4 µL (1 µL = 10^{-9} m^3) for 1-butanol, benzene, toluene and 1,2-DCB, and 1 µL for MTBE and TCE to produce a relative vapor pressure (p/p_o) within 0.1 at equilibrium (except for 1,2-DCB partitioning into *S-clay*). Within such a low range of the relative vapor pressure, adsorption

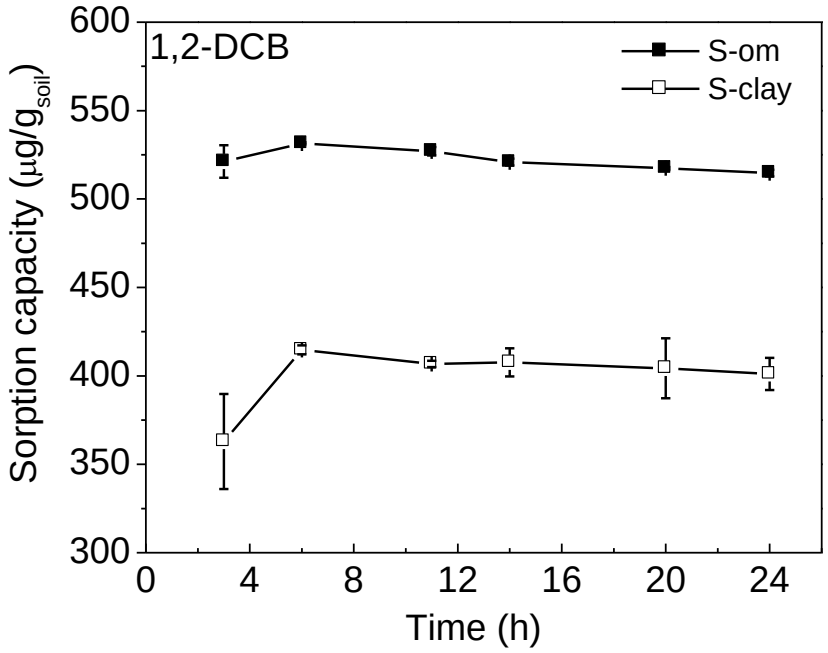

Figure 3.2 Partitioning of 1,2-DCB into clay and silt as a function of time.

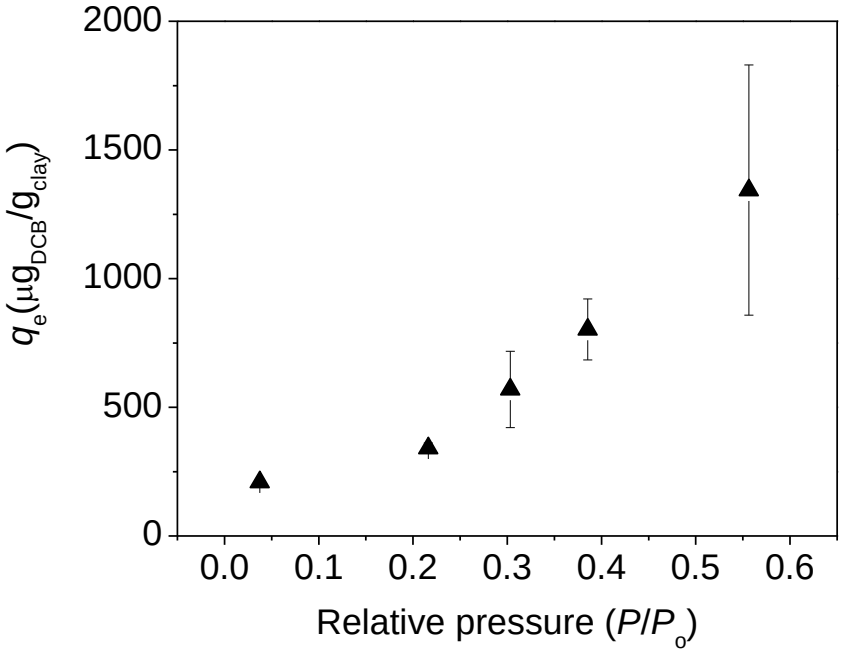

Figure 3.3 Adsorption of 1,2-DCB on the as-received *S-clay* at different relative pressures at equilibrium (q_e: adsorption capacity at equilibrium; 1 μL of pure liquid 1,2-DCB was injected into the glass bottle for the adsorption test).

can be approximated to be linearly related to the vapor pressure of the VOC; thus, the concept of a partition coefficient applies (Petersen et al., 1995). At high vapor pressures, BET theory can be used to describe the whole adsorption isotherm over the full range of the relative vapor pressures (Petersen et al., 1995). Our measurement of the adsorption isotherm suggested a linear increase of the partitioning of 1,2-DCB into *S-clay* at the investigated p/p_o range (Figure 3.3); thus, the partition coefficient concept can also be applied to describe the partitioning of 1,2-DCB into *S-clay*.

3.4 VOC sampling and analysis

We used the head-space sampling method to take gas samples from the borosilicate glass bottles at the end of the sorption experiment (Kremser et al., 2016; Mead et al., 2017). A volume of 30 µL of gas was taken from the headspace of the bottle using a 50-µL gas-tight syringe (Hampton 1705SL). Since we used borosilicate glass bottles, wall loss of the gaseous VOCs was negligible (Kim & Kim, 2015; Ahlberg et al., 2017).

A gas chromatograph (Clarus 680, PerkinElmer, Waltham, MA) and mass spectrometer (Clarus SQ-8T, PerkinElmer, Waltham, MA) (GC/MS) system equipped with an Agilent DB-5ms capillary column (30 m × 0.25 mm ID, 0.25-µm film coated with 5%-(phenylmethylpolysiloxane) were used to quantify the VOCs. Ultrapure helium was used as the carrier gas at a flow rate of 1 mL min^{-1} (1.67×10^{-8} m^3 s^{-1}). For each measurement, immediately after injecting the 30 µL of headspace sample, 1 µL of 500 ppb of the internal standard dissolved in methanol was also injected into the GC/MS. The ratio of the peak areas of the target VOCs and the internal standard (500 ppb) was measured. Five different concentrations of the VOCs and 500 ppb of their corresponding internal standard were prepared in methanol solutions to generate the calibration curve. Next, 1 µL of each

solution was injected into the GC/MS, and the peak areas (A) of both the VOC and internal standard were recorded as the response ratio. The response ratio against the concentration of the analyte to that of the internal standard was plotted to generate the calibration curves (r^2 = 0.996). The mass of VOC that partitioned into the soil was calculated by deducting the measured mass of the gas-phase VOC in the GC/MS analysis from the mass of the injected VOC (by multiplying the injection volume with the density of the pure liquid VOC). The mass spectrometer was operated in the single-ion monitoring mode.

3.5 Statistical analysis

We measured the K_{SA} at least in triplicate, which we then averaged with the uncertainty reported as one standard deviation. Regression analysis and statistical calculations were performed using *SigmaPlot* (Systat Software Inc.). We used equation 3.2 to perform regression analyses to determine which physicochemical parameters best correlated with the measured K_{SA}.

$$log\ K_{SA} = A \times log\ [\text{physicochemical parameters}] + B \quad (3.2)$$

We used these physicochemical parameters: log p_{sat}, log K_{ow}, log K_{oa}, log [water solubility], log [Henry's law constant], log [diffusion coefficient in air], log [diffusion coefficient in water] and log [molecular weight].

3.6 Partitioning of VOCs in water-saturated soil

The K_{SA} of VOCs in *S-clay* and *S-om* at different soil water contents are shown in Figure 3.4. We observed different partitioning patterns for the VOCs that we investigated, but we did not observe significant differences in the K_{SA} for similar VOC partitioning into both types of soil (Figure 3.4**)**, except 1,2-DCB and toluene, which partitioned

preferentially into *S-om* (red curve) than into *S-clay*. The average K_{SA} of 1,2-DCB on *S-om* was 2.6× to 10.9× higher than the average K_{SA} on *S-clay*. In contrast, the average K_{SA} of toluene on *S-om* was 2.3× to 4.1× the average K_{SA} on *S-clay*. Benzene had a similar K_{SA} on both types of soil. Although benzene was aromatic, it partitioned to a lesser extent into *S-om* compared with the substituted aromatic VOCs (1,2-DCB and toluene). We observed a similar phenomenon for the chlorinated alkane VOC (TCE) and polar VOCs (MTBE and 1-butanol), in which the extent of their partitioning was identical in both soil despite *S-om* containing higher organic matter (10.7%).

3.7 Relationship between K_{SA} of the VOCs and soil water content

We observed an almost linear decrease of *log* K_{SA} with soil water content for 1,2-DCB and toluene partitioning into *S-om* (Figure 3.5), while that of the other nonpolar VOCs (MTBE and TCE) exhibited poor linearity into both soils (not shown). As the water content of *S-om* increased, the K_{SA} of 1,2-DCB and toluene decreased by 80% and 55% respectively over the entire soil water content range. Partitioning of TCE into both soils increased with an increasing water content of the soil to ~35% by mass (~ 40% of the WHC for each soil) and then gradually declined. In contrast, for both soils, MTBE exhibited an opposite partitioning trend: initially, the K_{SA} slightly decreased, which then increased as the water content of the soil increased. Also, the K_{SA} was 15–20% greater on *S-om* than on *S-clay* at a soil water content of > 50% by mass, which suggested that partitioning into the soil organic matter also plays an important role for MTBE. For 1-butanol, the K_{SA} increased almost linearly for all water contents in both soils. Similar to MTBE, when the water content in soil was relatively high (> 50% by mass), the K_{SA} on *S- om* was nearly twice that

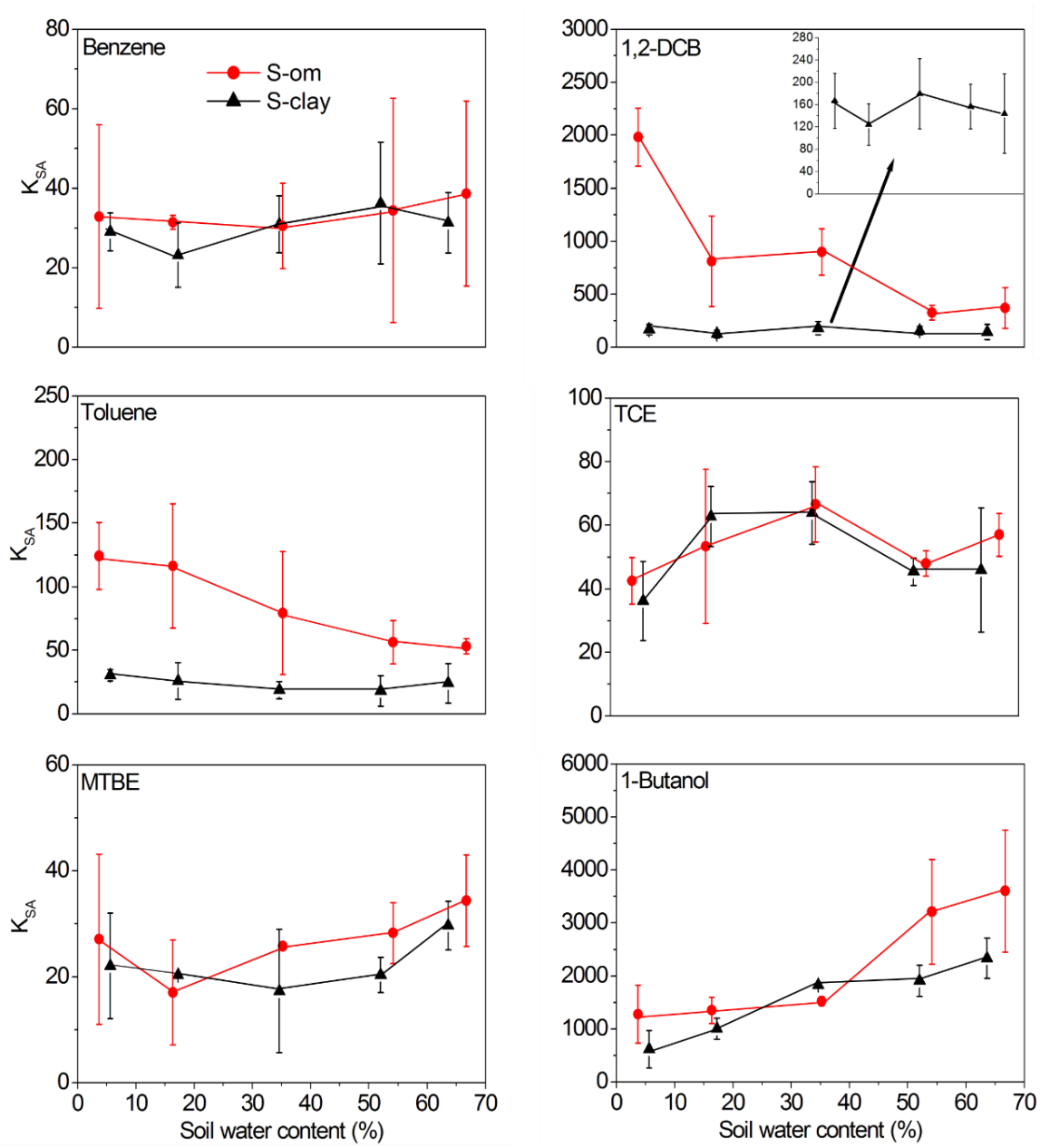

Figure 3.4 Soil/air partition coefficient of VOCs at different soil water contents at 25ºC. Measurements were performed at least in triplicate. Error bars are one standard deviation from the average K_{SA}.

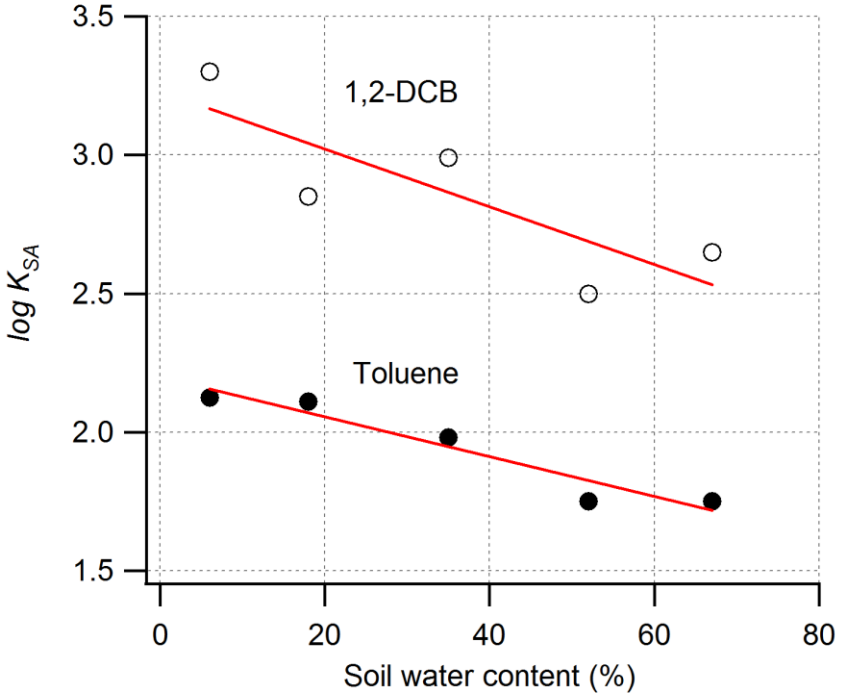

Figure 3.5 Soil water content dependence of the soil/air partition coefficient for 1,2-DCB and toluene partitioning into *S-om.*

of the K_{SA} on *S-clay*. As the water content of *S-om* increased, the K_{SA} of 1,2-DCB and toluene decreased by 80% and 5 % respectively over the entire soil water content range.

3.8 Correlation of the physicochemical parameters with *log* K_{SA}

We investigated which physicochemical properties of the VOCs best correlated with the measured log K_{SA} for both soils under varying water contents for predicting K_{SA} using linear regression. For this analysis (performed under a confidence interval of 95%), we used the following physicochemical properties of the VOCs: *log* P_{sat}, *log* K_{ow}, *log* K_{oa}, *log [water solubility]*, *log [Henry's law constant]*, *log [diffusion coefficient in air]*, *log [diffusion coefficient in water]*, and *log [molecular weight]*. Since the organic carbon partitioning parameter (K_{oc}) was strongly correlated with K_{ow} (r^2 = 0.9996), we only used K_{ow} for our analysis. Among the physicochemical parameters, p_{sat} and K_{oa} have been extensively used as the correlation parameters in modelling studies to predict the K_{SA} of VOCs partitioning into soil with a small amount of water (Goss & Schwarzenbach, 1998, 1999a; Pankow, 1998; Rao & Vejerano, 2018). The K_{ow} has also previously been incorporated in modelling (Hippelein & Mclachlan, 1998). The Henry's law constant describes the dissolution of VOCs into soil water (Ong & Lion, 1991a; Goss & Eisenreich, 1996); and the partitioning of VOCs into soil is described as the diffusion of VOCs into the soil micropores (Cheng et al., 2012; Jochum et al., 2015); thus, these parameters were investigated in this study as well. Since K_{oc} was strongly correlated with K_{ow} (r^2 = 0.9996), we only used K_{ow} in the analysis. The physicochemical parameters of log K_{ow}, log [water solubility], log [Henry's law constant], log [diffusion coefficient in air], log [diffusion coefficient in water] and log [molecular weight] were weakly correlated with log K_{SA} with r^2 < 0.23, 0.18, 0.30, 0.44, 0.24 and 0.23 respectively, compared with the other parameters

regardless of soil type.

3.9 Correlation of K_{SA} with p_{sat} and K_{oa} in different soil types

Only log p_{sat} and log K_{oa} correlated strongly with log K_{SA} compared with the other physicochemical parameters that we investigated but this was dependent on soil class. The summary of the results of the correlation analysis for the two parameters (log p_{sat} and log K_{oa}) is give in Table 3.3. The graphs of the analysis depicting the correlation between log K_{SA} and log p_{sat} or log K_{oa} are shown in Figure 3.6 and Figure 3.7. Both parameters weakly correlated with log K_{SA} for *S-clay* at all water contents of the soil ($P > 0.05$, $r^2 = 0.377$–0.499) for log p_{sat} and log K_{oa} ($P > 0.05$, $r^2 = 0.582$–0.656) (Table 3.3) if all the VOCs were included.

For *S-om*, which contained a high amount of organic matter, the log K_{SA} was strongly correlated with log K_{oa} at 4–35% soil water content (corresponding to 5–40% WHC) ($r^2 \geq 0.94$, $P \leq 0.001$; Table 3.3). The log p_{sat} also showed a relatively strong correlation with log K_{SA} at these soil water content levels (r^2 of 0.835–0.943, $P < 0.011$). However, at the soil water content of 54–67 % (corresponding to a WHC of ~ 80–100 %), both parameters correlated weakly with log K_{SA} ($r^2 \leq 0.760$).

Among the VOCs, the highly polar 1-butanol was an outlier in most cases. Excluding 1-butanol from the analysis, the r^2 improved slightly, but the log K_{SA} was still weakly correlated with both log p_{sat} and log K_{oa} for *S-clay*. However, for *S-om*, excluding 1-butanol significantly improved the adjusted r^2 from 0.747 to 0.974 ($P \leq 0.007$, Table 3.3).

Table 3.3 Summary of the linear regression analysis of the *log* K_{SA} with *log* [P_{sat} or K_{oa}]

Soil type, water content by mass of soil	With 1-butanol				Without 1-butanol				Investigated variable
	A	B	*p*-value	r^2	A	B	*p*-value	*adjusted* r^2	
S-clay, 6%	-0.390	2.329	0.185	0.391	-0.202	1.876	0.016	0.855	
S-clay, 18%	-0.526	2.656	0.117	0.499	-0.337	2.204	0.047	0.709	
S-clay, 35%	-0.633	2.801	0.139	0.460	-0.395	2.231	0.098	0.538	P_{sat}
S-clay, 52%	-0.599	2.742	0.163	0.421	-0.350	2.144	0.097	0.641	
S-clay, 64%	-0.562	2.738	0.195	0.377	-0.298	2.105	0.076	0.603	
S-clay, 6%	0.571	-0.008	0.070	0.601	0.221	0.853	0.021	0.828	
S-clay, 18%	0.608	-0.186	0.051	0.656	0.348	0.560	0.088	0.563	
S-clay, 35%	0.780	-0.788	0.064	0.618	0.409	0.300	0.142	0.423	K_{oa}
S-clay, 52%	0.771	-0.762	0.069	0.604	0.373	0.400	0.122	0.471	
S-clay, 64%	0.756	-0.665	0.078	0.582	0.329	0.585	0.081	0.587	
S-om, 4%	-0.990	3.590	0.001	0.943	-0.905	3.388	0.001	0.982	
S-om, 16%	-0.868	3.345	0.007	0.869	-0.744	3.048	0.001	0.984	
S-om, 35%	-0.834	3.330	0.011	0.835	-0.701	3.010	0.002	0.961	P_{sat}
S-om, 54%	-0.720	3.113	0.087	0.561	-0.481	2.540	0.001	0.970	
S-om, 67%	-0.709	3.143	0.094	0.544	-0.473	2.603	0.006	0.974	
S-om, 4%	1.010	-1.269	0.000	0.995	1.009	-1.266	0.000	0.991	
S-om, 16%	0.899	-0.960	0.001	0.944	0.807	-0.705	0.006	0.922	
S-om, 35%	0.881	-0.863	0.001	0.940	0.771	-0.560	0.005	0.934	K_{oa}
S-om, 54%	0.833	-0.755	0.024	0.760	0.532	0.082	0.003	0.956	
S-om, 67%	0.825	-0.680	0.026	0.747	0.524	0.182	0.007	0.915	

log K_{SA}= A × *log* [P_{sat} or K_{oa}] + B was used for the analysis

water content was calculated relative to the soil mass, corresponding to ~ 5, 20, 40, 60, and 80% of the WHC

3.10 Mechanisms of soil/air VOC partitioning

The emission of VOCs from the soil and into the air is primarily affected by the soil moisture dynamics and carbon availability (*i.e.,* presence of organic matter) (Rossabi et al., 2018). The high mass fraction of water and organic matter affect VOC partitioning, and ultimately the emission of VOCs into the air. We measured the soil–air partition coefficient for three classes of VOCs: non-polar aromatic, slightly polar alkanes and highly polar compounds, as representatives of chemicals that may be present in chemical spills and environmental contamination. Our results regarding 1,2-DCB and toluene partitioning more into *S-om* than into *S-clay* indicate that aromatic VOCs preferentially partitioned into the organic matter fraction rather than into the mineral fraction of the water-saturated soil, which is consistent with those in the literature (Costanza & Brusseau, 2000; Han et al., 2013). These results indicate that the chlorine substituents likely enhanced the affinity of the VOC to sorb onto the organic matter fraction (*e.g.*, the hydrophobic sites) of the water-saturated soil, which is consistent with the finding that chlorinated aromatic VOCs partition into soil with high organic matter suspended in aqueous water (Pierce et al., 1974). We expect that the association of the chlorinated aromatic VOCs with soil organic matter may be enhanced if the soil is saturated with water.

In soil that contained high amounts of organic matter, we attributed the decline in K_{SA} as the water content increases to the impact of water covering the hydrophobic sites of the organic matter, which rendered them less available to interact with the VOC. Benzene had a similar K_{SA} on both types of soil. Although benzene is aromatic, it partitioned to a lesser extent into *S-om* compared with the substituted aromatic VOCs (1,2-DCB and toluene). We observed a similar phenomenon for the chlorinated alkane VOC (TCE) and

polar VOCs (MTBE and 1-butanol), in which the extent of their partitioning was similar in both soils, despite *S-om* containing higher organic matter (10.7%). This phenomenon may likely arise because these VOCs are less hydrophobic compared with aromatic VOCs (1,2-DCB and toluene). Therefore, for the less hydrophobic nonaromatic VOCs, the organic matter fraction in soil was not the primary partitioning medium.

The comparable partition coefficients for benzene, TCE, MTBE and 1-butanol into both soils indicated that neither the mineral soil's specific surface area nor the organic matter fraction in soil (Table 3.2) played a significant role on partitioning. The more dominant factor was the presence of condensed water on the soil surface at a high level of RH (~ 100%) (Goss & Eisenreich, 1996; Cabbar, 1999). This condensed water may form a thick layer on soil that prevents the components in the soil from interacting directly with the VOCs (Goss & Eisenreich, 1996) but enhances the dissolution of the VOCs. For instance, TCE has been observed to dissolve into a water film containing at least five layers of molecular water on a mineral surface (Ong & Lion, 1991a).

Although benzene is highly soluble in water (~ 1.79 g L^{-1}), the dissolution of benzene into the water in soil may not be the only mechanism of its partitioning; otherwise, we would have observed an increased in K_{SA} as the water content increased (Goss & Eisenreich, 1996), but in fact, the K_{SA} remained constant (Figure 3.1). Thus, it was likely that some mass fraction of benzene adsorbed at the air-water interface (Heath & Valsaraj, 2015; Costanza & Brusseau, 2000). As the water content of the soil increased, more mesopores and macrospores were filled with water, which led to a decrease in the surface area of the air-water interface (Cabbar, 1999). The increased dissolution of benzene with increasing soil water content might have offset the decrease in the mass of adsorbed

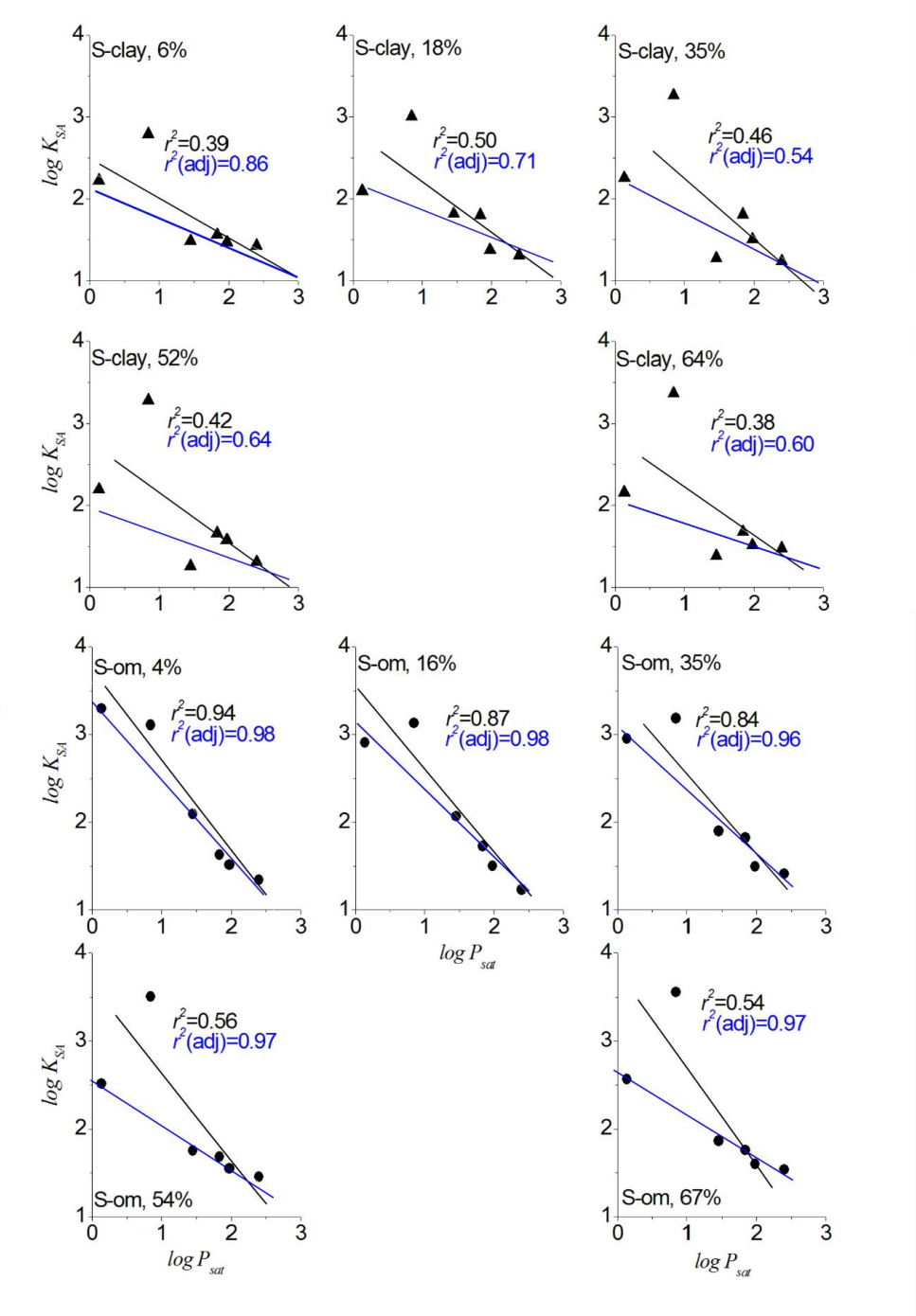

Figure 3.6 Correlation analysis between *log* K_{SA} and log P_{sat}. Line and r^2 text in black represent the regression that includes 1-butanol; line and $r^2(adj)$ text in blue represent the regression that excludes 1-butanol).

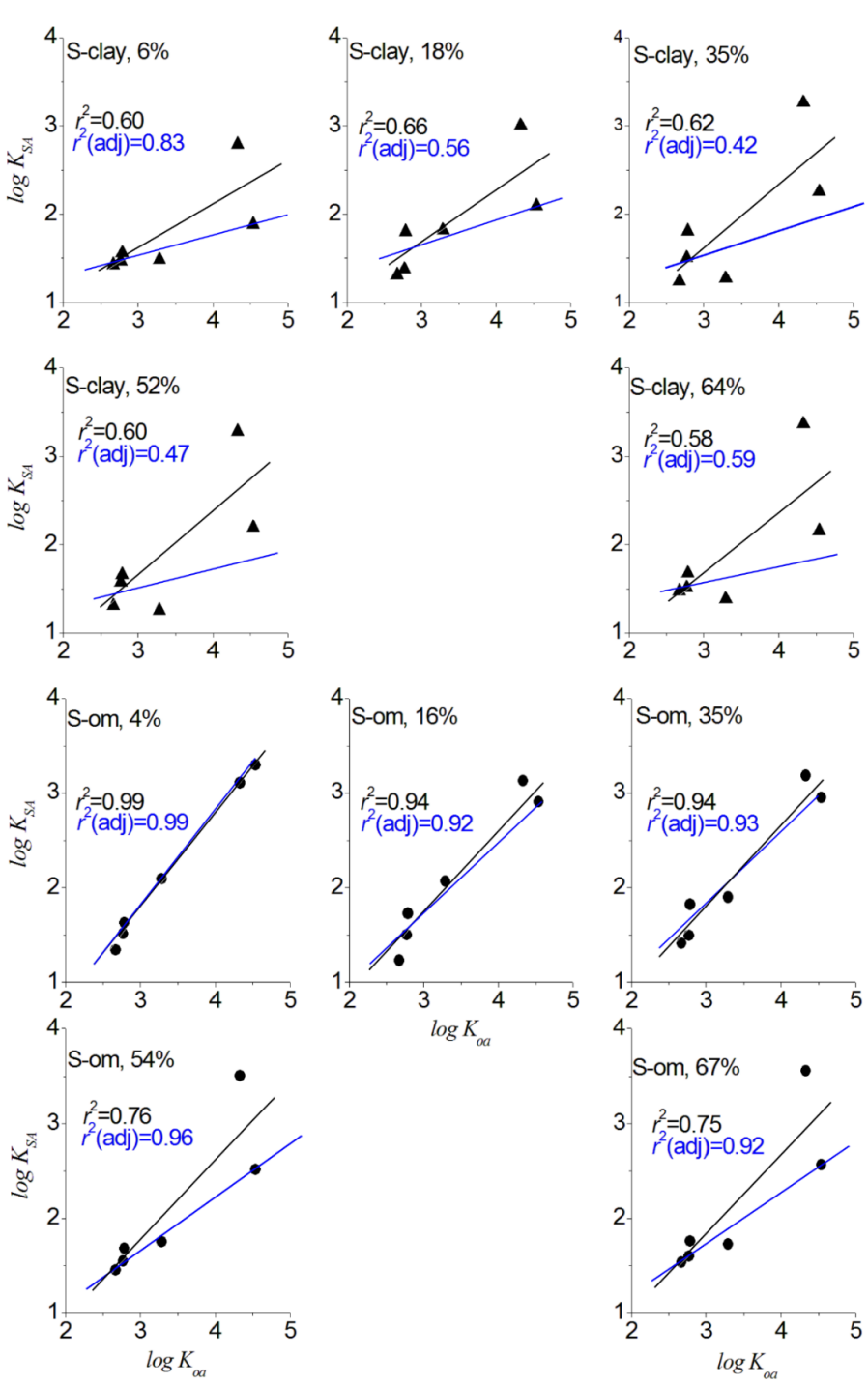

Figure 3.7 Correlation analysis between *log* K_{SA} and *log* K_{oa}. Line and r^2 text in black represent the regression that includes 1-butanol; line and r^2*(adj)* text in blue represent the regression that excludes 1-butanol).

benzene at the air-water interface, leading to an almost constant K_{SA}. Such mechanisms may also explain the near constant K_{SA} with increasing soil water content observed for 1,2-DCB and toluene partitioning into *S-clay*.

The increase of K_{SA} at the beginning was likely a result of a larger mass fraction of TCE dissolving at higher soil water content levels and less adsorption at the air-water interface, and the dissolution partly contributed to the overall partitioning (Ong & Lion, 1991a, 1991b). The chlorine substituents of the alkane VOC may also increase the sorption by interacting strongly with sites on the water film that have high interfacial energy through induced electrostatic forces (Tekrony & Ahlert, 2001). As the water content increased up to the WHC, the area at the air-water interface and the availability of high interfacial energy sites on the water film were significantly reduced, which resulted in the overall decline in the K_{SA}. We attributed the slight decrease of K_{SA} to the adsorption-dominated partitioning mechanism at the air-water interface when the water content of the soil was relatively low. Although the weakly polar VOCs (*e.g.*, MTBE) have stronger tendency to adsorb at the air-water interface than the nonpolar VOCs, the high aqueous solubility of MTBE may have limited the relative importance of interfacial sorption to the overall MTBE partitioning (Costanza & Brusseau, 2000), in which we observed an increase in K_{SA} at higher soil water content. Also, the K_{SA} was 15–20% greater on *S-om* than on *S-clay* at a soil water content of > 50% by mass, which suggested that partitioning into the soil organic matter also played a vital role in the overall MTBE partitioning.

Dissolution of 1-butanol into the water in soil was likely the dominant partitioning mechanism because this VOC is highly polar ($\log K_{ow} < 1$), and because we observed an almost linear increase in the K_{SA} under all water contents for both soil. However, because

1-butanol has the lowest dimensionless Henry's law constant that is two to three orders magnitude lower than the other VOCs, the air-water partitioning mechanism might have also contributed to the overall partitioning of 1-butanol into soil. Similar to MTBE, when the water content in soil was relatively high (> 50% by mass), the K_{SA} on *S-om* was nearly twice that on *S-clay*, which suggests the importance of the organic matter on partitioning for this class of VOC.

We are interested in determining if p_{sat} and K_{oa} are good predictors of K_{SA} for VOCs sorbing in soil that are saturated with water or those that contain water close to the WHC. Although the p_{sat} and K_{oa} parameters have been extensively applied in modelling studies to predict the partitioning of VOCs into unsaturated soil, they are not applicable for mineral soil that contains almost no organic matter under a water-saturated condition. Both parameters were weakly correlated with log K_{SA} for *S-clay* at all water contents of the soil ($P > 0.05$, $r^2 = 0.377$–0.499) for log p_{sat} and log K_{oa} ($P > 0.05$, $r^2 = 0.582$–0.656) (Table 3.3). The adjusted r^2 rather than r^2 was reported when we excluded 1-butanol from the analysis because this regression contained only a part of the targeted VOC parameters (Miles, 2005). Therefore, in this case, p_{sat} and K_{oa} may be used to predict K_{SA} of VOCs partitioning into *S-om*. However, using these parameters may underestimate the partitioning of highly polar VOCs (*e.g.*, 1-butanol, log $K_{ow} << 1$) when the soil water content is relatively high.

We also compared our correlation analysis results with the work reported by Hippelein and Mclachlan (Hippelein & Mclachlan, 1998), where the partitioning of semivolatile organic compounds (SVOCs; chlorinated benzenes, PCBs and PAHs) into the water-saturated soil that contained mainly sand with 1% of organic carbon and 1.9% of soil

water was studied. In their study, the log K_{SA} correlated well with log K_{oa} (r^2 = 0.972, A = 0.987, B = –1.686), which is comparable to the results of our analysis of VOCs partitioning into the as-received *S-om* (Table 3.3; r^2 = 0.995, A = 1.01, B = –1.269). Hippelein and McLachlan (Hippelein & Mclachlan, 1998) also found a strong correlation between log K_{SA} and log p_{sat} (r^2 = 0.974, A = –0.912, B = 4.304) after excluding PAHs from the regression, which again was comparable to our analysis for VOCs partitioning into the as-received *S-om* (Table 3.3; r^2 = 0.943, A = -0.99, B = 3.59). Therefore, soil with an organic matter as low as 1 wt% may be considered as an *S-om* type soil for SVOCs partitioning. However, it is unclear if a similar organic matter content of 1 wt% is also applicable to VOC partitioning since our *S-om* contained 10.7% organic matter by soil mass. Also, the VOCs may partition differently from SVOCs (*e.g.*, PAHs), thus models explicitly developed for VOC-soil partitioning are desirable.

Based on these results, we have three recommendations: (1) p_{sat} or K_{oa} is not applicable to predict K_{SA} for mineral-type soil that is water-saturated and contains minimal organic matter; (2) for water-saturated soil that contains a relatively high amount of organic matter, p_{sat} and K_{oa} are good parameters (K_{oa} is slightly better than p_{sat}) in modelling studies to predict K_{SA} if the soil contains a low mass fraction of water; (3) for soil with a high water content (> 50% of soil mass using K_{oa} and > 35% of soil mass using p_{sat} in this study), highly polar VOCs need to be separated from other types of VOCs in modelling studies to predict K_{SA}. Therefore, for most soils in the environment that contain a high amount of organic matter and are saturated with water, p_{sat} or K_{oa} can be used to predict K_{SA}.

3.11 Environmental implication

Only a limited number of protocols exist for estimating VOC emission from the soil into the air. A predictive equation, as in this case, can be used to determine the average long-term emissions of VOCs released into the air. Because it is relatively easier to measure the concentration of contaminants in water and soil, our results can be used to estimate the emission of a broad class of non-polar and slightly polar VOCs into the atmosphere if air quality measurement is difficult to obtain or unavailable, especially after a natural disaster. Here, we described an application scenario of our results. The estimations described here illustrate a worst-case scenario with several assumptions and simplifications. The most important, but not limited to these, were: (1) the contaminants were ultimately deposited into the soil at a high concentration, (2) emission was homogenous over time, (3) the soil and air temperatures were assumed to be isothermal at 25°C, (4) the contaminants accumulated in the air and were stagnant. Of course, the actual air concentrations of the VOCs would be lower than these estimates since the prevailing meteorological conditions disperse the contaminants. Also, emission rates into the air will decline as the VOCs in the soil are metabolized by microorganisms or undergo biogeochemical processes over time.

In August 2017, Hurricane Harvey dumped massive rain damaging chemical and industrial plants across south-eastern Texas. During and following the storm, 46 chemical plants and refineries released 4.6 million pounds of hazardous chemicals into the air, land and water over a 13-county area (Nicole, 2018). Harris County, a highly-populated area with a large number of industrial or chemical facilities and refineries, had 63% of the accidents (Qin et al., 2020). During the hurricane, 40% of the spilled chemicals was released into the air, 35% into the water and 6% into the soil (Misuri et al., 2019). Harris

County has a total area of 4600 km^2, of which 4410 km^2 consists of land and the rest is covered with water. Dark gumbo clay is the dominant soil type covering half of the non-impervious surface in Harris county (USDA, 2019).

In our calculation, we considered the mass concentration of chemicals deposited in the soil and those in the water, which we assumed would eventually sorb in the soil. We only considered one refinery that released 106,781 kg of chemicals during the hurricane (Qin et al., 2020). The amount released into the soil was 43,780 kg (41%). The refinery usually emits 2.8–7.8 wt% of benzene and 3.1–5.9 wt% of toluene (Wei et al., 2014; Mo et al., 2015). If each VOC (benzene, toluene, ethylbenzene and xylenes (BTEX)) contained only 5 wt% in the spilled chemical, each VOC was present at ~ 2189 kg in soil. We calculated the concentration of VOCs that partitioned into the air using equation 3.3:

$$C_{air} = \frac{m_s}{\left(k_{SA}\frac{d_s}{h_s}+1\right)V_a} \tag{3.3}$$

where C_{air} (μg m^{-3}) is the concentration in air, m_s (μg) is the mass of the VOC in soil, d_s (m) is the depth of the soil, h_s (m) is the depth of the surface layer and V_a (m^3) is the volume of air. We used a volume of 4.42×10^{10} m^3. The depth of the surface layer, the region of the atmosphere in which heat and momentum fluxes are negligible (< 10%), is ~ 100 m during a typical daytime unstable condition and ~ 10 m during a typical nighttime situation (Zannetti, 2013). In the calculations, we used h_s at 10 m, which depicted a worst-case scenario. For the surface area, we used the percent of non-impervious surface in Harris County, which was estimated to be 50% (2205 km^2) (Han & Burian, 2009). We used a soil depth of 0.2 m as it contained a high concentration of organic matter (Kramer & Gleixner, 2008). We calculated the concentrations BTEX using the experimental K_{SA} derived from

our study, which was 40 for benzene and 56.2 for toluene under *S-om* at 67% WHC. For ethylbenzene, xylenes and other VOCs that may be present during the chemical spill, we used the K_{oa} to determine the K_{SA} using $\log K_{SA} = 0.524 \times \log K_{oa} + 0.182$ in Table 3.3**,** which we obtained from our correlation analysis. The conditions used in the calculation and the air concentration for BTEX are depicted in Figure 3.8D.

At the nighttime condition, the emitted VOC concentrations into the air were 8.6 ppb for benzene, 6.2 ppb for toluene, 3.3 ppb for ethylbenzene and ~ 3.0 ppb for isomers of xylenes. These values were well below the National Institute of Occupational Safety and Health Recommended Exposure Limits (NIOSH REL). During the daytime, the air concentrations for similar VOCs were 10× less because of the higher depth of the surface layer. The masses of the VOCs remaining in the soil were three orders of magnitude lower than the initial masses after 30 days (Figure 3.8A), and the concentrations of BTEX emitted into the air were less than 10 ppb (Figure 3.8B). The concentration of VOCs emitted into the air decreased with soil depth. Note, we assumed that the VOCs accumulated into the surface layer for 24 h. At a soil depth of zero, which represents the maximum emission rate, the air concentrations of BTEX at a surface layer of 10 m were ~ 31 ppb (Figure 3.8C). This value is also the maximum concentration if we assumed that all the emitted BTEX accumulated in the air for ~30 days in the absence of a removal mechanism. Note that we estimated only from one-point source; therefore, a higher air concentration owing to a localized emission of the VOCs is expected. Air sampling in Houston after Hurricane Harvey was ~ 99 ppb, which suggested that other sources contributed to that spike or from localized emissions (Tabuchi, 2017). A summary of the calculated air concentrations for a larger subset of VOCs is presented in Table 4.4.

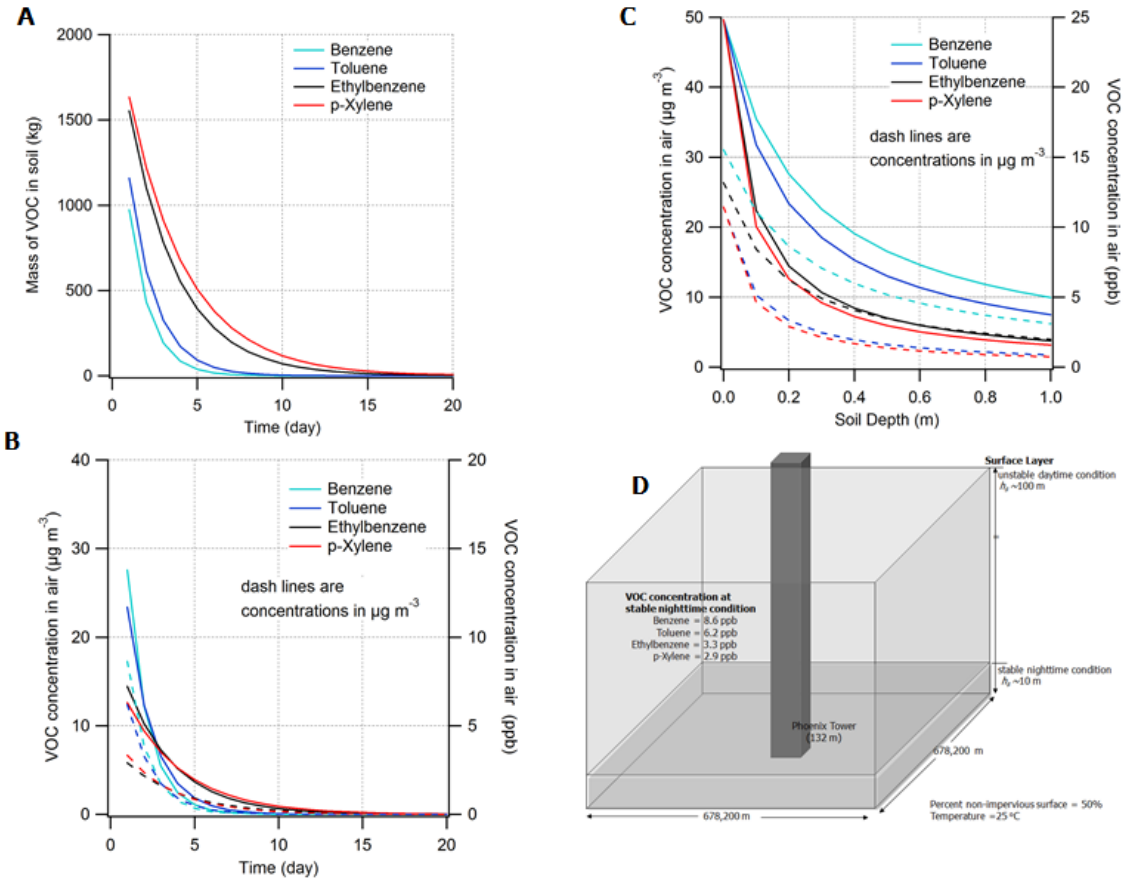

Figure 3.8 (A) Mass of the VOCs remaining in soil. (B) VOC concentration that accumulated in the air under nighttime stable condition. (C) Variation of the emitted VOC concentrations in air as a function of soil depth. (D) Conditions used in the calculations. For height comparison, Phoenix Tower in Houston has a height of 132 m.

Table 3.4 Estimated concentration of typical VOCs released from the soil into the air as estimated from the experimental K_{SA} or from the K_{SA} using the K_{oa} as a parameter.

	log K_{oa} (log L/kg)	K_{SA} (at 67% soil water content, 25°C)	Air concentration (Nighttime)		NIOSH REL (ppm)
			µg m^{-3}	ppb	
Aromatics					
Benzene	2.77	40[A]	27.6	8.63	0.1
Toluene	3.29	56.2[A]	23.4	6.20	100
Ethyl benzene	3.63	122[B]	14.4	3.32	100
o-Xylene	3.91	170[B]	11.3	2.60	100
p-Xylene	3.65	147[B]	12.6	2.90	100
m-Xylene	3.72	145[B]	12.7	2.92	100
1,2-DCB	4.49	125[A]	14.2	2.36	50
Chlorinated Hydrocarbon					
TCE	2.79	48[A]	25.3	4.71	2
Chloroethane	2.10	19.2[B]	35.8	13.4	-
Chloroform	2.79	43.8[B]	26.5	5.42	2
Vinyl chloride	0.92	4.60[B]	45.5	17.8	-

[A] Values were obtained under *S-om* at 67% from experimental results.
[B] Values were calculated from the linear regression analysis of *S-om, at 67% of WHC* without 1-butanol using $log\ K_{SA} = 0.524 \times log[K_{oa}] + 0.182$ in **Table 3.3**.
Values at daytime condition are 10× less.

CHAPTER 4

PARTITIONING OF 1,2-DICHLOROBENZENE ONTO ORGANIC AND INORGANIC AEROSOLS[2]

4.1 Experimental setup

We fabricated the cylindrical chamber (diameter = 0.3 m, height = 0.1 m, and volume ~ 7 L) from aluminum. The chamber was enclosed in a temperature-controlled cabinet (CEO932, Lunaire Environmental, New Columbia, PA) to maintain a constant temperature. The chamber has a removable lid that can be attached to the base with screws. An *o*-ring rested in the groove on the top rim of the chamber base to ensure a tight seal between the lid and base.

Figure 4.1 illustrates the schematic of the experimental setup. Three flows, namely, the diluted 1,2-dichlorobenzene (1,2-DCB, 99% purity from Sigma-Aldrich) flow, aerosol flow, and humid air flow were supplied to the chamber. All sample lines were made of polytetrafluoroethylene (PTFE) tubing. However, we used carbon-coated tubing for the aerosol flow to reduce particle loss during transport from the diffusion dryer to the chamber. In a parallel experiment, we monitored the flow rate and the pressure drop across the filter using a pressure sensor (PC series, Alicat Scientific). The pressure drop changed

[2] Reprinted here with permission of publisher: Jeonghyeon Ahn *et al*., Partitioning of 1,2-dichlorobenzene onto organic and inorganic aerosols. Environmental Chemistry 18(2) (2021) 61-70.

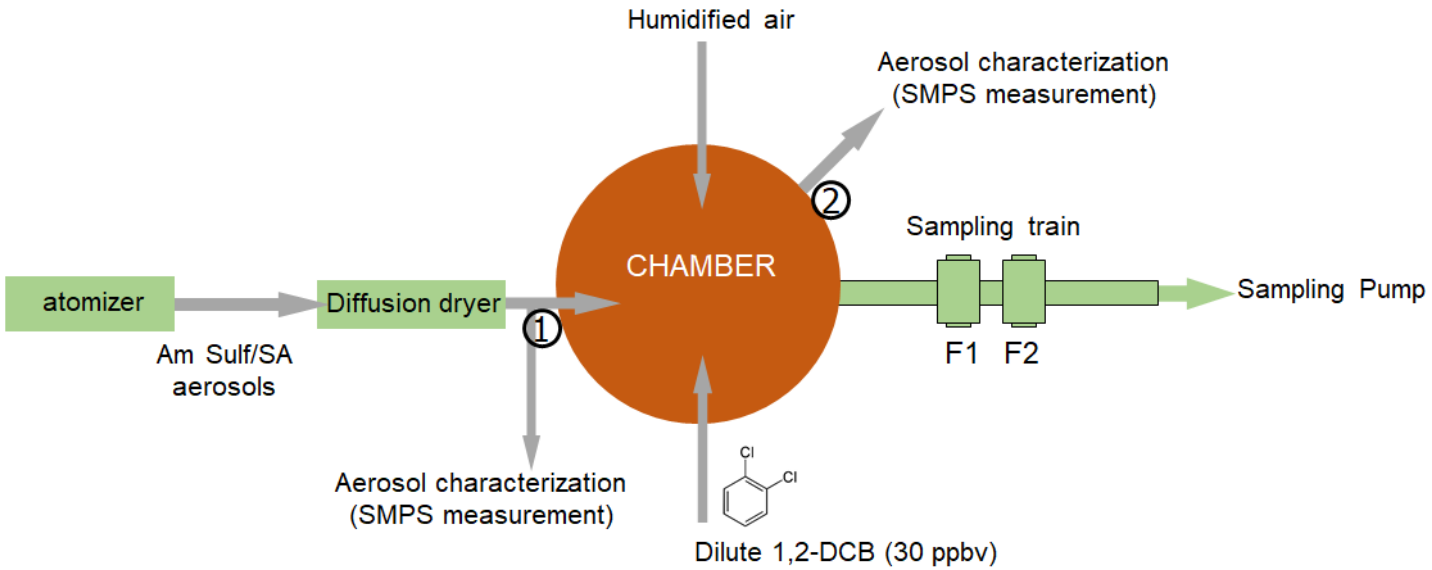

Figure 4.1 Schematic of the experimental setup.

only by < 5% during the entire sampling duration as well as the flow rate.

We generated the dilute 1,2-DCB flow stream by placing a 2-mL amber vial containing 1 mL of pure 1,2-DCB liquid in the chamber of the Precision Standard Gas Generator (491M-B, KIN-TEC Laboratories Inc, La Marque, TX). Pure 1,2-DCB vapor effused through a 400-µm deactivated glass capillary, which we then diluted with purified compressed air. We supplied compressed air at a pressure of 240 kPa as the air source, which we passed through a hydrocarbon trap (BHT-4, Agilent) to remove organics and then through a high-efficiency particulate air (HEPA) filter (83690H, Pall Life Sciences) to remove particles. Hereafter, air refers to clean- and particle-free air. By adjusting the flow rate of the compressed air stream passing through the gas generator chamber, we obtained a dilute 1,2-DCB mixing ratio of 30 ppbv in air, determined experimentally. We used this mixing ratio in all the tests in this study. We diluted the 40 mL min^{-1} 1,2-DCB flow stream that entered the chamber with 260 mL min^{-1} of air. RH level in the chamber was 50%. We sampled 300 mL min^{-1} of the mixed airflow exiting the chamber for 1.5 h using a thermal desorption tube that contained Tenax TA as the sorbent. We measured 1,2-DCB using a thermal desorption-gas chromatograph/mass spectrometer (TD-GC/MS, PerkinElmer, Waltham, MA) in triplicates.

We generated the organic and inorganic aerosols by atomizing 200 ppm succinic acid (SA, ≥ 99%, Alfa Aesar) and 100 ppm ammonium sulfate (Am Sulf, ≥ 99%, Sigma) dissolved in water, respectively, to obtain a comparable dry aerosol mass of ~ 500 µg m^{-3}. We used SA because it is one of the dicarboxylic acids often identified in atmospheric aerosols and is representative of the water-soluble component in aerosols (Svenningsson et al., 2006; Jing et al., 2018). Am Sulf is a major inorganic component in aerosols (Song

et al., 2012). We operated the atomizer (TSI 3076, TSI Incorporated, Shoreview, MN) using compressed air at 2.5 L min^{-1} and 207 kPa. The MFC was interfaced with a LabVIEW program that controlled the flow rate of the air. We dried the aerosol exiting the atomizer by passing it through a diffusion dryer (Model 3062, TSI Inc., Shoreview, MN) containing silica beads as the desiccant before routing the flow into the chamber. We installed a tee connector with needle valves to control the flow rate of the aerosol entering the chamber while we vented the excess into the atmosphere.

We generated the humid air flow by mixing the dry air (RH of ~ 4%) with the wet air. Wet air was generated by passing the dry air through two 20-gallon saturators filled with water that were connected in series. We obtained the desired RH of humid air by adjusting the flow rates of the dry air and wet air using needle valves. We measured the RH using a temperature and humidity probe (USBQTENKI-T-RH-CC2, Dracal Technologies, Inc.). Note that the RH meter is not rated above 95%.

To investigate the effect of temperature on K_p, we varied the chamber temperature from 5 to 35°C. We set the 1,2-DCB, humid air, and aerosol flow streams at 40, 60, and 200 mL min^{-1}, respectively, to achieve a total flow rate of 300 mL min^{-1} entering the chamber. We maintained the RH in the chamber at 35%. To investigate the effect of RH on K_p, we kept the chamber temperature at 25°C for SA aerosols and 15°C for Am Sulf aerosols since the amount of DCB that partitioned into Am Sulf aerosols at 25°C was below the detection limit. We used 100 ppm SA solution, and 50 ppm Am Sulf solution at the lowest RH to obtain ~ 500 μg m^{-3} of dry aerosol mass to be comparable with the dry aerosol masses under other RH levels. We increased its concentration in the chamber by supplying 100 mL min^{-1} of 1,2-DCB flow rate into the chamber under dry air condition to improve

detection of 1,2-DCB in aerosols at high RH. The aerosol flow rate was set at 200 mL min^{-1}, and the humid air flow was set to 0 mL min^{-1}. We varied the RH in the chamber from 5 to 95% by adjusting the flow rate of the dried and humid air flows. We achieved low RH levels by using highly dried silica beads in the diffusion dryer, whereas fully water-saturated beads led to the highest RH. The uncertainty (relative standard deviation) in the RH was < 3%. The TSP readings by the SMPS were verified gravimetrically. We used dried Am Sulf aerosol as the test aerosol. We sampled dried Am Sulf aerosol for 354 min at a flow rate of 345 mL min^{-1} onto a clean filter that was preconditioned at an RH of 30%. At the instrument's parameter settings, the SMPS recorded a TSP of 540 μg m^{-3}, whereas we obtained 560 ± 20 μg m^{-3} from the gravimetric measurement. Since the measured average TSP value differed only by < 4 %, we used the TSP recorded by the SMPS to calculate the K_{ip} without correcting for them. In most This TSP is much higher than most ambient PM concentration in most cities, occurring only during severe episodes of haze in highly polluted cities (Huang et al., 2018).

4.2 Aerosol sampling

We sampled the aerosols that contained 1,2-DCB for 18 h by pulling the air stream from the chamber that was passed through two glass microfiber filters using a vacuum pump (Model 10473, Environmental Monitoring System). The pump was coupled to an MFC at a sampling flow rate of 300 mL min^{-1} (isokinetic). The filter holders were connected in series with one piece of the glass microfiber filter (I.D. ~13 mm, pore size 1.0 μm, Whatman™) embedded in each filter holder. We used the first filter to capture the aerosol particles into which 1,2-DCB partitioned. Preliminary tests suggested that one filter can retain most of the aerosol particles (~ 99.8% capture efficiency). We used the second

filter to correct for the gas-phase 1,2-DCB that sorbed on the filter fibers. We calculated the mass of the 1,2-DCB that partitioned into the aerosol particles by subtracting the mass of 1,2-DCB from the second filter from that on the first filter. Before introducing the aerosols, the two filters were equilibrated with the diluted 1,2-DCB flow at a total flow rate ~ 300 mL min^{-1} for 2 h. In Figure 4.1, F1 and F2 are the glass fiber filter sampling assemblies. The measured mass of 1,2-DCB on F1 was < 2% higher than that on F2. We deemed this difference to be negligible and did not correct for it.

4.3 1,2-DCB quantification

After sampling, the two filters were transferred into separate 10-mL gas-tight borosilicate vials to extract 1,2-DCB using solid-phase microextraction (SPME). Briefly, an SPME fiber holder (Supelco^{TM}) that was assembled with a Carboxen®/ Polydimethylsiloxane (CAR/PDMS) fiber (Supelco^{TM}) was inserted into each vial through the Teflon-lined rubber septum of the cap. The SPME fibers were then suspended in the headspace of each vial. We then desorbed the filter for 30 min at 22 °C and measured the amount of 1,2-DCB that sorbed onto the SPME fibers. However, the measured initial desorption recovery under this condition was only 79 ± 6%. Desorption recovery was determined by spiking a clean filter with 1 ppm each of 1,2-DCB and internal standard (IS, 1,2-DCB-*d*4, AccuStandard), measured in triplicates. We ensure a high recovery of 1,2-DCB from the filter by desorbing it for another 4 h at the same temperature; the recovery increased to 94 ± 5% (determined from three replicates). For all subsequent desorption procedures, we desorbed the 1,2-DCB from the fibers at 22°C for 30 minutes and then for 4 h. We chose this desorption time because beyond 4 h, the further amount of 1,2-DCB desorbed was below the detection limit. We quantified the mass fraction of 1,2-DCB that partitioned onto the SPME fiber.

We injected 1 µL of 1 ppm IS into the GC/MS to quantify the VOC extracted by the SPME fibers. For each filter, we summed the amount of 1,2-DCB. We analyzed the mass of 1,2-DCB extracted by the SPME fiber using a GC (Clarus 680, PerkinElmer, Waltham, MA) and MS (Clarus SQ8T, PerkinElmer, Waltham, MA) (GC/MS) system for quantification, with a capillary GC column (Agilent DB-5ms) of length 30 m, ID 0.25 mm, coated with 0.25-µm 5% (phenyl)-methylpolysiloxane. The GC/MS spectra were acquired using the following parameters: oven temperature 50°C (1 min hold); heating rate 15°C min^{-1}, maximum oven temperature 140°C, ionization mode EI (electron impact, 70 eV), ion source temperature 200°C, transfer line temperature 200°C, helium (99.999%) carrier gas.

We quantified the concentration of 1,2-DCB using a four-point calibration curve generated with 1,2-DCB solutions in 2-mL amber GC vials using methanol (> 99.99%, Fisher Chemical) as the solvent. For each concentration, we added 1 µL 1 ppm IS. We injected 1 µL of each solution into the GC/MS to measure the peak areas of the 1,2-DCB and the IS. We plotted the response ratio *v.* the mass of 1,2-DCB to obtain the calibration curve. The response ratio is the peak area of 1,2-DCB (A_{DCB}) to that of 1,2-DCB-*d*4 (A_{IS}).

We identified based on its retention time (4.63 ± 0.1 min) and its abundant ions ($C_6H_4{}^{35}Cl^+$ and $C_6H_4{}^{35}Cl{}^{35}Cl^+$) in the mass spectrum. For the sensitive trace level detection of 1,2-DCB, we acquired the mass spectra in selected ion monitoring (SIM) mode to monitor the specific mass-to-charge (*m/z*) ratios of 111 and 146.

4.4 Aerosol characterization

We characterized aerosol properties, including the particle median diameter, particle number concentration, and TSP, using an SMPS (electrostatic classifier model 3082 with a condensation particle counter model 3775, TSI Inc., Shoreview, MN). The SMPS was operated at 300 mL min^{-1} with a sheath flow of 3 L min^{-1}. The residence time of the aerosol in the chamber was ~ 24 min. At each RH level, we monitored the properties of the aerosols that exited the chamber for at least 18 h, at 20 min intervals. The dry aerosol mass was used to calculate K_p using Equation 1.1. The dry mass was used because at very high RH, the amount of water that sorbed to the aerosols resulted in an increased in TSP. We obtained the dry aerosol mass by routing the aerosol flow exiting the chamber to an additional diffusion dryer using dry air (RH < 10%.) The water content of aerosols at each RH level was then calculated after determining the masses of the wet and dry aerosols. We measured the aerosol properties in location 1 or location 2 in Figure 4.1.

4.5 Effect of RH on K_p

The K_p of 1,2-DCB partitioning into Am Sulf and SA aerosols was dependent on RH (Figure 4.2). Although temperature conditions were different (Am Sulf aerosols at 15°C *versus* SA aerosols at 25°C), the K_p values for both aerosols decreased as RH increased. For Am Sulf aerosols, K_p values decreased sharply at ~ 45% but did not significantly increase even at an RH of 95%, whereas for SA aerosols, K_p slowly declined as RH increased (Figure 4.2). Although the fit used only three data points, sorption of 1,2-DCB on Am Sulf aerosol followed the expected classic exponential relationship between K_p and RH (Figure 4.2a). However, the sorption of 1,2-DCB on SA aerosol departed from

this relationship (Figure 4.2b). We calculated that 1.39, 1.19, 0.81, and 0.40 pg of 1,2-DCB partitioned to 1 μg of SA aerosol (dry mass) at RH levels of 5, 45, 70, and 95%, respectively (Table 4.1). The mass fraction of 1,2-DCB that partitioned onto both aerosols was < 0.001% as nearly all of the 1,2-DCB was expected to be in the gas phase (Matsumoto et al., 2010).

4.6 Effect of temperature on K_p

The K_p values of the 1,2-DCB partitioning into the SA aerosol particle at 15, 25, and 35°C were (13.1 ± 3.98) × 10^{-8}, (3.94 ± 0.68) × 10^{-8}, and (0.89 ± 0.70) × 10^{-8} m^3 μg^{-1}, respectively. The dry aerosol mass of 1,2-DCB corresponded to 3.27, 1.03, and 0.23 pg (Table 4.1). RH was fixed at 35 ± 3% in this experiment. These values were greater than the 0.1 pg that we calculated using the data from the literature that sampled urban aerosols (Odabasi et al., 2005). Our K_p values were in a similar range to the data reported for non-polar organics (mainly SVOCs) partitioning into urban, suburban, coastal, and rural aerosol particles owing to the comparable vapor pressure (Arp et al., 2008a).

At 15 and 25°C, K_p of 1,2-DCB partitioning on Am Sulf aerosol particle was almost two orders of magnitude smaller than on SA aerosol particle (Figure 4.3). At 35°C, the K_p could not be determined because the amount of 1,2-DCB was below detection limit. For each aerosol type, the sorption of 1,2-DCB followed the classic van't Hoff relationship (ln K_p linearly related to $1/T$) (Figure 4.3**)** (Goss, 1993a). The slopes of the regression lines for SA and Am Sulf aerosols were 11,938 and 15,305, respectively. We calculated the heat of desorption (ΔH_{des}) using equation (4.1):

$$ln\, K_{ip} = \frac{\Delta H_{des}}{RT} + constant. \quad (4.1)$$

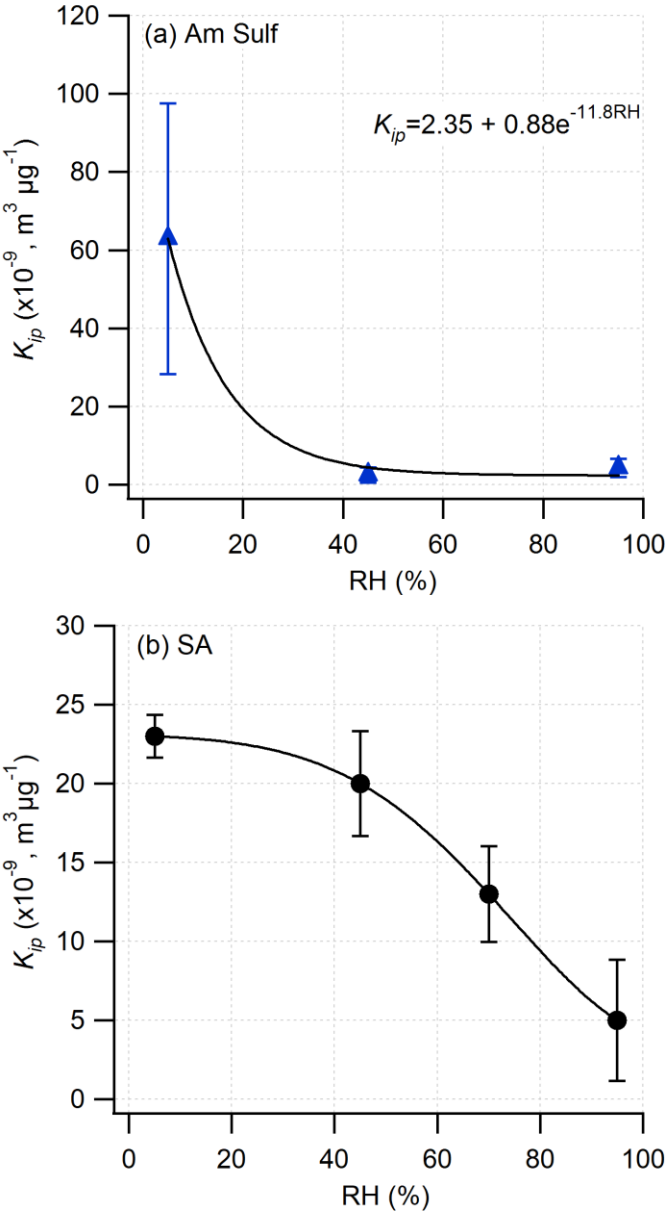

Figure 4.2 The K_p of 1,2-DCB partitioning into (a) Am Sulf aerosol at 15°C and (b) SA aerosol at 25°C at different RHs. Solid line for (a) Am Sulf is a fitted function, and for (b) SA, the line is drawn only as a guide.

Table 4.1 The K_p value and dry aerosol mass of 1,2-DCB partitioning into the aerosols.

Aerosol type	Temperature (°C)	RH (%)	K_p ($\times 10^{-8}$, m^3/μg Aerosol)	C_{ip}/TSP (pg VOC/μg Aerosol)
Succinic acid 200 ppm	15	35	13.1±3.98	3.27
	25		3.94±0.68	1.03
	35		0.89±0.70	0.23
	25	5	2.27±0.13	1.39
		45	1.96±0.33	1.19
		70	1.34±0.30	0.81
		95	0.48±0.38	0.4
Ammonium sulfate 100 ppm	5	35	2.59±0.74	0.63
	15		0.27±0.26	0.07
	25		0.07±0.008	0.02
	35		BDL	BDL
	15	5	6.30±3.47	3.82
		45	0.25±0.02	0.15
		95	0.43±0.23	0.26

BDL: Below the detection limit

where R is the ideal gas constant and T is the absolute temperature. The estimated ΔH_{des} was 109.5 ± 5 kJ mol^{-1} for SA aerosol and 127.0 ± 6 kJ mol^{-1} for Am Sulf aerosol. Errors ($\sigma_{\Delta H_{des}}$) were derived as the propagated uncertainties, which were calculated as $\sigma_{\Delta H_{des}} = \pm \sigma_{slope} R \times 10^{-3}$. Uncertainty in the slope (σ_{slope}) was derived from fitting the data in *Igor Pro*™, and was defined as one standard deviation from the mean. These values were more endothermic than the measured ΔH_{des} for more than 50 S/VOCs and VOCs partitioning into atmospheric aerosol particles, in which most ΔH_{des} ranged from 40 to 70 kJ mol^{-1} (Arp et al., 2008b).

To understand the reason leading to the K_p change of SA aerosol at each RH level, we continuously monitored the evolution of aerosol exiting the chamber for more than 18 h. The particle median diameter for SA aerosol at an RH of 5% was much larger than at RH levels of 45% and 70%. The particle number concentration was lower under dry conditions (5% RH), suggesting that the SA particles aggregated (Figure 4.4a-c**)**. Increasing RH from 45% to 95% led to a larger particle median diameter and higher TSP for the SA aerosol. We measured a water content of 24, 37 and 71% by aerosol mass at RH level of 45, 70 and 95%, respectively, for the SA aerosol.

Similarly, we monitored the properties of the Am Sulf aerosol at each RH level (Figure 4.4d-f). Unlike SA aerosol, the particle median diameter for Am Sulf aerosol at an RH of 10% was comparable with those at an RH of 45%. We measured a water content of 42% at an RH of 45% and the particle median diameter was 64 nm. The particle number concentration at RH. 10% was lower than that at RH 45% and 95%; thus, the dry aerosol aggregated. The particle median diameter at an RH of 95% was larger than that at an RH

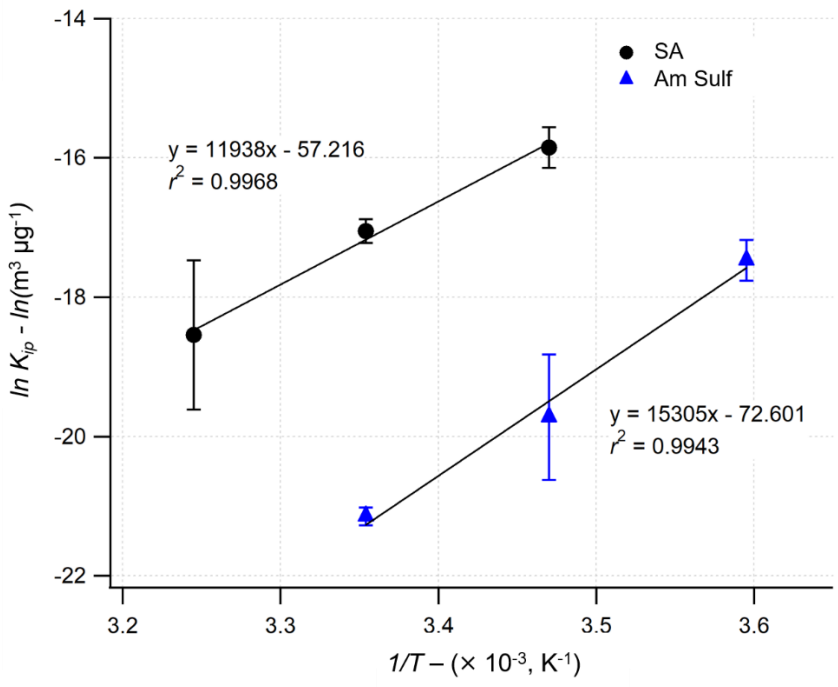

Figure 4.3 Correlation of 1/T with *ln* K_p for 1,2-DCB partitioning into SA and Am Sulf aerosol particles at 35% RH. Error bars are one standard deviation from the mean, from triplicate measurements.

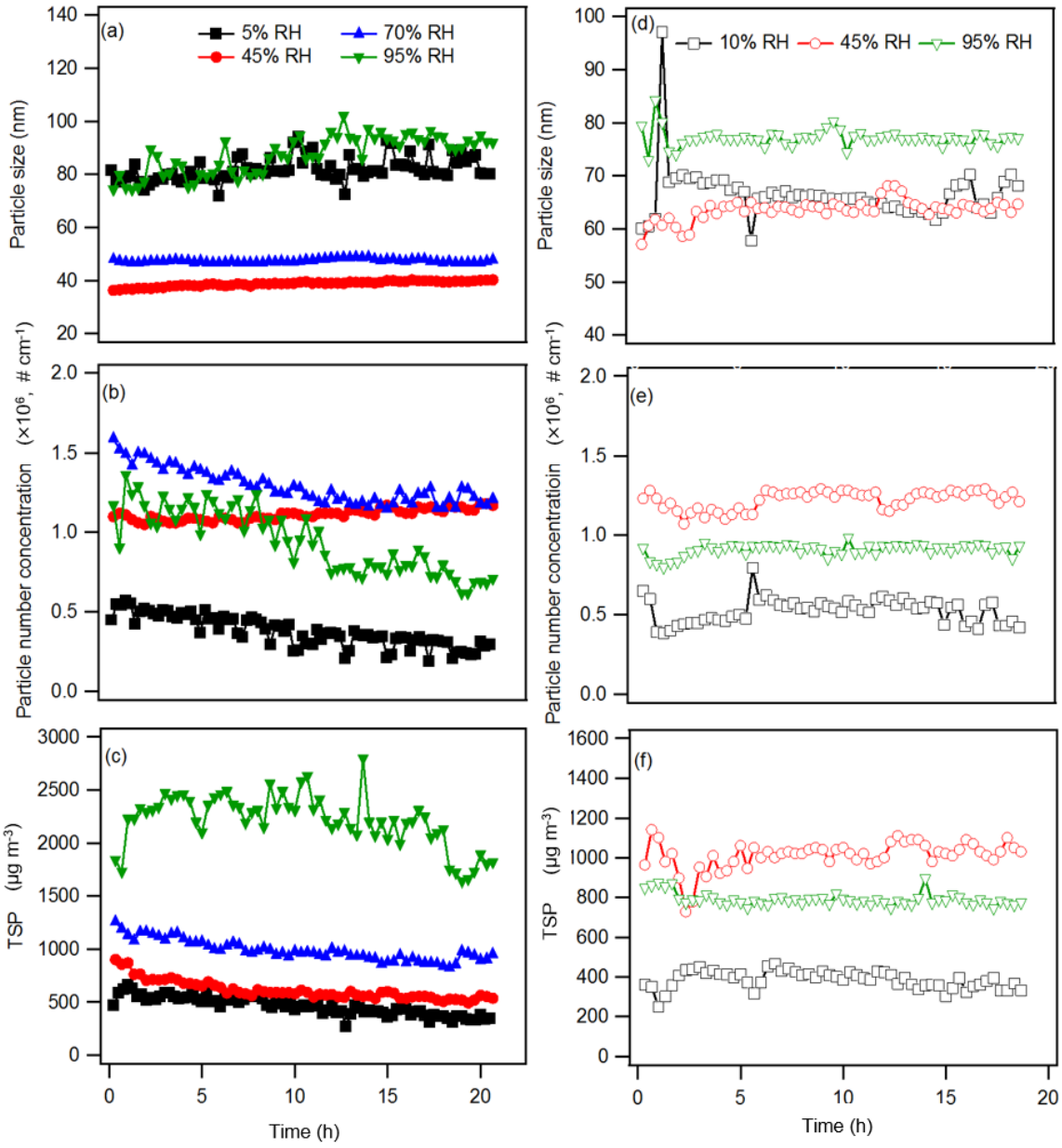

Figure 4.4 Evolution of the properties of the SA aerosols (a-c); and Am Sulf aerosols (d-f) for 24 hours at different RH levels.

of 45%, suggesting that more water sorbed into the Am Sulf particles because it is highly hygroscopic. However, both the particle number concentration and TSP at RH 95% were smaller than those obtained at RH 45%. Also, the measured water content at RH of 95% was only 52%, and the particle median diameter was 77 nm. Thus, it is likely that large particles that contained a high mass of water may have settled in the chamber owing to gravity. At an RH of 95%, we observed that liquid water formed on the chamber walls at the end of the measurement, which explained the observed lower TSP and particle number concentration.

4.7 Partitioning of 1,2-DCB in aerosol particle

Assessing the contribution of VOCs in aerosol particle has been limited by the experimental challenge in detecting their extremely low mass fraction in aerosol particle compared to that in the gas phase. Here, we present our study on the measurement of the partitioning coefficient for 1,2-DCB under different RHs and temperatures. Our K_p values (Figure 4.2 and Table 4.1) were in a similar range to the data reported for non-polar organics (mainly SVOCs) partitioning into urban, suburban, coastal, and rural aerosol particles due to the comparable vapor pressure (Arp et al., 2008a). Because of the lower vapor pressure of SVOCs, a higher mass of SVOCs is expected to partition into aerosol particles compared with VOCs. The K_p for 1,2-DCB in our study being comparable with those reported in the literature for some SVOCs suggests the WSOM fraction in aerosol particles plays an important role in the overall partitioning of VOCs (Arp et al., 2008a). Sorption of 1,2-DCB into both types of aerosol particle was favorable, as deemed from their higher endothermic ΔH_{des} compared with some S/VOCs that partitioned into atmospheric aerosol particles (Arp et al., 2008b). The ΔH_{des} values we obtained were more

endothermic than those measured for more than 50 S/VOCs partitioning into atmospheric aerosol particles, in which the majority of the ΔH_{des} ranged from 40 to 70 kJ mol^{-1} (Arp et al., 2008b).

In the earlier work by Pankow, gas-phase organics partition into aerosol particle *via* two mechanisms: adsorptive and absorptive (Pankow, 1994). Absorptive gas-particle partitioning occurs when organics diffuse into the bulk of the aerosols *via* dissolution. Adsorptive gas-particle partitioning occurs when organics interact with the active surface sites on the aerosol particle. However, in many cases, it is unclear which is the dominant partitioning mechanism (Goss & Schwarzenbach, 1998). One mechanism primarily drives the partitioning depending on the RH level and the composition of the aerosol. For Am Sulf aerosol, at low RH levels (~< 35%), partitioning of 1,2-DCB was potentially driven by adsorption, whereas at RH ~> 35%, the extremely low amount of sorbed 1,2-DCB may be driven by absorption. 1,2-DCB partitioning on SA aerosol particle was driven by adsorption at all RH levels, perhaps excepting at saturated RH level. The dependence of K_p on RH for 1,2-DCB partitioning onto SA aerosol particle was much lower than onto Am Sulf aerosol particle, as depicted in Figure 4.2a, b.

The sorption of 1,2-DCB on Am Sulf aerosol particle followed the expected exponential relationship between K_p and RH at RH > 30% ($\ln K_p = - C \times RH + E$, where C and E are VOC- and aerosol-specific constants) (Goss, 1992; Goss & Eisenreich, 1997). Our results are consistent with the findings in the literature that RH ranges of 50–90% have a negligible effect on the partitioning of non-polar VOCs (*e.g.*, 1,2-DCB) because 1,2-DCB preferentially partitions into the hydrophobic phase of aerosol particle (Cotham & Bidleman, 1992a; Arp et al., 2008a; Jathar et al., 2016) and is poorly water-soluble. For a

simplified aerosol consisting of two components, such as our study, the lower K_p may be due to the absence of a hydrophobic phase. Sorption of 1,2-DCB on Am Sulf aerosol particle is primarily due to the aerosol's higher number of active surface sites at low RH (Goss & Schwarzenbach, 1999). At higher RHs (≥ 35%), 1,2-DCB partitioned onto Am Sulf aerosol particle primarily *via* dissolution into the aqueous phase, although at extremely low mass fraction because of the poor solubility of 1,2-DCB (1.47 wt% at 25 ^{o}C). Since Am Sulf is highly hygroscopic, at higher RH levels (45% and 95%), water solvated and ionized Am Sulf, which prevented 1,2-DCB from interacting directly with the active surface sites of the aerosol. We ascribed the larger K_p at an RH of 10% compared to those at higher RH levels to the adsorption of VOCs into the aerosol particle surface *via* Van der Waals interactions. For an aerosol consisting of a hydrophobic phase, we expect that 1,2-DCB would partition more into the aerosol particle, leading to a higher K_p. Note that although the deliquescence RH of Am Sulf is ~ 82% (Brooks et al., 2002), Am Sulf is highly hygroscopic and even a low amount of water (RH ~ 40%) is enough to cover these active sites (Goss & Schwarzenbach, 1999). Thus, the K_p at an RH of ~ 40% was similar to that at saturated RH level.

However, the sorption of 1,2-DCB on SA aerosol particle did not fit the exponential dependence of K_p with RH (Figure 4.2b). Comparing the trendline of each aerosol type, the decrease in K_p for SA was more gradual than that for Am Sulf. The partitioning of 1,2-DCB on SA aerosol particle primarily occurred *via* adsorption. Under this condition, 1,2-DCB adsorbed onto the aerosol particle surface *via* Van der Waals interactions (Goss, 1993b; Schwarzenbach et al., 2016). At higher RH levels (> 45%), the carboxylic acid functional group in SA formed a strong complex with water. In an earlier study by Pankow,

gas-phase organics (primarily SVOCs) were described as absorbing onto aerosol particle by dissolving into the bulk of the organic phase. However, such a scenario may only apply at higher RH levels since the deliquescence RH of submicron SA particles (particle median diameter ~ 200 nm) occurs only at nearly saturated humidity (99%) (Bilde & Svenningsson, 2004). Moreover, the deliquescence of small particles (such as in our study, particle median diameter < 100 nm) consisting of slightly soluble compounds such as SA (solubility at 25°C ~ 8.3 wt%) (Brooks et al., 2002; Wex et al., 2007) requires overcoming an activation barrier (Bilde & Svenningsson, 2004). Additionally, dry SA particles are not highly hygroscopic compared with Am Sulf particles.

These physicochemical behaviors of SA may explain: (1) their higher K_p relative to Am Sulf; (2) the gradual decline in K_p with increasing RH levels; and (3) the small difference in the K_p at low (< 50%) and high RH levels (> 95%) compared to sorption on Am Sulf aerosol particle. It appears that for SA and at RH levels lower than saturation, the dominant mechanism is the adsorption of 1,2-DCB. We attribute this observation to two possible explanations. First, the slow decline in K_p suggests that 1,2-DCB competes well with water. Otherwise, we would have observed a similar behavior to that of Am Sulf, in which the K_p decreased exponentially with RH and then remained almost constant. Indeed, a modeling study demonstrates that the interaction of chlorine with a hydrogen bond donor (-OH) is comparable to the canonical hydrogen bond (*i.e.*, -OH in SA with water) (Lin & MacKerell, 2017). However, this comparable strength of interaction was tempered by an orientation requirement. The chlorine atom should be oriented perpendicularly to interact successfully with the hydroxyl group in SA (Lin & MacKerell, 2017). Second, at a higher RH level, an increasing number of water molecules will compete with the hydroxyl group

in SA in interacting with the chlorine atom, dominating the low concentration of gas-phase 1,2-DCB (Lin & MacKerell, 2017). Theoretical calculation of SA's interaction with water shows that proton transfer increases with increasing hydration cluster (Taheri et al., 2011). As a result of this competitive interaction, only a few molecules of 1,2-DCB can interact with the available sorption sites on SA aerosol particle, thus, K_p decreased.

We used a high TSP to shorten the sampling time, obtain a sufficient mass of 1,2-DCB and minimize their breakthrough from the filter fibers. Such a TSP level occurs only during severe haze episodes in some cities (Huang et al. 2018). The dependence of K_p with temperature (equation 5.1) can be expressed as $\ln K_p = A / T + B$, where T is temperature, and A and B are constants (Pankow 1987). A depends on ΔH_{des}, whereas B depends on the properties of the compound and the specific surface area of the aerosol (Pankow 1987). At constant temperature, for the same type of aerosol and under the same ambient conditions (*e.g.*, RH), A and B would be similar (Pankow & Bidleman 1991). Hence, a high TSP level would not affect the measured K_p. If equaion (4.1) is used to derive ΔH_{des}, as long as the fraction of non-exchangeable organics between the two phases is low, then $\ln C_{ip} / (C_{ig} \cdot \text{TSP})$ is closer to the true thermodynamic partition coefficient (K_p) (Pankow & Bidleman 1991). In the case of a highly volatile VOC such as 1,2-DCB, its fraction in the particle phase was < 0.001%, and the non-exchangeable fraction is even lower. The equilibration timescale for VOCs is rapid, seconds to minutes (Shiraiwa & Seinfeld 2012). 1,2-DCB has a sufficient time to reach equilibrium between the gas and aerosol phases in the chamber (residence time ~ 24 min). Overall, a high TSP level should not affect the kinetic and thermodynamic parameters during the partitioning of 1,2-DCB onto SA and Am Sulf aerosol particles. The mass fraction of an organic compound that partitioned onto the

aerosol particle also depends on the particle size. For instance, for the polychlorinated biphenyls SVOCs, most of the mass partitions into the smaller size-fraction (< 1 μm) (Zhu et al. 2017). This observation is consistent with the explanation that for an equivalent aerosol mass, the number concentration for small particles is higher, therefore, there is a larger total surface area compared with larger particles.

4.8 Comparison of experimental K_p with VOC partitioning models

Partitioning models for SVOCs, which are derived empirically, can be used to estimate K_p. Although modeling studies have been carried out for VOCs using models mainly developed for SVOCs partitioning into the WIOM fraction of aerosol particles since the 1980s (Abraham, Andonian-Haftvan, et al., 1994; Abraham, Chadha, et al., 1994; Pankow, 1994), only the saturated vapor pressure (P_i^0) and the octanol-air partition (K_{OA}) models (Finizio et al., 1997) were applicable to VOCs (Table 4.2). Both the P_i^0 and K_{OA} model can be applied to nonpolar VOCs and some polar/nonionizable VOCs (Harner & Bidleman, 1998; Rao & Vejerano, 2018). The P_i^0 model is applicable to organic and inorganic aerosols, and assumes that the chemical potential of the VOC is equal in the gas and aerosol phases (Rao & Vejerano, 2018). Since *n*-octanol is considered as WIOM in the K_{OA} model, it can be expressed as the simplified K_{OA} model in Table 4.2. At 25°C and RH of 5% with SA aerosol, the K_{OA} model predicted the K_p of 1,2-DCB better than the P_i^0 model. The K_p predicted by the P_i^0 model was 2.5× higher than the experimental value. Indeed, the K_{OA} model predicts the K_p better than the P_i^0 model for different classes of nonpolar organics that exhibit a similar ratio of activity coefficients between the inorganic and organic matter fractions (Pankow, 1998). Our calculation, which estimated the K_p with VOC partitioning models, agrees well with our experimental value (Table 4.1 and 4.2)

compared to the predicted K_p of 31 for an isomer of 1,2-DCB (*e.g.*, 1,4-dichlorobenzene) in an earlier calculation (Odabasi et al., 2005). However, the K_{OA} model is limited to organic aerosols (Rao & Vejerano, 2018) because *n*-octanol is used as a surrogate for organic matter fractions. Note that while the equation by Pankow contains absorptive and adsorptive contribution, we calculated only the absorptive contribution for Am Sulf. We assumed that the active surface sites are covered with water at an RH of 35% as deemed from the low K_p in Figure 4.3a and Table 4.1. At 5°C and RH of 35%, the experimental K_p of 1,2-DCB partitioning on Am Sulf aerosol was comparable to that predicted by the P_i^0 model. However, when applied at a low RH (~ 5%), assuming a low number of active sites (N_s ~ 100 cm^{-2}), the predicted K_p (~ 22.9) deviated substantially from the experimental K_p. Although the dominant mechanism was the adsorption of 1,2-DCB onto SA aerosol particles at RH levels lower than saturation, the adsorptive or absorptive component of the K_p predicted by P_i^0 model departed substantially from the experimental value (Table 4.2).

Table 4.2 K_p predicted by VOC partitioning models.

VOC Partitioning Model	Predicted K_p ($\times 10^{-8}$, m^3 μg^{-1} aerosol)	Equation
Succinic acid @25°C, 5% RH		
Experimental value	2.27±0.13	–
Saturated vapor pressure model (P_i^0) (Goss 1994; Goss and Schwarzenbach 1998)	$18.8^{adsorptive}$ $7.85^{absorptive}$	$K_p = \frac{1}{P_i^o}\left[\frac{N_s\, a_{TSP}\, T\, e^{(Q_l - Q_v)RT}}{1600} + \frac{760\, f_{om}\, RT}{10^6\, MW_{om}\, \zeta_{i,\,om}}\right]$
Octanol-air partition model (K_{OA}) (Pankow, 1998)	3.21	$K_p = \frac{K_{OA}\, f_{om}}{\rho_{oct}}\ \frac{\zeta_{i,\,oct}}{\zeta_{i,\,om}}\ \frac{MW_{oct}}{MW_{om}}$
Simplified octanol-air partition model (K_{OA}) (Harner & Bidleman, 1998)	1.69	$\log K_p = \log K_{OA} + \log f_{om} - 11.91$
Ammonium sulfate @5°C, 35% RH		
Saturated vapor pressure model (P_i^0) (Goss 1994; Goss and Schwarzenbach 1998)	$3.52^{absorptive}$	$K_p = \frac{760\, f_{im}\, RT}{10^6\, MW_{im}\, P_i^0\, \zeta_{i,\,im}}$
Experimental value	2.59±0.74	–

octanol/air partition coefficient (K_{OA}); organic proportion of the particle (f_{om}); inorganic proportion of the particle (f_{im}); octanol density (ρ_{oct}); activity coefficient of compound *i* in octanol ($\zeta_{i,\,oct}$); activity coefficient of compound *i* in organic matter ($\zeta_{i,\,om}$); activity coefficient of compound *i* in inorganic matter ($\zeta_{i,\,im}$); molecular weight of octanol (MW_{oct}); molecular weight of organic matter (MW_{om}); molecular weight of inorganic matter (MW_{im}); vapor pressure of compound *i* (P_i^0); gas constant (R); absolute temperature (T); surface concentration of sorption sites (N_s); specific surface area for the TSP (a_{TSP}); the enthalpy of desorption of compound *i* from the adsorbing solid surface (Q_s); enthalpy of vaporization of i as a liquid (Q_v)

*Only the absorptive part was used to calculate the predicted K_p as N_s was assumed zero at an RH of 35%.

CHAPTER 5

TEMPERATURE DEPENDENCE OF THE GAS-PARTICLE PARTITIONING OF SELECTED VOCS[3]

5.1 Materials

n-BuOH (≥ 99%) and TCE (≥ 99%) were purchased from Sigma Aldrich and used without purification. Deuterated analogs of *n*-BuOH (1-butanol-d_{10}, ≥ 99%) and TCE (trichloroethylene-*d*, ≥ 99%) were purchased from AccuStandard. Methanol (> 99.99%, Fisher Chemical) was used as the solvent for preparing the internal standard (IS) and calibration solutions. Succinic acid (≥ 99%, Alfa Aesar) and ammonium sulfate (≥ 99%, Sigma) were used to generate the organic and inorganic aerosols, respectively. Here, Am Sulf and SA refer to the aerosol particles generated from ammonium sulfate and succinic acid, respectively.

5.2 Quantification

The mass of *n*-BuOH and TCE was measured by using a GC/MS system for quantification. The calibration curve was generated by preparing different concentrations of *n*-BuOH and TCE solutions in methanol. For each concentration, 1 µL of 1 ppm of the

[3] Reprinted here with permission of publisher: Jeonghyeon Ahn *et al*., Temperature dependence of the gas-particle partitioning of selected VOCs. Environmental Science Process & Impacts 23 (2021) 947-955

corresponding IS was added. We injected 1 µL of each solution into the GC/MS to measure the peak areas of *n*-BuOH or TCE was plotted to obtain the calibration curve. The response ratio is the peak area of *n*-BuOH or TCE to that of the IS. For each filter, the VOC masses from the two desorption steps were combined.

The VOCs were identified based on their retention time (2.50 ± 0.1 min for *n*-BuOH, and 2.45 ± 0.1 min for TCE) and their abundant ions (C_2HO^+, $H_4H_8^+$ for *n*-BuOH, and $C_2HCl_3^+$ for TCE) in the mass spectrum. We monitored specific mass-to-charge ratios of 41 and 56 for *n*-BuOH and 130 and 132 for TCE. Mass spectra were acquired in selected ion monitoring mode for trace level detection of the VOCs.

5.3 Temperature dependence of the gas-particle partitioning of VOCs

Assessing the particle-phase VOCs has been limited by the experimental challenge in detecting the extremely low mass fraction of VOCs in aerosol particles compared to that in the gas phase. Here, we present our study on the quantitative laboratory measurement of K_p of *n*-BuOH and TCE and compare them to our previous results for 1,2-DCB under a fixed RHs and varying temperatures.

The *ln* K_p values for the three VOCs are summarized in Table 5.1. The *ln* K_p values for TCE partitioning into SA and Am Sulf aerosol particles at 278.15, 285.15, 298.15, and 308.15K measured at a fixed RH of 35 ± 3% ranged from -26.4 to -28.3. These values were four to five orders of magnitude lower than the K_p obtained for 1,2-DCB. Whereas the *ln* K_p values for *n*-BuOH ranged from -13.9 to -17.4 on both aerosols. K_ps for *n*-BuOH

Table 5.1 Experimental data of *ln* K_p for three VOCs partitioning into aerosols at an RH of 35%.

	ln K_p *(SA)*			
VOC	*278.15K*	*288.15 K*	*298.15 K*	*308.15 K*
1,2-DCB[a]	*nm*	-15.9 ± 0.29	-17.0 ± 0.17	-18.5 ± 1.07
TCE	-27.0 ± 0.70	-27.3 ± 0.17	-27.7 ± 1.20	-27.9 ± 0.01
n-BuOH	-13.9 ± 0.03	-14.9 ± 0.09	-15.2 ± 0.02	-17.4 ± 0.17
	ln K_p *(Am Sulf)*			
1,2-DCB[a]	-17.5 ± 0.29	-19.7 ± 0.90	-21.2 ± 0.13	*nm*
TCE	-26.4 ± 0.26	-27.3 ± 0.18	-27.4 ± 0.71	-28.3 ± 0.01
n-BuOH	-14.1 ± 0.16	-14.5 ± 0.17	-15.2 ± 0.17	-17.1 ± 0.12

[a]Data were taken from a companion study for comparison

nm not measured

were comparable to that of 1,2-DCB but were ~ 10× higher at 298.15 and 308.15K. At 288.15 and 298.15K, K_p of 1,2-DCB partitioning on Am Sulf aerosol particles was almost two orders of magnitude smaller than those on SA aerosol particles. In general, the $ln\ K_p$ increased as the temperature increased (K_p decreased with increasing temperature) for all the VOCs partitioning in both aerosol types. In our earlier result for 1,2-DCB, the mass fraction of 1,2-DCB at 308.15K was below the method's detection limit.

To deduce the ΔH_{des} and ΔS_{des}, we plotted $ln\ K_p$ with 1/T, which are depicted in Figure 5.1 for the VOC partitioning into Am Sulf aerosol particles, and in **Figure 5.2** for those partitioning on SA aerosol particles. On both aerosols types, the sorption of TCE followed the classic van't Hoff relationship ($ln\ K_p$ linearly increased with to 1/T, $r^2 = 0.944$) (Figure 5.1 and 5.2) (Goss, 1993a). We also observed similar behavior for 1,2-DCB in our earlier report ($r^2 = 0.988$). We included the plot for 1,2-DCB for comparison. Partitioning of TCE behaved similarly to 1,2-DCB (Ahn, Rao, & Vejerano, 2021a). However, moderately polar compound *n*-BuOH did not fit well with the classic van't Hoff plot. The r^2 for *n*-BuOH was only ~ 0.84. We calculated the enthalpy of desorption (ΔH_{des}, kJ mol^{-1}) using equation (5.1):

$$lnK_p = -\frac{\Delta H_{des}}{RT} + \frac{\Delta S_{des}}{R} \tag{5.1}$$

where R is the ideal gas constant (J K^{-1} mol^{-1}), and T is the absolute temperature (K). The enthalpy of sorption ($\Delta H_{sorption}$) = $-\Delta H_{des}$. Values of the linear fitting parameters are summarized in Table 5.2. The slopes of the regression lines for SA and Am Sulf aerosol

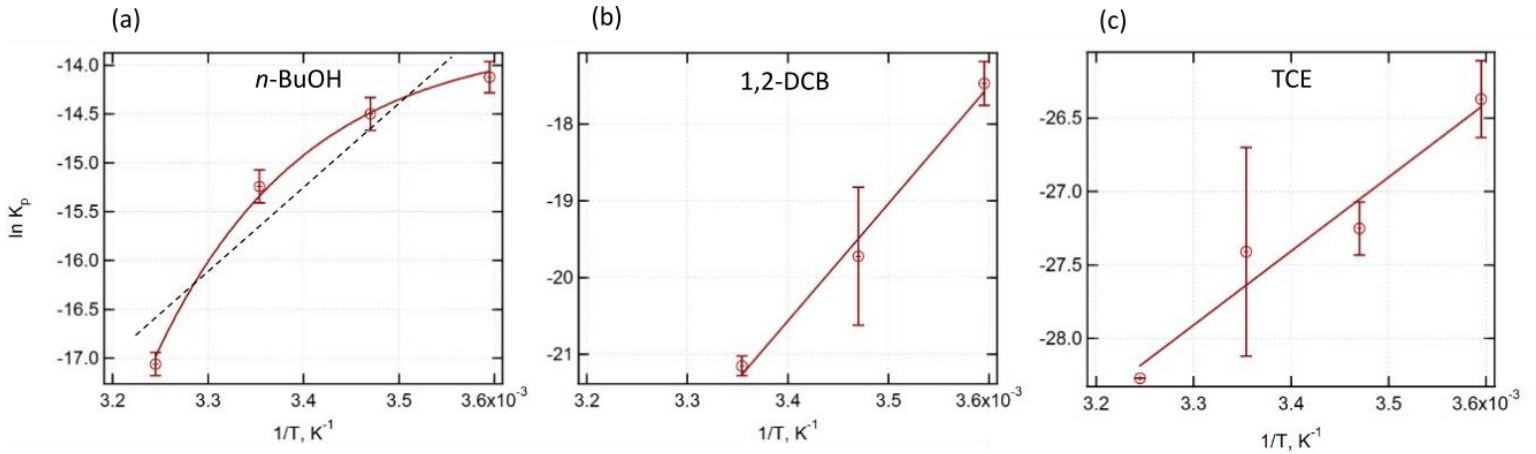

Figure 5.1 van't Hoff plot of (a) *n*-BuOH, (b) 1,2-DCB, and (c) TCE partitioning on SA aerosol. Data for 1,2-DCB was taken from an earlier study. The red curve is the best-fit function for the data. The black dash line is the linear fit to the data for *n*-BuOH.

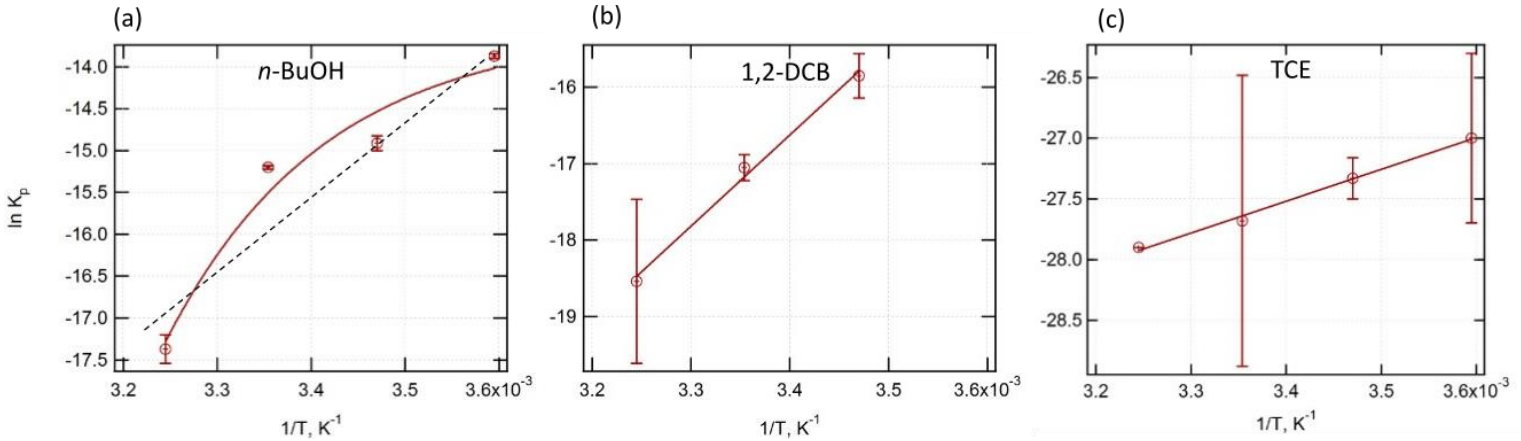

Figure 5.2 van't Hoff plot of (a) *n*-BuOH, (b) 1,2-DCB, and (c) TCE partitioning on Am Sulf aerosol. Data for 1,2-DCB was taken from an earlier study (Ahn, Rao, & Vejerano, 2021a). The red curve is the best-fit to the data. The black dash line is the linear fit to the data for *n*-BuOH.

Table 5.2 Linear fit parameters and thermodynamic values for three VOCs.

	Fitting parameters and thermodynamic value					
VOC	*Intercept*	*Slope*	r^2	ΔH_{des} (kJ mol^{-1})	ΔS_{des} (kJ mol^{-1})	ΔH_{vap*} (kJ mol^{-1})
n-BuOH	-42.9±4 (-46.7±4)	8105±1020 (9183±1080)	0.875 (0.883)	*nc*	*nc*	52.0 ± 3.0
1,2-DCB[a]	-72.8±10 (-61.5±8)	15249±2830 (13173±2420)	0.988 (0.993)	-126.8±6 (-109.5±5)	-0.605±0.02 (-0.511±0.02)	48.5±0.1
TCE	-41.5±3 (-30.5±3)	4173±958 (924±947)	0.944 (0.995)	-34.7±1 (-7.7±2)	-0.345±0.007 (-0.254±0.007)	34.7±0.4

Values without and with parentheses are for Am Sulf and SA, respectively. The uncertainty was defined as one standard deviation from the mean. ΔH_{des} and ΔS_{des} were calculated from equation 2 as $\Delta H_{des} = R \cdot Slope \cdot 10^{-3}$ and $\Delta S_{des} = R \cdot Intercept \cdot 10^{-3}$, respectively, where *R* is the gas coefficient. *nc* not calculated

* ΔH_{vap} values were taken from the National Institute of Standards and Technology.(*Chemical Name Search*, n.d.)

particles were 11,924 and 15,275, respectively. The enthalpy (ΔH_{des}) and entropy (ΔS_{des}) of desorption were calculated using the following equation, $\Delta H_{des} = R \times \text{slope} \times 10^{-3}$ and $\Delta S_{des} = R \times \text{intercept} \times 10^{-3}$, respectively. The estimated ΔH_{des} for TCE on Am Sulf aerosol particles was 34.7 ± 1 kJ mol^{-1}, which was ~ 4× higher than on SA 7.7 ± 2 kJ mol^{-1}. Whereas ΔH_{des} values for 1,2-DCB partitioning on Am Sulf aerosol particles were almost similar to that on SA aerosol particles. Fitting the data to a line, 1,2-DCB yielded the highest r^2 (0.993) compared to TCE and *n*-BuOH, in which the latter did not fit well to a line. For all VOCs, $|\Delta S_{des}|$ were < 1 kJ mol^{-1}.

Nonlinear temperature dependence observed for *n*-BuOH may be attributed to the interactions with the organic or inorganic aerosol particles or a different three-dimensional structure of *n*-BuOH due to its interaction with the 'bulk' water leading to different enthapies (Tanase et al., 2019). One possible explanation is observed from a computational modeling study on *n*-BuOH/water adsorbing on zeolite composed of silica (DeJaco et al., 2016), which resembles our experimental condition. In our experiment, we fixed RH at 35%, but absolute humidity increases with increasing temperature. DeJaco *et al*. demonstrate an increasing number of water molecules form more hydrogen bonds with *n*-BuOH, bridging two *n*-BuOH molecules (DeJaco et al., 2016). Such structures will interact differently with the aerosol resulting in different enthalpies. However, additional investigation is needed to determine if other moderately or strongly polar VOCs behave similarly at this RH level and higher. In this case, the overall dimensionless partitioning coefficient (D_p) can be expressed as

$$D_p = \frac{\sum_{i=1}^{n} C_{p_i}}{C_g} \tag{5.2}$$

where i is the number of distinct *n*-BuOH-water structures in the aerosol particle phase. For simplicity, assuming only two different complexes of *n*-BuOH with water in the aerosol particle phase (C_{p1} and C_{p2}) as described above, we define D_p as

$$D_p = \frac{C_{P_1} + C_{P_2}}{C_g} \tag{5.3}$$

We assume that both complexes have different equilibrium constants,

$$k_1 = \frac{C_{P_1}}{C_g} \tag{5.4}$$

and

$$k_2 = \frac{C_{P_2}}{C_g} \tag{5.5}$$

Additionally, we assume that the conformations of *n*-BuOH in the aerosol particle phase are in equilibrium and is defined by

$$k_{2,1} = \frac{C_{P_2}}{C_{P_1}} \tag{5.6}$$

Dividing the numerator and denominator of equation (5.3) by C_{p1}, and substitution k_1 and $k_{2,1}$ yield,

$$D_p = \frac{1 + k_{2,1}}{k_1^{-1}} \tag{5.7}$$

which is independent of k_2. Since the equilibrium constants are defined by the Gibbs free energy (ΔG_n^0), which incorporates the dependence of D_p with $1/T$, equation (5.7) becomes

$$D_p = \frac{1 + e^{-\Delta G_{2,1}^0 / RT}}{e^{\Delta G_1^0 / RT}} \tag{5.8}$$

where R and T are the ideal gas constant and absolute temperature, respectively.

Taking the natural logarithm yields

$$ln\, D_p = ln\,(\,1 + e^{-\Delta G^0_{2,\,1}\,/\,RT}) - \frac{\Delta G^0_1}{RT} \tag{5.9}$$

which can be expanded as a Taylor series (ESI) with a general form of

$$ln\, D_p = a + bx + cx^2 + dx^4 + ex^6 \ldots \tag{5.10}$$

where $x = 1/T$ and a, b, c, d, e… are coefficients.

Since we only have four points, we fitted the data to a second-order approximation. Fitting the data from *n*-BuOH improved the r^2 from 0.875 to 0.980 for Am Sulf and from 0.883 to 0.937 for SA. Values of the fitting parameters a, b, and c are listed in Table 5.3. To determine ΔH_{des} and ΔS_{des}, we took the first derivative with respect to x of equation (5.11),

$$\frac{\partial\, lnD_p}{\partial x} = b + 2cx \tag{5.11}$$

Since $\frac{\partial\, lnK_p}{\partial \frac{1}{T}} = \frac{\Delta H_{des}}{R}$ is the slope in equation (5.1), we can approximate that $\frac{\partial\, lnD_p}{\partial x} = b + 2cx \cong \frac{\Delta H_{des}}{R}$ therefore,

$$\Delta H_{des} \cong R\left(b + {}^{2c}/_{T}\right) \tag{5.12}$$

Combining equations (5.1), (5.11), and (5.12) yield

$$\Delta S_{des} \cong R\left(\,a - {}^{c}/_{T^2}\right) \tag{5.13}$$

ΔH_{des} derived from equation (5.12) is only a good approximation if $\frac{\partial \Delta S_{\mathrm{des}(T)}}{\partial 1/T}$ is close to zero. Equation (5.12) and (5.13) have been used to derive thermodynamic values for compounds displaying nonlinear temperature dependence of van't Hoff plots (Galaon & David, 2011).

The ΔH_{des} for *n*-BuOH partitioning on Am Sulf ranged from 16 to -149.9 kJ mol^{-1}. ΔH_{des} exhibited strong temperature dependence, increasing ~ 10× within a 30 ^{o}C/K temperature interval for both aerosol composition. The gas-particle partioining on SA had a slightly different ΔH_{des} than on Am Sulf aerosol particles. Similar to the ΔH_{des}, ΔS_{des} exhibited temperature dependence. However, for both aerosol composition, $|\Delta S_{des}|$ at all temperatures were < 1 kJ mol^{-1}. The ΔS_{des} values on both aerosol compositions were all negative, ranging from -0.06 to -0.63 kJ mol^{-1}. Error propagation is described in the ESI (Table 5.4).

For the narrow temperature range used in the study, ΔH_{des} for *n*-BuOH partitioning into Am Sulf aerosol particles can be approximated using ΔH_{des} (kJ mol^{-1}) ~ 4.91T - 1370. The ΔH_{des} for *n*-BuOH ranged from 12.4 to 144.2 kJ mol^{-1} on SA aerosol particles with increasing temperature and followed the equation ΔH_{des} (kJ mol^{-1}) ~ 3.90T - 1062. T is the absolute temperature. The ratio of ΔH_{des} (Am Sulf:SA) partitioning on each type of aerosol increased with increasing temperature, with the ratio being slightly above unity at 300K (Figure 5.3). Also, ΔH_{des} exhibited a strong temperature dependence from 278 to 300K. The minimum ratio occurred at the lowest temperature, ~278.15K (Figure 5.3).

Partitioning of the VOCs on SA was less endothermic than on Am Sulf aerosol particles as the temperature increased. However, these values were more endothermic than

Table 5.3 Fitting parameters for *n*-BuOH using a second-order polynomial.

Aerosol	a	b ($\times 10^5$)	c ($\times 10^7$)	r^2
Am Sulf	-376 ± 45.7	2.03 ± 0.267	-2.85 ± 0.390	0.980
SA	-311 ± 91.9	1.64 ± 0.538	-2.26 ± 0.786	0.937

Experimental data was fitted to equation (6.2), $ln\, D_p = a + bx + cx^2$, where $x = 1/T$

Table 5.4 Temperature dependence of ΔH_{des} and ΔS_{des} for *n*-BuOH.

T, K	$\Delta H_{des,\ Am\ Sulf}$	$\Delta S_{des,\ Am\ Sulf}$	$\Delta H_{des,\ SA}$	$\Delta S_{des,\ SA}$
278.15	16.0 ± 0.6	0.0633 ± 0.002	12.4 ± 3	0.157 ± 0.03
288.15	43.1 ± 1.7	0.272 ± 0.009	59.3 ± 14	0.323 ± 0.06
298.15	98.2 ± 3.7	0.460 ± 0.015	103.0 ± 24	0.472 ± 0.09
308.15	149.9 ± 5.7	0.630 ± 0.020	144.0 ± 34	0.607 ± 0.12

Using the fitting parameter in Table 5.4, ΔH_{des} and ΔS_{des} in kJ mol^{-1} were calculated as $\Delta H_{des} \cong R\left(b + {}^{2c}/_{T}\right) \times 10^{-3}$ and $\Delta S_{des} \cong R\left(a - {}^{c}/_{T^2}\right) \times 10^{-3}$, respectively, where R is the gas coefficient. The factor 10^{-3} appears because of the conversion from J to kJ.

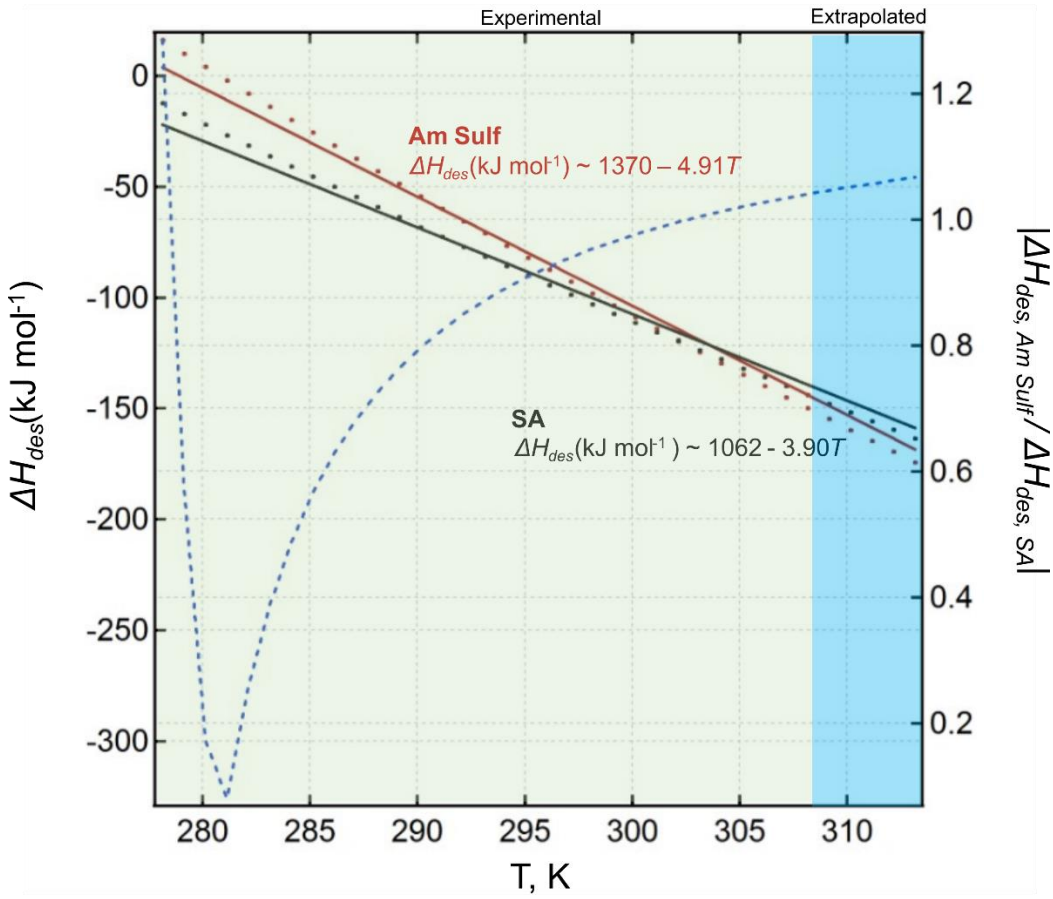

Figure 5.3 Temperature dependence of ΔH_{des}, for the partitioning of *n*-BuOH on Am Sulf (red line) and SA aerosols (black line). The blue curve is the ratio of ΔH_{des} for the VOCs partitioning in Am Sulf and SA aerosols. The green region is the calculated value within the experimental temperature range and values on the blue region are the extrapolated above 308K.

the measured ΔH_{des} for more than 50 S/VOCs partitioning onto atmospheric aerosols. The majority of the ΔH_{des} ranged from 40 to 70 kJ mol^{-1} (Arp et al., 2008b) for aerosols obtained from diverse environments. Sorption of the VOCs into both types of aerosol were both favorable as deemed from their higher endothermic ΔH_{des} compared to some SVOCs that partitioned into atmospheric aerosols (Arp et al., 2008b). The calculated values for the amount of VOCs were larger than those reported for a select class of VOCs measured from urban aerosols. VOCs associate with fine particles (d_p < 2.5 µm) (Matsumoto et al., 2010; Odabasi et al., 2005). Matsumoto and colleagues showed that the aerosol's VOC loading depends strongly on the aerosol mass than the VOCs' gas-phase concentration (Odabasi et al., 2005; Matsumoto et al., 2010). Measurement of the K_p values for VOCs remained scant. The limited study that measured them was acquired from field sampling that is susceptible to dynamic and static factors (*e.g.*, wind speed, RH, temperature, sampling artifacts, non-equilibrium conditions, *etc*.) confounding the measured gas-particle coefficients' accuracy (Wang et al., 2014; Kristensen et al., 2016).

On Am Sulf aerosol particles, TCE matched the ΔH_{vap} (34.7 ± 0.4 kJ mol^{-1}) closely with ΔH_{des} (34.7 ± 1 kJ mol^{-1}). The excellent agreement between the ΔH_{des} obtained from our experimental data and the ΔH_{vap} obtained from the National Institute of Standards and Technology (NIST) for TCE on Am Sulf demonstrates that our experimental system was accurate. Arp and collegues have recommended using the enthalpy of vaporization (ΔH_{vap}) for estimating K_p since the average values of the ΔH_{vap} and ΔH_{des} are close (Arp et al., 2008b). However, this recommendation cannot be generalized and may only apply to weakly polar compounds. For 1,2-DCB, there is a substantial difference between these parameters. Even more so for *n*-BuOH; ΔH_{des} exhibited a nonlinear temperature

dependence on organic and inorganic aerosols as depicted in Figure 5.1 and 5.2. We expect these differences to be larger for complex aerosols relative to the simple model aerosols used in this study.

Although the typical RH range at the lower troposphere is ~ 70–80% (Ruzmaikin et al., 2014), we determined the temperature dependence at RH ~ 35%, since, in our earlier study (Ahn, Rao, & Vejerano, 2021a), the VOC's mass fractions above this RH were not significantly different. Additionally, the state of Am Sulf aerosol particles was most likely a crystalline solid since ammonium sulfate effloresces at ~ 35–40% RH (Ciobanu et al., 2010). However, at RH ~ 35%, the absolute humidity approximately doubles for each 10 °C/K rise in temperature. The absolute humidity is ~ 8× at 308.15K relative to that at 278.15K. At this condition, the aerosol can transform into a supersaturated liquid electrolyte solution depending on the aerosol's inorganic components. Although, for SA and Am Sulf aerosol particles, such a state is less likely because of their high deliquescence RH. At 298.15K, small SA (< 100 nm) and Am Sulf aerosol particles deliquesce only at RH of ~ 99% (Bilde & Svenningsson, 2004) and ~ 82% (Brooks et al., 2002), respectively, because of the Kelvin effect. Therefore, the aerosol particle's state will most likely be a crystalline solid at RH ~ 70%. Additionally, dry SA aerosol particles are less hygroscopic compared to Am Sulf aerosol particles. For Am Sulf aerosol particles (Goss & Schwarzenbach, 1999), water molecules will cover the particle's active sites, thus compete with the VOC for adsorption.

Ammonium sulfate and SA aerosol particles more likely exist as crystalline solids at an RH lower than the deliquescence RH. If only a monolayer of water molecules on the surface of particles, there may be competition for active sites, and partitioning is driven by

adsorption. Equation (5.14) depicted the adsorptive part of the saturated vapor pressure (P_i^0) model described by Pankow (Pankow, 1987).

$$K_p = \frac{N_s\, a_{TSP}\, T\, e^{(Q_l - Q_v)RT}}{16\, P_i^0} \tag{5.14}$$

where P_i^0 is the vaper pressure of compound i, R is the gas constant (8.314×10^{-3} kJ mol^{-1} K^{-1}), T (K) is the absolute temperature, N_s (mol cm^{-2}) is the surface concentration of sorption sites, a_{TSP} (cm^2 µg^{-1}) is the specific surface area for the TSP; Q_s (kJ mol^{-1}) is the enthalpy for desorption of compound *i* from the adsorbing solid surface (always positive), Q_v (kJ mol^{-1}) is the enthalpy for vaporization of compound *i* as a liquid (always positive). If significant layers of water cover the particle's surface, or if the particles consist of a supersaturated liquid electrolyte solution, particularly at higher RH level, then the partitioning mechanism will be absorptive as described by equation (5.15),

$$K_p = \frac{760\, f_i\, RT}{10^6\, MW_i\, \zeta_i\, P_i^0} \tag{5.15}$$

where f_i is the inorganic/organic fraction of the aerosol particle, ζ_i is the activity coefficient of compound *i* in inorganic/organic matter fraction, MW_i (g mol^{-1}) is the molecular weight of inorganic/organic matter, P_i^0 is the vapor pressure of compound *i*, R is the gas constant (8.314×10^{-3} kJ mol^{-1} K^{-1}) and T (K) is the absolute temperature. Although we experimented with only one TSP level, K_p will increase linearly with TSP (a_{TSP}) due to the increasing number of active sites (N_s). Hygroscopic aerosol particles such as ammonium sulfate are likely to be covered by a thicker water layer. At lower RH and temperature, we attribute the high K_p to the aerosol's higher active surface sites (Goss & Schwarzenbach, 1999) because of less competition with water molecules due to their low concentration. For

an aerosol consisting of multiphase systems, the hydrophobic phase may provide a large partitioning matrix for a VOC.

Partitioning is not only affected by the VOC's nature (*e.g.*, solubility and polarity). Aerosol-specific properties, which are dependent on the components contained in them, will also modulate VOC partitioning. The ad/absorptive partitioning will depend on whether the process occurs onto or into solid, or (aqueous) organic or inorganic solution phases, and the composition of those phases or phase transitions as a function of temperature and aerosol composition. In this study, we generated aerosols consisting only of a single solute. Ambient atmospheric aerosols contain multiple components that form multiphase systems depending on environmental conditions, more importantly, RH. Aerosol consisting of an equimolar amount of ammonium sulfate and nitrate drastically deliquesces at a lower RH (63.6%) (Tang & Munkelwitz, 1993; Wu et al., 2019); therefore, will affect VOC partitioning differently from a model aerosol consisting of one solute. Phase separations have been known to correlate well with the O : C ratio (Dallemagne et al., 2016; You et al., 2012, 2014). Aerosols containing ammonium sulfate and less-oxidized organic components (O : C < 0.5) undergo phase separation (You et al., 2012), whereas aerosols with O : C > 0.8 (relatively more oxidized) do not (You et al., 2012). These types of aerosol are good models to investigate the effect of phase separation on partitioning.

Phase separation can result in aerosols with different morphologies: homogeneous, core-shell, partially engulfed, or structures containing multiple inclusions (Freedman, 2017; Dallemagne et al., 2016). Depending on the dominant morphology, sorption of VOCs will result in significantly different gas/particle enthalpies due to differences in the VOC's interaction with phase-separated components. Modeling studies should not neglect

the contribution of slightly water-soluble organic fraction of aerosols to overall VOC partitioning to prevent underestimating the K_p of VOCs (Ahn, Rao, & Vejerano, 2021a). Since we used a simple aerosol model, the observed K_p and partitioning behavior should be carefully interpreted when applying them to complex aerosols to prevent misattribution to VOC-specific properties alone. Future studies should incorporate a more complex model aerosol to determine partitioning enthalpies due to combined aerosol- and VOC-specific properties and behaviors.

For a weakly polar organic (TCE), K_p varied linearly with the inverse of the absolute temperature. In contrast, *n*-BuOH, a moderately polar compound, followed a Langmuir-type behavior. Our results differed from those of Matsumoto and colleagues that concluded that the VOCs' gas-particle partitioning did not exhibit temperature dependence (Matsumoto et al., 2010). In their study, the K_ps were very weakly and negatively correlated with ambient temperature and RH (Matsumoto et al., 2010). The reason for their conclusion is that they measured primarily nonpolar and weakly polar VOCs. Therefore, their finding should not be generalized because it appears that the VOC's polarity affects temperature dependence. One reason for this non-sensitivity is the inherent limitation of the field sampling technique; environmental factors such as temperature and RH cannot be controlled compared to the precise modulation in a laboratory setting.

CHAPTER 6

DEPENDENCE ON HUMIDITY AND AEROSOL COMPOSITION OF THE GAS-PARTICLE PARTITIONING OF WEAKLY AND MODERATELY POLAR VOCS[4]

6.1 Effect of RH on *Kp* of weakly polar and strongly polar VOCs

Figure 6.1 depicts the dependence of K_p with RH at a constant temperature of 25°C for TCE and *n*-BuOH partitioning onto Am Sulf aerosols. The trendlines for the K_p values for both organics decreased with increasing RH levels. For Am Sulf aerosol, the K_p for both *n*-BuOH and TCE were highest at a low RH and declined continuously at higher RH levels. The K_p values at an RH of ~ 40% decreased sharply for Am Sulf aerosol. These behaviors were similar to that of 1,2-DCB. However, compared to 1,2-DCB partitioning onto the same aerosol, the decline in K_p with RH was more gradual (Figure 6.1). Compared to TCE and 1,2-DCB, the K_p values were higher for *n*-BuOH, suggesting that it preferentially sorbed onto Am Sulf aerosols.

Figure 6.2 depicts the dependence of K_p with RH at a constant temperature of 25°C for TCE and *n*-BuOH partitioning onto SA aerosols. Compared to the partitioning of these

[4] Reprinted here with permission of publisher: Jeonghyeon Ahn *et al*., Dependence on humidity and aerosol composition of the gas-particle partitioning of weakly and moderately polar VOCs. Aerosol and Air Quality Research *In Press*

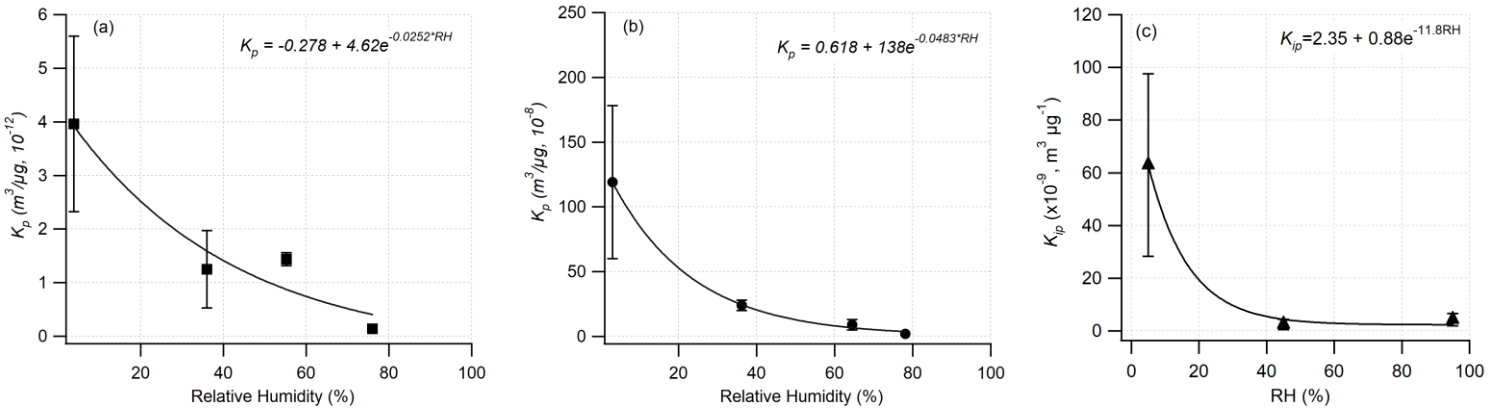

Figure 6.1 The K_p of (a) TCE, (b) *n*-BuOH, and (c) 1,2-DCB (Ahn, Rao, & Vejerano, 2021a) partitioning into Am Sulf aerosol at 25°C at different RHs. Error bars are one standard deviation from the mean, which were taken from triplicate measurements.

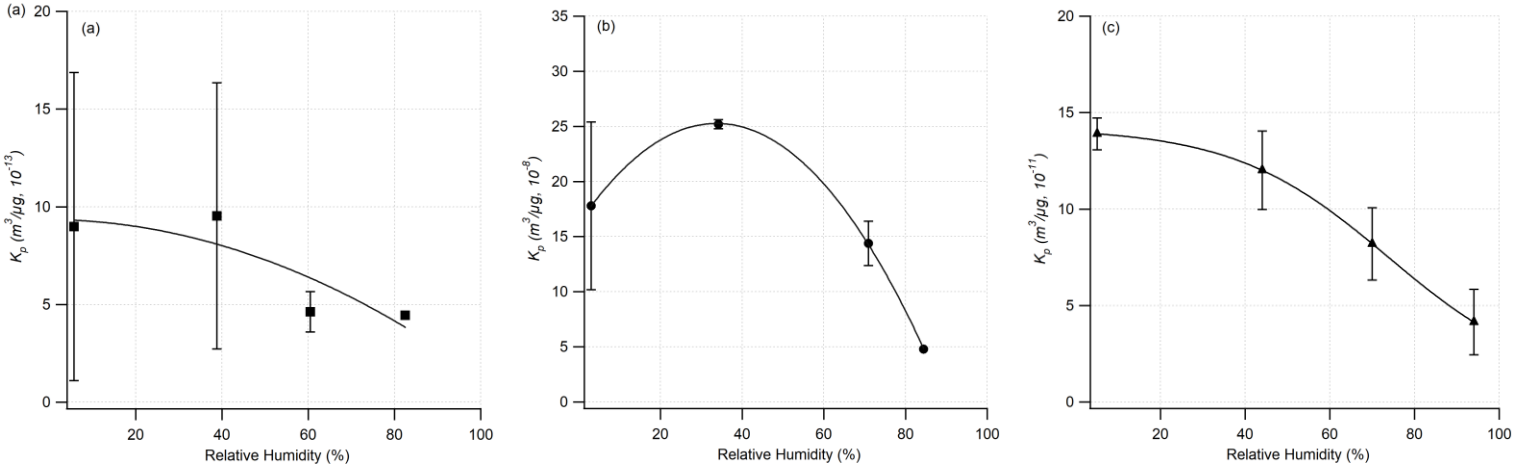

Figure 6.2 The K_p of (a) TCE, (b) *n*-BuOH, and (c) 1,2-DCB (Ahn, Rao, & Vejerano, 2021a) partitioning into SA aerosol at 25°C. Error bars are one standard deviation from the mean, which were taken from triplicate measurements. Solid lines are not fit but were drawn as a guide only.

organic onto Am Sulf aerosols, the K_p decline slowly with increasing RH levels. At all RH levels, the K_p varied only within an interval of ~ 5×10^{-13} for TCE (Figure 6.2a) and ~ 10×10^{-13} for 1,2-DCB. The most extensive interval range was for *n*-BuOH, which fluctuated by an interval of ~ 20×10^{-13}. However, compared to 1,2-DCB partitioning onto the same aerosol composition, K_p's decline with RH was more gradual. The K_ps for *n*-BuOH were higher than those for TCE and 1,2-DCB (Figure 6.1 and 6.2), consistent with their observed behavior on Am Sulf, suggesting preferential sorption.

Overall, the K_ps for the three VOCs partitioning into Am Sulf aerosol were higher than those onto SA aerosol. In general, the K_p for TCE, *n*-BuOH, and 1,2-DCB partitioning onto Am Sulf aerosols were ~ 5×, ~ 10×, and ~ 600× higher than onto SA aerosols. As the K_p of Am Sulf aerosol were 1.36×10^{-13} to 3.96×10^{-12} for TCE and 1.57×10^{-8} to 1.19×10^{-6} for *n*-BuOH, the K_p of *n*-BuOH was four orders of magnitude higher than those for TCE. For the partitioning onto SA aerosols, the K_p were 4.45×10^{-13} to 8.99×10^{-13} for TCE and 4.80×10^{-8} to 1.78×10^{-7} for *n*-BuOH. The K_p of *n*-BuOH was five orders of magnitude higher than those of TCE.

6.2 Evolution in aerosol properties at different RH levels

We monitored changes in the properties of Am Sulf and SA aerosols for ~ 8 h at different RH levels (Figure. 6.3). The particle median diameter appeared to be less affected by RH even at higher RH levels. The particle size of SA aerosols was slightly larger than those of Am Sulf aerosol; average particle median diameter was 95 ± 7 nm for Am Sulf

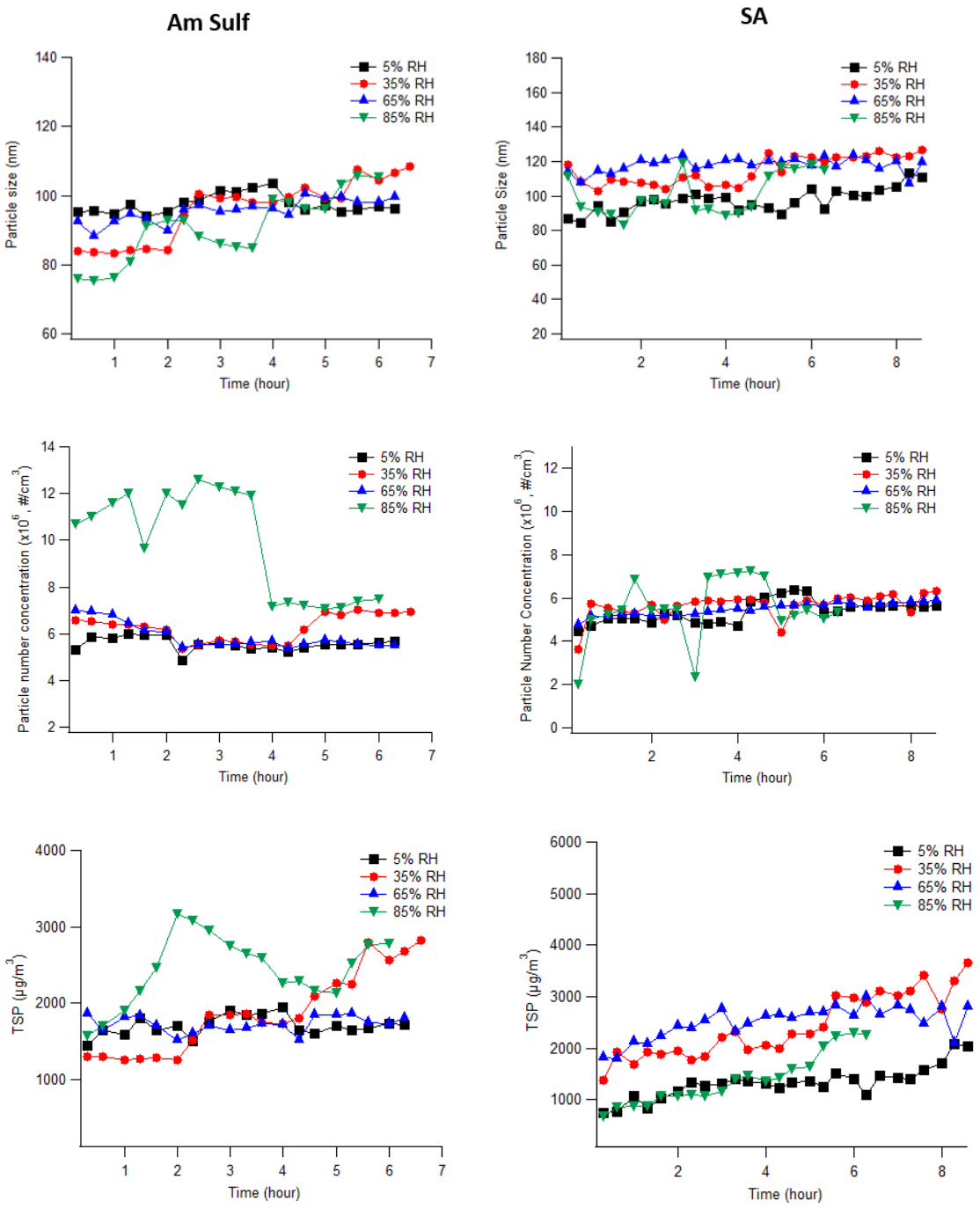

Figure 6.3 Time-evolution of the particle size, particle number concentration, and TSP of Am Sulf and SA aerosols for 8 hours at different RH levels.

aerosol and 108 ± 12 nm for SA aerosol. For both aerosols, we observed that the TSP and particle number concentration fluctuated more at an RH of ~ 85% but were stable at lower RH during the 8-h monitoring. The particle number concentrations for Am Sulf aerosol were 5.37×10^6 cm^{-3} at an RH of 5% RH, 5.65×10^6 cm^{-3} at 35% RH, 5.48×10^6 cm^{-3} at 65% RH, and 5.52×10^6 cm^{-3} at 85% RH. Although the particle number concentration as depicted in Figure 6.3 fluctuated the concentration remained within 10^6 cm^{-3}, except at an RH of 85%, which increased by an order of magnitude. Particle number concentrations of SA aerosol were 5.56×10^6 cm^{-3}, 6.24×10^6 cm^{-3}, 5.86×10^6 cm^{-3}, and 9.90×10^6 cm^{-3} at RH levels of 5%, 35%, 65%, and 85%, respectively. At an RH of 85%, the particle number concentration for Am Sulf aerosol fluctuated intensely but had stabilized after 4 h and resulted to higher TSP compared to those at lower RH levels. At similar RH level, the particle number concentration for SA aerosol also fluctuated for 4 h, but the TSPs were within a similar level to those measured at lower RH levels. Higher fluctuations in TSP only occurred for Am Sulf aerosol. We did not observe intense fluctuations of the TSP for SA aerosol. The TSPs measured by the SMPS were at similar levels for Am Sulf and SA aerosols, which were 1,930 ± 461 and 1,952 ± 715 μg m^{-3}, respectively. Note that the high uncertainty was due to the strong fluctuations at an RH of ~ 85%. TSP and particle number concentration became slightly larger during the 8-h measurement at all RH levels.

6.3 Partitioning mechanism

Although the mass fraction of VOCs that partitions into aerosols is less compared to SVOCs, VOCs dominate the class of atmospheric and indoor pollutants. Therefore, some highly abundant VOC can reach concentration levels comparable to SVOCs with very low abundance (Hamilton et al., 2004; Odabasi et al., 2005; Matsumoto et al., 2010). This

companion paper described our measurement of the partitioning coefficient for TCE and *n*-BuOH under different RH levels and aerosol composition. We compared them with our earlier studies on 1,2-DCB (Ahn, Rao, & Vejerano, 2021a). The K_p values for TCE and *n*-BuOH were at similar ranges to those measured for different aerosols sampled from diverse sources (Arp et al., 2008a) and were at similar orders to that of 1,2-DCB (Ahn, Rao, & Vejerano, 2021a). Overall, results showed that: (1) VOC partitioning onto Am Sulf was higher than onto SA aerosols; (2) partitioning on SA was affected less at all RH levels, whereas partitioning onto Am Sulf was affected only at low RH level.

Gas-particle partitioning of organics can proceed via absorption (*i.e.*, diffusion into the bulk of the aerosol) and adsorption (*i.e.*, interacts with the active surface sites) (Pankow, 1994). Although the dominant partitioning mechanisms are unclear, it is well known that environmental conditions (Goss & Schwarzenbach, 1998), more importantly, RH and temperature, and aerosol composition modulate these processes. However, the effects of RH are tightly coupled with the surface chemistry of the particles (Sobanska et al., 2015). In general, partitioning of the VOCs onto Am Sulf was likely via adsorption at an RH < 40%, whereas above this RH, the partitioning was more plausibly via absorption. VOC partitioning onto SA aerosols appears to proceed via adsorption at all RH levels, perhaps except at saturated RH since dried SA aerosol only deliquesces at an RH ~ 99% (Bilde & Svenningsson, 2004). Our earlier paper described the effects of temperature (5 to 35°C) for the partitioning of TCE and *n*-BuOH (Ahn, Rao, & Vejerano, 2021b). Partitioning of TCE is independent of temperature as deemed from the constant enthalpy of desorption consistent with the classic van't Hoff relationship (ln K_p vs. 1/T). However, partitioning of *n*-BuOH strongly depends on temperature, resulting in a non-linear behavior (Ahn, Rao,

& Vejerano, 2021b). At a constant RH, but increasing temperature, absolute humidity increases; under such conditions, *n*-BuOH forms various complexes with water (DeJaco et al. 2016) with different desorption enthalpy (Ahn, Rao, & Vejerano, 2021b).

6.4 Effect of RH

Although the fit uses at most four data points, similar to that for 1,2-DCB (Ahn, Rao, & Vejerano, 2021a), the partitioning of TCE and *n*-BuOH onto Am Sulf aerosol followed an exponential relationship between K_p and RH in which $ln\ K_p = - C \times RH + E$, where C and E are VOC- and aerosol-specific constants) (Goss, 1992; Goss & Eisenreich, 1997). For the three VOCs we studied, regardless of the polarity, RH has a negligible impact above 50%, consistent with those reported in the literature (Cotham & Bidleman, 1992a; Arp et al., 2008a; Jathar et al., 2016). The results for TCE and *n*-BuOH, and that with our previous study with 1,2-DCB, suggest that aerosol-specific properties strongly affect partitioning behavior than do VOC-specific properties. The overall K_p values of TCE and *n*-BuOH decreased as the RH increased for organic and inorganic aerosols at 25°C. However, sorption of the VOCs onto SA aerosol regardless of their polarity did not fit the exponential dependence of K_p with RH. This result suggests that partitioning behavior is driven more by aerosol-specific properties than do the VOCs' properties; under such a mechanism, it appears that the VOC's polarity has less impact on partitioning.

6.5 Effect of water uptake

Absorption of water has a considerable impact on partitioning. At high RH, water vapor can compete with the adsorption sites on the aerosol. At RH levels of 50 to 70%, the liquid water content of atmospheric aerosols accounts for ~ 10% of the total particulate

mass and increases significantly at RH > 70% (Pilinis et al., 1989; Thibodeaux et al., 1991). For instance, organic-phase water can increase the aerosol mass, providing a larger absorbing matrix for organics (Jathar et al., 2016). Am Sulf particles deliquesce at high RH (~ 82%) (Brooks et al., 2002) and highly hygroscopic. Still, even under low RH, uptake of water can cover active sites on aerosol, which will decrease the mass fraction of adsorbed organics onto the aerosol. On Am Sulf aerosol, partitioning is dominated primarily by the aerosol's higher active surface sites at low RH (adsorption) (Goss & Schwarzenbach, 1999). On SA, water covering the active sites was less pronounced because SA is less hygroscopic than Am Sulf. Therefore, the number of active sites remained almost constant, which may explain the slow decline in K_p (Figure 6.2(b)) as the RH increased. For SA aerosols, the dissolution of the VOCs in the aerosols water was not likely the mechanism because SA deliquesces at a high RH (Bilde & Svenningsson, 2004). SA droplets do not deliquesce even at 90% RH as deemed from a single-droplet study at 25°C (Peng et al., 2001). Smaller particles of SA have a higher DRH of 99% (Bilde & Svenningsson, 2004). Moreover, the growth factor of SA (RH of 10% and 90%) was ~ 1, suggesting that they are not hygroscopic within this RH range (Peng et al., 2001). Therefore, below saturated RH, dry SA aerosol introduced into the chamber was not expected to grow. However, in Figure 6.3, we observed a slight change in the particle median diameter as the RH increased (Hämeri et al., 2000). It is known that small soluble and insoluble particles increase in size well below the DRH because of the adsorption of water onto their surfaces (Hämeri et al., 2000). The lesser effect of RH on the K_p of the VOCs partitioning onto SA is consistent with these observations. For small Am Sulf particles, DRH is influenced by two effects. First, the solubility of a crystal increases as its size decreases, lowering the DRH. Particles

smaller than 100 nm have a DRH of 79.9% (Tang & Munkelwitz, 1993). Even submicron particles of pure AS have a DRH = 80.7 ± 0.2% (Laskina et al., 2015; Q. Liu et al., 2016; X. Wang et al., 2017). Small SA particles < 200 nm require overcoming an energy barrier to uptake water (Brooks et al., 2002; Wex et al., 2007). Second, when the particles deliquesce, water vapor pressure increases, increasing the DRH (Hämeri et al., 2000). Aerosols consisting of mixed components have significantly different DRH than aerosol consisting of single solute, such as this study. Aerosol consisting of a mixture of salts effloresces at 15–40% RH, crystalizes simultaneously, and deliquesces at 63.6% (Tang & Munkelwitz, 1993; Wu et al., 2019). Thus, for a mixed aerosol, the partitioning behavior will differ from an aerosol consisting of one solute.

6.6 Effect of the VOC's physicochemical properties

As we observed that moderately polar, weakly polar, and nonpolar aromatic VOCs have similar behavior on Am Sulf aerosols as shown by their trendlines in Figure 6.1. However, the nature of the organics (for instance, polarity and solubility) dictates the VOC's mass fraction that will sorb onto aerosols. Below the DRH, aerosol can absorb sufficient amount of water. Hence, to some extent, the surface is covered with water layers, in which the VOCs can dissolve. At higher RHs (≥ 35%), the VOCs partitioned onto Am Sulf by dissolving into the aqueous phase. The amount of the VOCs that partitioned into the aerosols was inconsistent with the trend in water solubility of the VOCs. Although to some extent, compounds with high water solubility such as *n*-BuOH (66× higher than TCE) had a higher mass fraction partitioned onto both aerosols. However, solubility alone does not dictate mass transfer of a VOC onto aerosols. The solubility of the 1,2-DCB, TCE, and *n*-BuOH at 25°C were 1.56, 11.8, and 680 wt%, respectively. Whereas, in general, the K_p of

1,2-DCB, TCE, and *n*-BuOH at 25°C were on the order of 10^{-11}, 10^{-13}, and 10^{-8}, respectively (He et al., 2010). The saturated vapor pressure, dimensionless Henry's law constant (H_L), and octanol-air partition coefficient (K_{oa}) (Table 6.1) of the VOCs did not result in a consistent trend with K_p. For VOCs, K_{oa} is not applicable compared to their use for predicting K_p of SVOCs. The relationship of K_p with increasing RH (*i.e.*, being exponential) is identical for the three VOCs regardless of their polarity. However, at a similar RH level, the mass fraction that will sorb onto the aerosol is to some extent influenced by the VOC's polarity and their capacity to interact with the aerosols' active sites.

6.7 VOC/aerosol interactions

In general, for both aerosols, we ascribed the larger K_p at an RH ~ 10%, to Van der Waals interaction between the VOC and the aerosols' surface. TCE, a weakly polar compound, interacts strongly with the surface of Am Sulf aerosols *via* Van der Waal's interaction (Schwarzenbach et al., 2016), as deemed from the higher partitioning constant compared to those of SA aerosol. We observed a similar behavior with the other two VOCs as well. For real atmospheric aerosol consisting of hydrophobic components, this observation is applicable since nonpolar and weakly polar VOCs are less affected at RH levels of 50–90% because they preferentially partition into that phase (Cotham & Bidleman, 1992b; Jathar et al., 2016). At low RH, TCE interacts with molecular layers of water (Goss & Schwarzenbach, 1999), on the surface of Am Sulf aerosol *via* Van der Waal's interaction. Despite the relatively higher solubility of TCE in water to that of 1,2-DCB, the levels were similar because TCE is weakly polar and can interact with the water in the aerosols better by Van der Waals interaction. However, between the two types of

Table 6.1 Experimental and selected literature physicochemical properties of the VOCs.

VOC	*Experimental log K_p*	*Solubility (wt%)*	*Vapor Pressure (Torr)*	*Dimensionless Henry's Law Constant (H_L)*	*Octanol-air Partition Coefficient (K_{oa})*
1,2-DCB	-11	1.56	1.36	7.8×10^{-2}	4.36
TCE	-13	11.2	69	4.2×10^{-1}	2.99
n-BuOH	-8	680	7	3.6×10^{-4}	4.19

Data were taken from the National Institute of Standards and Technology except the experimental log K_p

aerosols, Van der Waals interaction of TCE with SA aerosol is weaker compared with Am Sulf aerosol.

The faster decline in the K_p values even at a lower RH for Am Sulf is due to water film (Goss & Schwarzenbach, 1999) covering the aerosol. Once the aerosol is covered with water the number of active sites available for the adsorption of the VOCs is reduced. At high RH, water solvates and ionizes Am Sulf aerosol. Dissolved ions interacted strongly with water, which reduced VOC uptake onto Am Sulf aerosol. The small mass fraction that partitioned onto the aerosol occurred via dissolution, the extent of which depends on the VOC's properties. However, deactivation of these sites due to water was less intense for SA aerosol since they deliquesce only at saturated RH. Moreover, SA aerosol is less hygroscopic than Am Sulf aerosol. Thus, at almost all RH levels, the partitioning of TCE and *n*-BuOH on SA primarily occurred *via* adsorption on the aerosol surface via Van der Waals interactions (Goss, 1993b; Schwarzenbach et al., 2016). Of the three VOCs, *n*-BuOH had the highest K_p. This behavior is expected since *n*-BuOH can form a strong hydrogen bond with the adsorbed molecular water layer on Am Sulf or SA aerosols and with the carboxyl groups in SA. At high RH, water vapor competes strongly with *n*-BuOH for the available sorption sites on the aerosol particle surface resulting in a slight decline in K_p.

Since we used a simple model aerosol, the interaction does not account for the complexity of aerosol systems. Ambient atmospheric aerosols contain multiple components that are susceptible to phase separate depending on the condition—more importantly—RH. Phase separation can induce the aerosol to form various structures (Freedman 2017, 2020; You et al. 2012). The formation of such structures and multiphase

systems may interact with VOC differently. Hence, a model aerosol we used in this experiment will substantially exhibit drastically different partitioning behavior.

Only limited studies have assessed the health impacts of aerosol-bound VOCs, partly because of the limited data on their partitioning. VOCs' contribution in aerosols is often excluded in inhalation exposure assessment because it is assumed that their amount in aerosol particles is negligible. However, aerosol- and VOC-specific properties and environmental conditions affect partitioning. Thus, chronic exposure to aerosol-bound VOCs may be a significant concern depending on the VOC type and the prevailing environmental condition (*e.g.*, RH, temperature, etc.). For example, formaldehyde is more polar and water-soluble despite being highly volatile relative to the VOCs we investigated in this study. Such a VOC class may amplify our inhalation risk because of the high mass partitioning onto aerosol particles. Our experimentally derived $K_{p,}$ when coupled with particulate matter (PM) concentration data in cities worldwide and the PM fractions deposited into the different regions of the respiratory system, can be used to calculate the regional mass deposition for some VOCs. These data can be used for assessing risk and improve our knowledge of the human health impacts of aerosol-bound VOCs.

CHAPTER 7

RESPIRATORY DEPOSITION OF AEROSOL-BOUND VOCS USING EXPERIMENTALLY DERIVED GAS-PARTICLE PARTITION COEFFICIENT[5]

7.1 $PM_{2.5}$ concentrations in Seoul and other countries

For the TSP, we used $PM_{2.5}$ data from Seoul and other countries in the calculation. Seoul is a dense metropolitan city in Korea with a complex urban environment, heavy traffic, high demand for public transportation, high population density, and an increasing portion of urbanized and built areas, especially in Seoul's center point (Eum et al., 2015). Recently, in South Korea, the concentration of particulate matter has become severe; the annual mean concentration of $PM_{2.5}$ in 2019 was 22.8 μg m^{-3}, and the highest concentration was 149 μg m^{-3} (March 5th, 2019) at the center point of Seoul (Korea Environment Corporation, 2019) According to national trends from EPA monitoring 649 sites throughout the US, the concentration of $PM_{2.5}$ was 8.66 μg m^{-3} on average in 2010–2018 (US EPA, 2016). For comparison, we selected two countries, Nepal and Niger, with the highest concentration of $PM_{2.5}$. Their $PM_{2.5}$ concentrations were 100 μg m^{-3} and 94 μg m^{-3} in 2017, respectively (*World Development Indicators*) Moreover, the $PM_{2.5}$

[5] Reprinted here with permission of publisher: Ahn *et al*., Respiratory deposition of aerosol-bound VOCs using experimentally derived gas-particle partition coefficient. Air Quality, Atmosphere & Health Research *Under review*

concentrations in 2019 (*World's Most Polluted Cities in 2020 - PM2.5 Ranking | AirVisual*) was 98.6 μg m^{-3} in Delhi, India; 89.5 μg m^{-3} in Lahore, Pakistan; 18.2 μg m^{-3} in Metro Manila, Philippines; and 42.1 μg m^{-3} in Beijing, China (Table 7.1). In addition, we estimated VOC deposition by applying the average global $PM_{2.5}$ concentration (~ 46 μg m^{-3}) in 2017 (*World Development Indicators*). These concentrations exceed the annual mean standard set by the World Health Organization (WHO, 10 μg m^{-3}), Environmental Protection Agency (EPA, 12 μg m^{-3}), and the Korea Ministry of Health (15 μg m^{-3}). We assumed that the K_p derived for particles with a median diameter of 77 nm applied to larger sizes; therefore, we used them for $PM_{2.5}$ to calculate the regional deposition of VOCs from cities worldwide.

7.2 Aerosol deposition from modeling by Strum

We used the deposition of ultrafine particles derived from a modeling study in the literature (Sturm, 2020). The modeling study by Sturm considered: (1) the effect of stochastic morphology of the respiratory system (airway length, diameter, branching angle); (2) inhaled particles are randomly transported into specific structures; and (3) the effect of various particle deposition mechanisms (diffusion, inertial impaction, interception, and sedimentation) (Sturm, 2020). We used this model since: (1) it considers the intrapulmonary transport and deposition behavior of the particles in children and adults, (2) it uses the current knowledge on particle aerodynamics in the respiratory system; (3) it simulates regional and local deposition scenarios (Sturm, 2020).

Loading of the particle considers intrasubject variability of the airway geometry due to age differences resulting in differing breathing physiologies (Sturm, 2020). Here,

Table 7.1 The $PM_{2.5}$ concentration of cities.

$PM_{2.5}$ concentration ($\mu g\ m^{-3}$)			
Seoul, Korea (2019)	22.8	Delhi, India (2019)	98.6
Seoul, Korea (highest, 2019)	149	Lahore, Pakistan (2019)	89.5
US (2010-2018)	8.66	Metro Manila, Philippines (2019)	18.2
Nepal (2017)	100	Beijing, China (2019)	42.1
Niger (2017)	94	Global (2017)	46

we summarized the key assumptions and conditions used in the modeling by Sturm. The detail is described elsewhere (Sturm, 2020). The breathing condition is simulated while sitting, and particles are inhaled through the nose in the modeling. A variable particle size with a unit density of 1.0 g cm^{-3} was assumed. The modeling assumes that an adult respiratory tract has a mean functional residual capacity of 3,300 cm^3 and a tidal volume of 750 cm^3. The length of a breath cycle was 4.2 s with a breath-hold of 1.0 s. Modeling was performed for 5-, 10- and 15-year (5-Y, 10-Y, and 15-Y) old children and adults considering their appropriate physiological data (Table 7.2). For the volume of air inhaled in 24 h, we used these values of breathing parameters. For this paper, we adopted the results for only the size range of 100 nm as this is the closest size for the size range of the data in which we obtained the experimental K_p. Although we used the $PM_{2.5}$ concentration for the data depicted in Figures 1, 2, and 3, we only considered the fraction of $PM_{0.1}$ deposited into the lungs as determined by Sturm since our data on K_p was obtained for a particle median diameter of 77 nm.

7.3 Aerosol deposition calculated from the ICRP model

We estimate the contribution of the mass fraction of VOCs entering the human body as transported by aerosols using the simplified and those calculated from the International Commission on Radiological Protection (ICRP) model (Hinds, 1999). In this estimation, we calculated particle deposition based on $PM_{2.5}$ and $PM_{0.1}$. The ICRP model calculates the inhalable fraction (IF) and deposition fraction (DF) for each region. We used

Table 7.2 Physiological breathing parameter used for determining the volume of air inhaled and for modeling particle deposition.

	Age			
Parameter	*5-Y*	*10-Y*	*15-Y*	*Adult*
Functional residual capacity (cm^3)	757	1230	2650	3300
Tidal volume (cm^3)	244	456	625	750
Breathing cycle (s)	2	2.5	3.2	4.2

the following equations:

$$IF = 1 - 0.5\left(1 - \frac{1}{1 + 0.00076\, d_p^{2.8}}\right) \quad (7.1)$$

where d_p is particle size in μm. The deposition fraction for the nasopharyngeal and laryngeal region (DF_{NPL}) is:

$$DF_{NPL} = IF\left(\frac{1}{1 + \exp(6.84 + 1.183 \ln d_p)} + \frac{1}{1 + \exp(0.924 - 1.885 \ln d_p}\right) \quad (7.2)$$

The deposition fraction for the tracheobronchial region (DF_{TB}) is:

$$DF_{TB} = \left(\frac{0.00352}{d_p}\right)[\exp(-0.234\,(\ln d_p + 3.40)^2) + 63.9\exp(-0.819\,(\ln d_p - 1.61)^2)] \quad (7.3)$$

The deposition fraction for the alveolar region (DF_{AL}) is:

$$DF_{AL} = \left(\frac{0.0155}{d_p}\right)[\exp(-0.416\,(\ln d_p + 2.84)^2) + 19.11\exp(-0.482\,(\ln d_p - 1.362)^2)] \quad (7.4)$$

A summary of the deposition calculated from the ICRP model and Sturm's work is depicted in Table 7.3. The ICRP model is not age-resolved; therefore, we used the breathing parameters for an adult in Table 7.2. $PM_{2.5}$ has an IF of 0.995. The DF values for each region were 68.8% (DF_{HA}), 6.07% (DF_{TB}), and 10.8% (DF_{AL}). $PM_{2.5}$ was deposited primarily to the head (nasopharyngeal laryngeal) region, while only 7% was deposited in the tracheobronchial region. $PM_{0.1}$ had the highest deposition in the alveolar region based on the ICRP model, which was twice larger than Sturm's model for an adult.

Table 7.3 Deposition of $PM_{0.1}$ in the three regions of the respiratory system.

	ICRP	PM deposition by age (%)*			
Region	*Adult*	*5-Y*	*10-Y*	*15-Y*	*Adult*
Nasopharyngeal laryngeal	2.1 / 68.8[a]	11	10	9	10
Tracheobronchial	2.66 / 6.07[a]	6.5	12	13.5	13.6
Alveolar	14.2 / 10.8[a]	1	3	3.8	6.6
Total deposition	19 / 86.7[a]	18.5	25	26.3	30.2

*Estimated from Strum (Sturm 2020)
The ICRP model is not resolved by age.
$PM_{2.5}$ was used for calculating deposition using the ICRP model, whereas we used the data for the particle deposition for $PM_{0.1}$ from Strum
[a] Regional and total deposition for $PM_{2.5}$

7.4 Calculation of the VOC mass deposited

The VOC mass (m_{VOC}, *pg*) deposited into the respiratory system was calculated using equation (7.5).

$$m_{VOC}\ (pg) = C_p \times V_{t,\ air} \times f_{PM} \times f_{rd} \times 10^6 \tag{7.5}$$

where C_p (μg m^{-3}) is the concentration of the VOC in the aerosol, which was calculated using equation (1.1). $V_{t,air}$ (m^3) is the total volume of air inhaled in 24 h using the data in Table 7.2. The ICRP model does not consider differences in geometry of the airway due to age. Therefore, in calculating the volume of air, we assume the breathing parameters of an adult. f_{PM} is the mass fraction of $PM_{0.1}$ in $PM_{2.5}$, which we assume to be 0.01. f_{rd} is the regional particle deposition taken from Sturm or calculated using the ICRP model (Table 7.3). C_g (μg m^{-3}) was calculated using equation (7.6).

$$C_g = \frac{pM_{voc}}{RT} M_r \tag{7.6}$$

where p (Pa) is the pressure, M_{VOC} is the VOC's molar mass (g mol^{-1}), T (K) the temperature, R is the ideal gas constant (8.314 J mol^{-1} K^{-1}), and M_r is the VOC mixing ratio (ppm). We used 0.5 ppm for each VOC in the calculation. We calculated the gas-phase VOC concentration at 5, 25, and 35°C. We assume that the VOC in aerosol is in equilibrium with that in the gas phase during inhalation and transport to regions of the respiratory system.

7.5 VOC deposition as a function of aerosol composition and VOC type

VOC depositions depend on the K_ps that depend on the aerosol composition, VOC type, and environmental factors. At TSP of ~ 50 μg m^{-3}, the deposited masses of *n*-BuOH ranged from 0.10 pg (Am Sulf at 35°C) to 580 pg (SA at 5°C) (Figure 7.1). The deposited masses of 1,2-DCB at 50 μg m^{-3} of TSP ranged from 0.004 pg (Am Sulf at 35°C) to 45 pg (SA at 5°C) (Figure 7.2). Those of TCE were from 3.6×10^{-6} pg (SA at 35°C) to 0.40 pg (SA at 5°C) (Figure 7.3). The deposited masses of *n*-BuOH were comparable to that of 1,2-DCB partitioning in SA at 5°C but were ~ 10 orders of magnitude higher than that of TCE partitioning in SA at 35°C. For the partitioning into Am Sulf, their difference was seven orders of magnitude compared *n*-BuOH at 5°C to TCE at 35°C. The ratio of the mass deposited in the body from Am Sulf to those from SA ranged from 0.0043 (1,2-DCB at 5°C) to 34.5 (TCE at 35°C). Except for *n*-BuOH and TCE at 35°C, SA aerosol contained more VOCs than Am Sulf aerosol into the respiratory system.

7.6 VOC deposition by models

The total deposited mass calculated using the ICRP model was 3× higher than the model from Sturm. The lower deposition is that because the Strum's model particles within similar size range are randomly transported into the various structures, whereas the ICRP assumes uniform deposition probability. Analysis of the regional deposition of the VOCs, the ICRP model calculated a higher amount at the nasopharyngeal region (~ 7×) but were only ~ 0.5× higher in the tracheobronchial region, and ~1.5× higher in the alveolar region relative to the deposition model by Sturm. Overall, there is a good agreement between the two models at the deeper regions of the respiratory system. The highest amount of VOC

deposited was 1640 pg of *n*-BuOH partitioning onto SA at 5°C, which was estimated by ICRP model (Figure 7.1). For an adult breathing VOC- and aerosol-laden air, the Sturm's model calculated 580 pg of *n*-BuOH assuming partitioning onto organic aerosol. On the other hand, the least amount of VOC deposited into the respiratory system was that TCE was negligible onto both aerosol type at 35°C as calculated by both particle deposition models (Figure 7.3).

7.7 VOC deposition by ages and regions of the respiratory system

The total volume of air inhaled for 24 h by age is 10.5 m^3 for 5-Y, 15.8 m^3 for 10-Y, 16.9 m^3 for 15-Y, and 15.4 m^3 for an adult. We used these data to calculate the mass of inhaled PM/VOC for each age group. VOC deposition for n-BuOH was higher than for TCE and 1,2-DCB for adults. Total deposited mass for 5-Y was ~ 2.5× less than for other ages, but those for 10-Y, 15-Y, and adult were comparable. For all ages, the mass of n-BuOH at 5°C deposited into the respiratory systems was comparably higher than for other VOCs. The mass of TCE deposited at 35°C was the lowest. In general, the younger the age, the less VOC amount deposited into the deeper pulmonary region, particularly in the alveolar region. However, the mass of VOC deposition into the nasopharyngeal region for 10-Y was slightly higher than for 15-Y and adults. The mass deposited in the tracheobronchial region for 15-Y was higher than that for adults. The deposition into the nasopharyngeal region was the highest for 5-Y group as calculated by the Sturm model (59%) and ICRP model (80%) relative to the total mass deposited. Especially in the 5-Y group, the amount deposited onto the deeper regions of the respiratory system was substantially lower.

7.8 VOC deposition as a function of temperature

The VOC mass in the aerosol particles decreased as temperature increased, as depicted in the smaller experimental K_p. As the temperature rose and corresponding enhanced volatility, less VOC partitioned onto the aerosol phase. For Am Sulf and SA aerosols, the ratios of the total VOC mass at 25°C to that at 5°C for *n*-BuOH and 1,2-DCB were ~ 2 and ~ 10, respectively. At 25°C and 35°C, the ratios were ~ 4× less for 1,2-DCB and ~ 30,000× less for TCE on Am Sulf to that on SA aerosols. Differences exist between the mass of the VOC that sorb Am Sulf and SA aerosol particles. The highest amount calculated was obtained at 5°C because of the lower vapor pressure of the VOCs at this temperature. The mass of 1,2-DCB was of similar order to that of *n*-BuOH. At all temperatures, only a negligible amount of TCE partitioned onto the aerosols. The partitioning trends for all the VOC/temperature/aerosol combinations are similar since we used similar regional particle deposition. The only parameter that would vary is the mass of the VOC for each age group. As the temperature increased, the experimental K_p values for each VOC decreased. Therefore, VOCs entering the body with the aerosol decreased with an increased in temperature (Figure 7.1). Due to the high volatility of compounds, they remain in the gas phase rather than partitioning on the aerosol phase as the temperature increased. At this condition, the VOC concentration inhaled through the aerosols decreased.

Error bars for the data in Figures 7.1, 7.2, and 7.3 were omitted. We calculated the uncertainty as the propagated uncertainty using the standard deviation from the experimental K_p. Errors were propagated based on the following equations.

$$\sigma_{m_v}{}^2 = \left|\frac{\delta m_{voc}}{\delta K_p}\right|^2 \times \left|\sigma_{K_p}\right|^2, \quad (7.7)$$

which yields

$$\sigma_{m_v} = C_p \times V_{t,\,air} \times f_{PM} \times f_{rd} \times 10^6 \times \sigma_{K_p} \quad (7.8)$$

Therefore, the corresponding uncertainty is the uncertainty in determining the experimental K_p. The temperature was not included as a variable in propagating the error because we precisely controlled it, varying only by 0.01°C. The relative standard deviations were 0.2–6%.

7.9 Estimate of VOC deposition in the respiratory system due to varying TSP levels

We calculated the VOC deposition on the respiratory system based on the $PM_{2.5}$ levels in cities worldwide. We used formaldehyde as it is more environmentally relevant. We assumed that the K_p for *n*-BuOH applies due to similar polarity, and we used a formaldehyde mixing ratio of 500 ppb (Kaden et al., 2010). However, we likely underestimated the mass of formaldehyde that partitioned onto aerosol particles since formaldehyde is a reactive carbonyl compound. In aqueous saline aerosols, formaldehyde can undergo irreversible chemical reactions, mainly to oligomers of its diol form (Matubayasi et al., 2007), whereas *n*-BuOH does not. Such reactive chemistry can drastically alter the toxicity of formaldehyde in aerosol particles.

We used mixing ratios of 680 ppb for 1,2-DCB (Chin et al. 2013) and 10 ppm for TCE (Bakke et al., 2007), and we assume similar mixing ratios for all cities depicted in Table 7.4. These concentrations represent the worst-case scenario as they are among the highest measured mixing ratios in indoor or outdoor environments. We assume that the

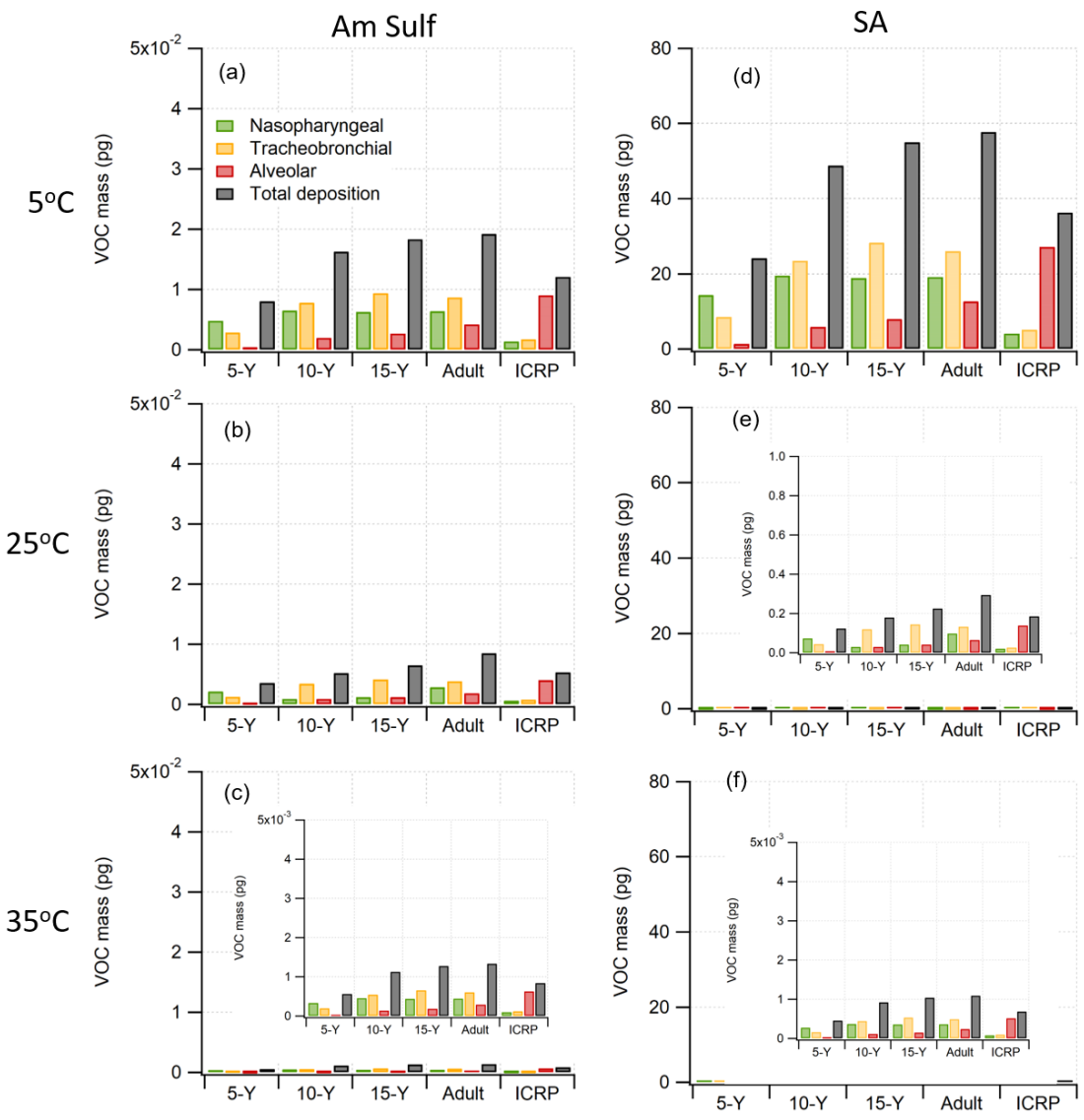

Figure 7.1 Mass accumulation of n-BuOH on Am Sulf (a, b, and c) and SA (d, e, and f) aerosols at 5, 25 and 35°C calculated from the deposition of 100 nm particles inhaled for 24 h different age groups.

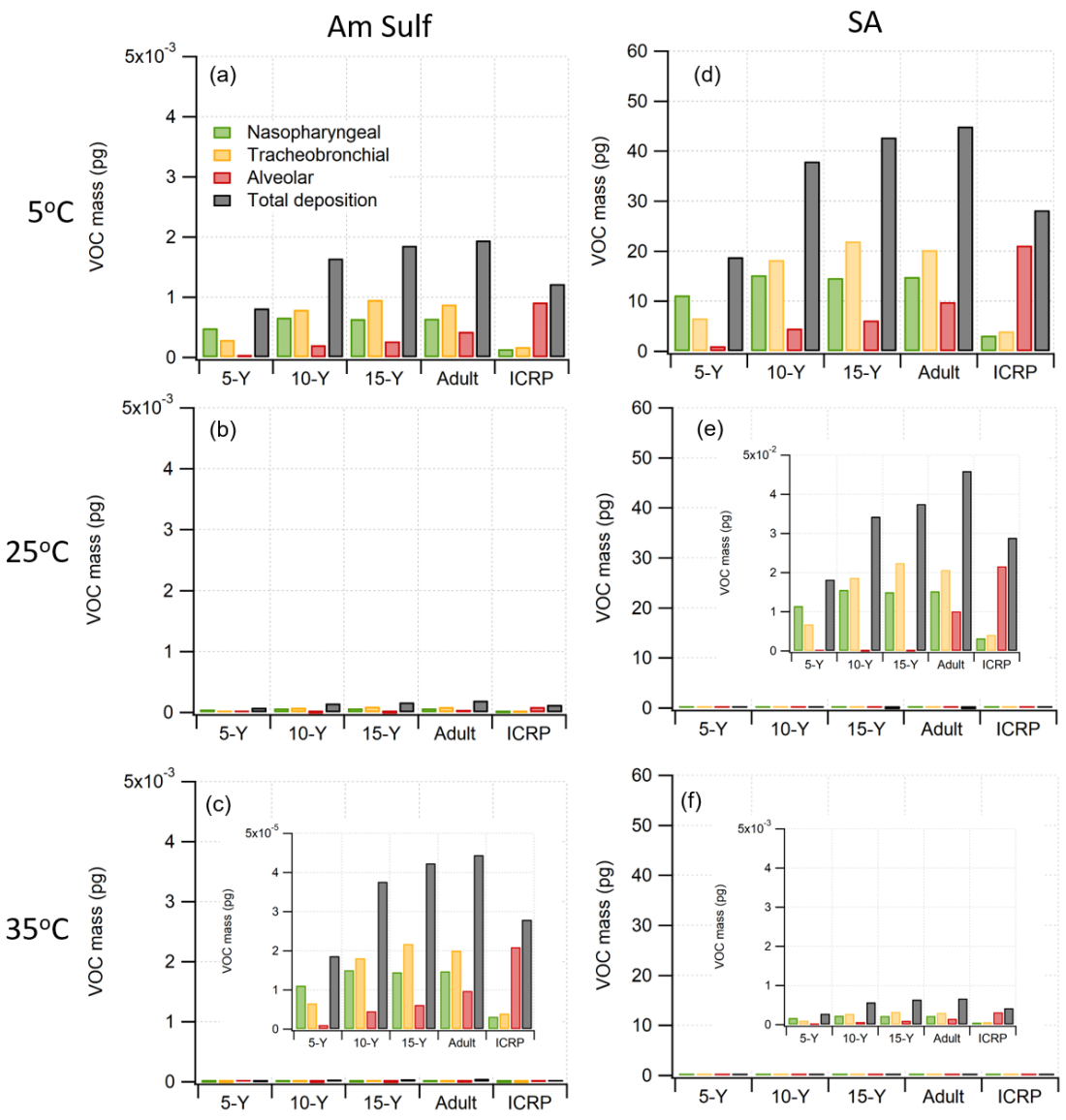

Figure 7.2 Mass accumulation of 1,2-DCB on Am Sulf (a, b, and c) and SA (d, e, and f) aerosols at 5, 25 and 35°C calculated from the deposition of 100 nm particles inhaled for 24 h by different age groups.

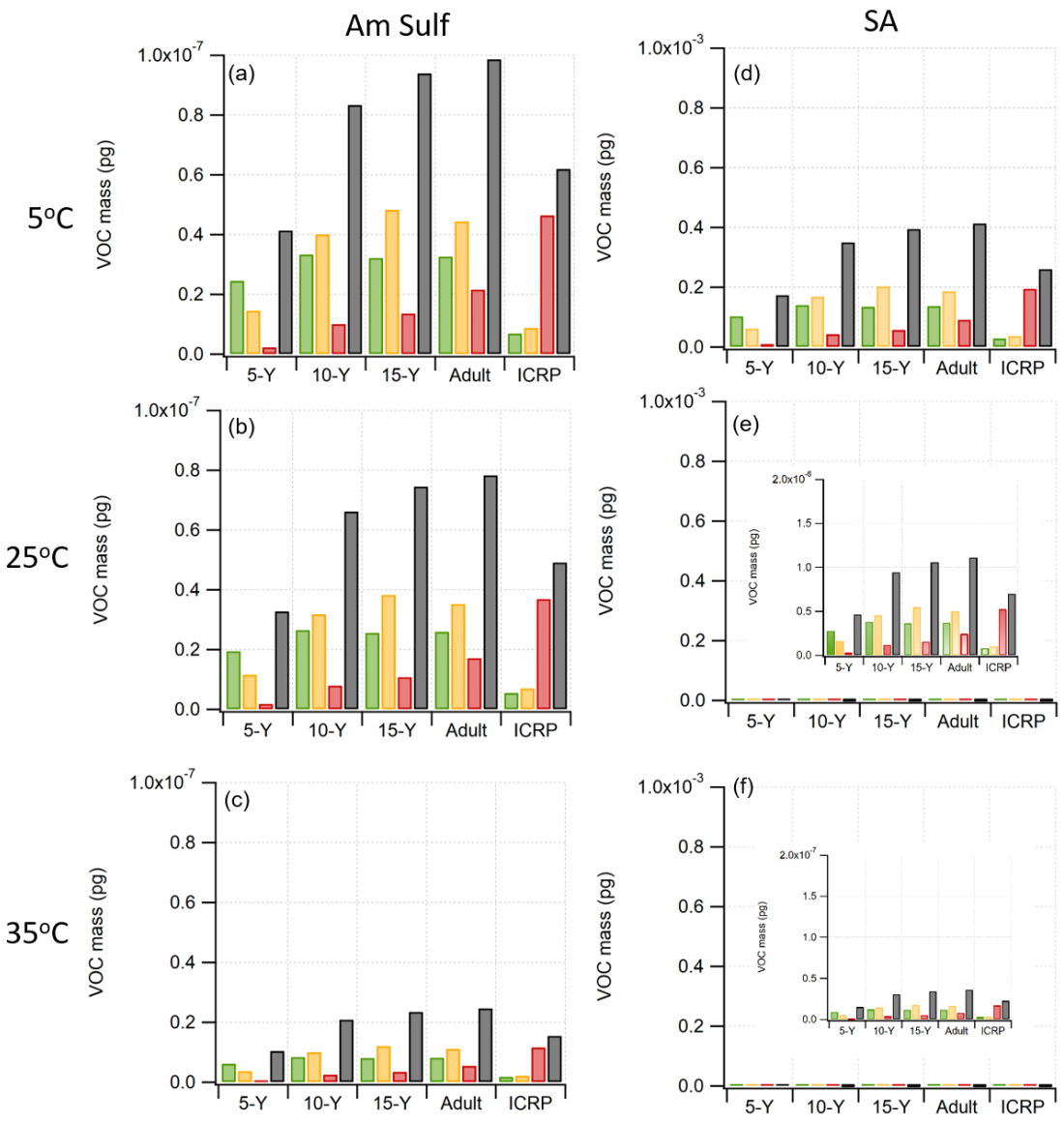

Figure 7.3 Mass accumulation of TCE on Am Sulf (a, b, and c) and SA (d, e, and f) aerosols at 5, 25 and 35°C calculated from the deposition of 100 nm particles inhaled for 24 h different age groups.

Table 7.4 Estimated VOC mass (pg) deposited in regions of the airway during a 24-h exposure at 25°C and RH ~35% using the ICRP model for $PM_{2.5}$.

		Mass (pg)					
		SA			Am Sulf		
		DF (NPL)	DF (TB)	DF (AL)	DF (NPL)	DF (TB)	DF (AL)
Formaldehyde	Seoul (max)	190	17	30	199	18	31
	Seoul (avg)	29	3	5	31	3	5
	US (avg)	11	1	2	12	1	2
	Nepal (2017)	127	11	20	134	12	21
	Niger (2017)	120	11	19	126	11	20
	World (2017)	59	5	9	62	5	10
1,2-DCB	Seoul (max)	2.1	0.2	0.3	31.2	2.7	4.9
	Seoul (avg)	0.3	0	0.1	4.8	0.4	0.8
	US (avg)	0.1	0	0	1.8	0.2	0.3
	Nepal (2017)	1.4	0.1	0.2	20.9	1.8	3.3
	Niger (2017)	1.4	0.1	0.2	19.7	1.7	3.1
	World (2017)	0.7	0.1	0.1	9.6	0.8	1.5
TCE	Seoul (max)	0	0	0	0	0	0
	Seoul (avg)	0	0	0	0	0	0
	US (avg)	0	0	0	0	0	0
	Nepal (2017)	0	0	0	0	0	0
	Niger (2017)	0	0	0	0	0	0
	World (2017)	0	0	0	0	0	0

[a]Values using the particle deposition from Sturm will be 0.7, 2, and 0.6× that for those calculated from the ICRP. We assume that the partitioning behavior for particles with median diameter of 77 nm applies to $PM_{2.5}$.
NPL, TB, and AL stand for nasopharyngeal/laryngeal, tracheobronchial, and alveolar regions, respectively.
A value of 0 is < 0.0001 pg

partitioning behavior for particles with median diameter of 77 nm applies to $PM_{2.5}$. The deposited masses into the various regions of the respiratory system had a maximum deposition of ~ 200 pg at the head airway during a 24-h exposure ignoring reduction due to the metabolism. Mass accumulation in the respiratory system will be higher for an adult engaging in light work as the data in Table 7.4 were obtained while sitting. Formaldehyde had the highest mass deposition with TCE being negligible despite the high mixing ratio (10 ppm). Formaldehyde mass exceeded that of 1,2-DCB by a factor of 89 and 6 on SA and Am Sulf aerosols, respectively. Other cities listed in Table 7.1 were not included as they have a similar $PM_{2.5}$ level to some cities listed in Table 7.4. Values using the particle deposition from Sturm will be 0.7, 2, and 0.6× for those calculated from the ICRP.

7.10 Discussion

Global VOC emission is estimated to be ~ 2.2 ± 0.48 Tg $year^{-1}$ by 2050 (Yeoman & Lewis, 2021). Increasing emissions of VOCs are due to their use as replacements for halocarbons as aerosol propellants (Yeoman & Lewis, 2021) and additives in personal care products (PCPs), exceeding those released from gasoline vehicles (Yeoman & Lewis, 2021). For many VOCs, their indoor concentration far exceeds outdoors (John D. Spengler et al., 2001). Most studies on VOCs measure total VOCs (TVOCs), representing the concentration of diverse groups of compounds present indoors and outdoors. However, TVOC concentration is not an accurate metric for assessing VOC exposure since each compound's threshold toxic concentration varies. More harmful but less abundant VOCs may drive the overall toxicity than those at high concentration but less toxic. Therefore, differentiating VOCs is essential, particularly highly toxic VOCs that may partition at significant concentrations onto aerosols. VOC in aerosol phases might be a significant

additional burden to their already high gas-phase concentration. In some homes, ethanol levels can exceed 1000 μg m^{-3} (~ 500 ppb), while 1,4-dichlorobenzene, *α*-pinene, and *d*-limonene concentrations have been detected at ~ 100 μg m^{-3} (Logue et al., 2011). This mixing ratio is similar to that we used in the calculation (0.5 ppm). Cells poorly absorbed gas-phase VOCs because of kinetic and diffusion limitations. However, the contribution of aerosol-bound VOCs that may be deposited to deeper regions of the respiratory systems studies has been understudied. To our knowledge, only Ebersviller et al. investigated the impact of aerosol-bound acrolein (Ebersviller et al., 2012a).

Although limited to three VOCs, we chose them as the parent structure to some common VOCs. We used 1,2-DCB as a surrogate of benzene, toluene, ethylbenzene, and xylene (BTEX), which are present in some household solvents and industrial formulations. We used trichloroethylene as a surrogate of chlorinated aliphatic organics; TCE is used as a degreaser and solvent (Bakke et al., 2007). In occupational settings, TCE concentration in air can be as high as ~ 45 ppm (Bakke et al., 2007). TCE and tetrachloroethylene but also vinyl chloride, methylene chloride, benzene, toluene, *cis*- and *trans*-1,2-dichloroethylene (DCE), and 1,1-DCE, were identified as the major drinking-water contaminants at Camp Lejeune (National Research Council (US) Committee on Contaminated Drinking Water at Camp Lejeune, 2009). These VOCs can migrate from subsurface soil or groundwater into the air in basements (vapor intrusion) (National Research Council (US) Committee on Contaminated Drinking Water at Camp Lejeune, 2009). If ventilation is insufficient, VOC concentration can reach high levels in basements (Du et al., 2015). We chose *n*-BuOH as representative of moderately polar compounds. BTEX concentrations measured in cities globally in outdoor environments are 154 ppt - 38

ppb for benzene, 186 ppt - 27 ppb for toluene, 30 ppt - 8 ppb for ethylbenzene, and 99 ppt - 12 ppb for xylenes (Cerón Bretón et al., 2020). The average indoor concentration in Spain is ~ 600, 969, 140, 140 ppt (Esplugues et al., 2010). In one measurement in Iran, BTEX concentration was at least 2–6× higher indoors than outdoors, with indoor mixing ratios of 5, 18, 3, 11 ppb, respectively (Hazrati et al., 2016). BTEX concentration is highly variable, but indoor concentrations exceed that outdoors (Cerón Bretón et al., 2020).

For an equal amount of aerosol and VOC concentration, *n*-BuOH (moderately polar compound) contributes ~ 98%, nonpolar aromatic such as 1,2-DCB contributes to ~ 2–3% (Figure 7.3). The weakly polar chlorinated aliphatic compound, TCE, has the highest vapor pressure than the other two VOCs and had a negligible contribution (0.001%) even at high concentration. Overall, moderately polar compounds, or presumably more polar VOCs, will drive the VOC mass in aerosols depending on the aerosol's composition. Since we used only one VOC, other VOCs of similar polarities should be investigated. In general, more VOC partitioned into Am Sulf aerosol particles (Figure 7.4) than onto organic aerosol particles; partly because Am Sulf is hygroscopic, holds more liquid water content, and dissolves more water-soluble VOCs (Ahn, Rao, & Vejerano, 2021a, 2021b).

Risk is a function of hazard and exposure; some VOCs despite being present at low concentration are more hazardous. Assuming that gas-phase VOCs have similar toxicity level, highly polar VOCs will increase the adverse health risk due to their higher partitioning onto aerosol particles. For this reason, in a VOC mixture, polar compounds such as formaldehyde may drive the toxicity of TVOCs detected indoors. In a typical commercial formulation, formaldehyde is dissolved in water (40 vol%) with methanol (6–13 vol%) as a stabilizing solution ('OSHA Fact Sheet: Formaldehyde | Occupational Safety

and Health Administration') Building materials, coatings, and combustion are the largest sources of formaldehyde indoors (Salthammer et al., 2010). Burning incense can produce formaldehyde at a concentration of ~ 300 μg m^{-3} measured in an 18.3-m^3 chamber when burning incense sticks (Baek & Jeon, 2014). Under quiescent condition, formaldehyde emission from smoking six cigarettes can reach a concentration of 234 μg m^{-3} when confined in a 30-m^3 chamber (Lee & Wang, 2004).

The amount that can partition on aerosols can be applied to formaldehyde (2.28 D) and methanol (2.87 D), which is more polar than *n*-BuOH (1.66 D) based on dipole moments. We predict more formaldehyde and methanol will partition onto organic aerosol particles than *n*-BuOH because they are relatively more polar and more soluble in water despite being more volatile. This behavior has been observed for acrolein (3.11 D), an extremely volatile VOC. Aerosols passed over acrolein vapor induce a significant adverse biological response than the pure aerosols alone (Ebersviller et al., 2012a). One plausible reason for this behavior consistent with our study is acrolein's relatively higher polarity and water solubility. However, Ebersviller and colleagues did not ascribe the enhanced toxicity to these physicochemical properties. Despite the vapor pressure of formaldehyde being ~ 3.6× higher than acrolein, we expect a significant concentration of it to partition in aerosols, specifically at higher RH levels. However, acrolein is a highly reactive *α, β*-unsaturated aldehyde that reacts with chemical and biological nucleophiles (Kehrer and Biswal, 2000). Thus, both the mass and chemical reactivity of acrolein drive the toxicity of the aerosol particles.

Formaldehyde is a highly water-soluble polar molecule with a large sticking coefficient (Toda et al., 2014). Indeed, measured formaldehyde concentration from

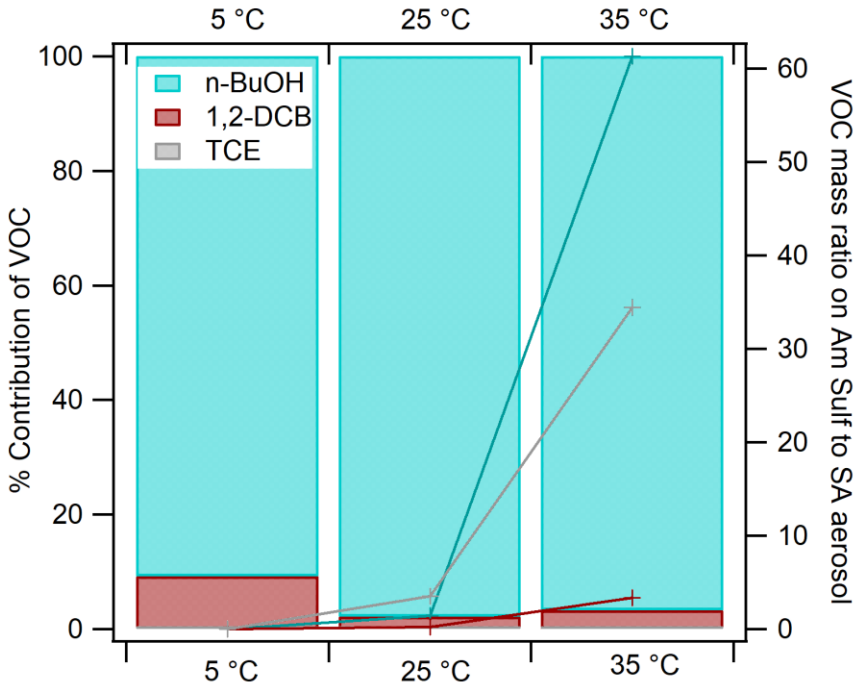

Figure 7.4 Contribution of the three VOCs to the amount deposited in the respiratory system that sorbed on model organic and inorganic aerosols. Values for the line graphs correspond to the parameter on the right axis. Values for the bar graphs correspond to the parameter on the left axis.

aerosols collected above forests in Japan, predominantly being organic, accounts for 5% of the total formaldehyde concentration (gas + aerosol) (Toda et al., 2014). This concentration is substantially higher than those expected for a VOC. Our partitioning study was measured at RH 35%. Increasing RH levels can increase the mass in the aerosols depending on the aerosol and VOC properties. Aerosol-phase concentration of formaldehyde increases with higher liquid water content in aerosol (Toda et al., 2014). At high RH level (> 90%), the measured formaldehyde mass for aerosol consisting of Am Sulf exceeds that predicted by Henry's law by two orders of magnitude (Toda et al., 2014) and as high as three orders of magnitude (Klippel & Warneck, 1980). The authors attribute this enhancement to formaldehyde oligomerizing in highly saline aerosol (Toda et al., 2014). Our data and this information suggest that VOCs' contribution, specifically those with high water solubility and more polar organic, *e.g.*, moderately polar and highly polar compounds, should be revisited as they may contribute to some of the adverse impacts of aerosols. We do not assert that only solubility and polarity will drive the partitioning of these VOCs in aerosol particles. Therefore, at similar VOC and TSP level, we expect higher mass deposition of formaldehyde than those in Table 7.4, particularly for aerosol particles containing ammonium sulfate at higher RH levels. The water solubility of chlorinated aliphatic and aromatic VOCs increases with decreasing numbers of carbon or halogen atoms (National Research Council (US) Committee on Contaminated Drinking Water at Camp Lejeune, 2009). *n*-BuOH was less affected by increasing temperature, probably because of the strong hydrogen bonding with the water molecule in the aerosol particle. Presumably, formaldehyde will behave similarly to *n*-BuOH as it forms a strong hydrogen bond with water (Ramelot et al., 1994).

VOC-specific properties and aerosol-specific properties drive the VOC mass that sorbed on aerosol. We used the data from the pure aerosol components (mixture of organic and inorganic aerosols). We assumed that each component contributes independently to the VOC that partitioned at different aerosols masses (Figure 7.5). The *x*-axis is the varying fraction of organic and inorganic aerosols. A value of 1 means that the aerosol consists of only the inorganic component (Am Sulf), and 0 means that the aerosol consists of only the organic component (SA). The mass *n*-BuOH, a moderately polar VOC, increases as the organic aerosol fraction increased. The mass of 1,2-DCB, a nonpolar VOC, increases as inorganic content increases. The composition of ambient aerosols in indoor and outdoor air is more complex. Indoors aerosols more likely contain higher organic contents, particularly those generated from cooking activities such as frying. Cooking is one indoor activity that generates a high $PM_{2.5}$ mass concentration exceeding 250 μg m^3 when using gas burners (Patel et al., 2020). The emission rate of PM_{10} and $PM_{2.5}$ during cooking can be as high as when 0.39–20.45 mg min^{-1} (Kang et al., 2019). In countries that use wood and biofuels, $PM_{2.5}$ concentrations are even higher. The data presented in Figure 7.5 should be taken for illustrative purposes only and subject to limitations. We assume that the VOC mass is contributed independently by each aerosol type. Ambient aerosols are more complex containing multiple components. Ambient aerosols are susceptible to phase separate depending on environmental conditions (Freedman, 2017, 2020; You et al., 2012). Hence, upon phase separation, different VOCs will interact differently with these components, and therefore are not simply independent contributions of their masses in aerosols. The behavior of aerosol at high RH levels, particularly above the deliquescence RH drastically differ under less humid conditions.

Total and regional deposition of $PM_{2.5}$ increases with age due to the higher air volume and variation in airway geometry, increasing particle deposition efficiency. Regional deposition of particles increases with age (Sturm, 2020). This fact is responsible for the increase in regional and total deposition of a VOC (Figure 7.1, 7.2, & 7.3). 5-Y Age group had lower inhaled aerosol-bound VOCs compared to older age groups. Deposition of $PM_{0.1}$ in the alveolar region is overestimated by the ICRP, particularly for the 5-Y group, and 2× higher for older age groups. There was a slight increase in the VOCs deposited with increasing ages. Adults appear to be more vulnerable to the risk of VOC exposure due to higher particle deposition.

Additionally, adults in homes and occupational settings perform many VOC and aerosol-generating activities in homes and occupational settings (Salthammer, 2014; Sriram et al., 2014; Lin et al., 2019). Aerosol-bound VOC had more detrimental effects on lung cells than did the PM alone (Ebersviller et al., 2012a). Aerosols can penetrate deeper into regions of the respiratory system, whereas soluble gases are removed mainly by the upper respiratory tract (Last et al., 1980). Although particles deposited into the respiratory system are removed effectively by the mucociliatory clearance, these defenses are slower relative to VOC diffusion. Hence, VOCs in aerosol may diffuse into components of the respiratory system before the aerosol can be cleared from the system (Hofmann & Sturm, 2004; Sturm, 2011, 2012). Although these VOC exposure amounts are below the guidelines, chronic exposure from aerosol-bound VOC is a concern (Bernstein et al., 2008).

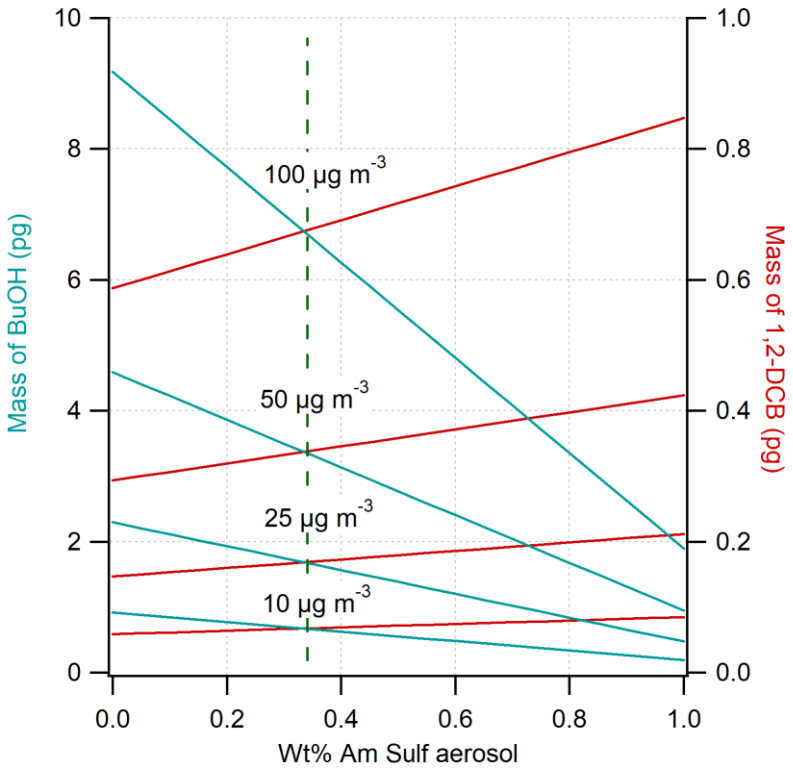

Figure 7.5 Variation of VOC loading at different $PM_{2.5}$ levels in which the fraction of $PM_{0.1}$ was assumed to be 1 wt%. The VOC mass was calculated as independent contribution from those that sorbed onto organic and inorganic aerosols. Partitioning data at 25°C were used. Intersecting lines have a similar TSP level.

CHAPTER 8

OVERALL CONCLUSIONS

This study investigated the partitioning of VOCs into the multiple environmental compartments to predict their fate and transport under various conditions. We controlled the types of soil and aerosol particles, water contents, relative humidity, and temperature to predict the partitioning coefficient of VOCs. Furthermore, the impact on the environment and human health were estimated by assuming the accidental chemical spills and emissions of contaminants.

In chapter 3, we assessed the partitioning of six polar, weakly polar or nonpolar VOCs into two types of soil under environmentally relevant conditions (*i.e.*, water-saturated condition) to find a physicochemical parameter for predicting the K_{SA} for these VOCs. The soil water content is important for the partitioning of VOCs, particularly, for highly polar VOCs and some aromatic VOCs. Partitioning of non-polar substituted aromatics was sensitive to the organic matter content in water-saturated soil. p_{sat} and K_{oa} correlated best with K_{SA} compared with the other physicochemical parameters; the K_{SA} of VOCs on soil with high organic matter content correlated well with p_{sat} and K_{oa} but not on mineral soil (clays). The VOCs partitioned into the soil by a combination of different mechanisms; associating with the soil organic matter, dissolving into the water in soil and adsorbing at the air-water interface. We applied the results of our study to calculate the air concentration of the VOCs. The air concentration for some VOCs was substantially lower

than NIOSH REL even under a worst-case scenario. Results can be used to estimate emissions for similar types of VOCs emitted from the soil to the atmosphere. For future studies, we recommend developing a separate model for predicting the partition coefficient of highly polar and nonpolar or weakly polar VOCs. Also, we recommend investigating further the impact of organic matter on the partitioning of aromatic VOCs.

In chapter 4, our results suggest that the contribution of a pure and slightly water-soluble organic fraction of aerosols to the overall VOC-aerosol partitioning was significant. Ignoring the contribution of WSOM and focusing only on the WIOM fraction of aerosols may underestimate the K_p of VOCs in modeling studies for predicting K_p. Arp and colleagues (Arp et al., 2008a) proposed a dual-phase sorption model that included both the partitioning of organics into the WIOM and the hydrophilic phase of aerosols. However, only the dissolution of organic acids and bases in aerosol water was included in the model to represent the partitioning of organics into the hydrophilic phase of aerosols, which may be oversimplified. In this case, we did not use the dual sorption model as we did not obtain data for aerosols that contained both organic and inorganic components. Later, a water-air partition coefficient model was developed for nonpolar organics partitioning into the aqueous phase of aerosols (Lohmann & Lammel, 2004; Efstathiou et al., 2016). Yet, this model looked at the effect of aerosol water on the organic partitioning and ignored the effect of WSOM. We observed that SA interacts strongly with 1,2-DCB than the inorganic or aerosol water.

In chapter 5, VOCs' environmental and health impacts need to be reexamined as a dominant class of outdoor and indoor air pollutants. We employed our previously developed method to discriminate the low mass fraction of the VOCs in aerosols to their

gas-phase concentration. Using this method enabled us to accurately determine the mass fraction of three surrogate VOCs on simple organic and inorganic aerosols. For a highly abundant VOC, its mass fraction in aerosols can reach a similar level to some SVOCs with very low abundance in the atmosphere, consistent with earlier findings. For a weakly polar organic, K_p varied linearly with the inverse of the absolute temperature. In contrast, for a moderately polar compound, *n*-BuOH, K_p varied quadratically. The sorption of the VOCs into both types of aerosol was favorable compared to some S/VOCs partitioning onto atmospheric aerosols. Using ΔH_{vap} as a proxy for and ΔH_{des} for calculating K_p cannot be generalized because of the wide differences in polarity for VOCs and the nonlinear dependence of ΔH_{des} on temperature. For weakly polar VOCs, ΔH_{vap} can be used as a surrogate for estimating K_p but may not be suitable for moderately and highly polar organics. In developing models, the nature of VOCs has to be considered, particularly for moderately/highly polar VOCs, as well as aerosol-specific properties. This study will contribute to creating models for VOCs' gas-particle partitioning that can inform in assessing their environmental and health impacts.

In chapter 6, many contaminants of concern in the environment are VOCs, which may be released into the environment from chemical spills, use and disposal of chemicals, and other activities. VOCs are subject to transfer between media. Partition coefficients are critical for predicting the fate and transport of VOCs in the environment and assessing exposure to them. In general, partitioning of the VOCs onto Am Sulf was likely via adsorption at an RH < 40%, whereas above this RH, the small amount detected on the aerosol potentially partitioned via absorption. On Am Sulf aerosol, partitioning proceeds via by adsorption due to the aerosol's higher active surface sites at low RH. It appears that

aerosol-specific properties strongly affect partitioning behavior than do VOC-specific properties. For TCE, a weakly polar compound, interacted strongly with the surface of Am Sulf aerosols *via* Van der Waal's interaction, as deemed from the higher partitioning constant compared to those of SA aerosol. The faster decline in the K_p values even at a lower RH for Am Sulf is due to water film covering the aerosol and is more hygroscopic than SA aerosol. Deactivation of active sites by water was less intense for SA aerosol because they deliquesce only at nearly saturated RH. *n*-BuOH had the highest K_p, which we attribute to its ability to form strong hydrogen bond with the adsorbed molecular water layer on both aerosols. These studies were conducted on simple model aerosols. Future studies should investigate more complex aerosols as aerosol-specific properties appear to dictate partitioning. We expect that a more complex aerosols would behave substantially different from our model aerosols. These experimental gas-particle partitioning data can be used for developing VOC-specific models. Results can be used to improve the prediction of the impacts of VOCs on health and the environment.

In chapter 7, We calculated the regional and total deposition of VOC-containing aerosols in the respiratory system using *n*-butanol, 1,2-dichlorobenzene, and trichloroethylene as proxy compounds. VOCs dominate the class of contaminants indoors and outdoors. Most exposure assessment of PM excludes the contribution of VOCs because it is assumed that only a negligible mass partitions into aerosol particles. Using experimentally-derived K_p, we calculated the mass of some VOCs deposited into the various structures of the respiratory systems. VOCs that partition in aerosol particles are likely moderately polar and aromatic organic compounds. Aliphatic chlorinated compounds had negligible contribution to TVOCs in aerosol particles due to their very low

K_p. Older age group appears to inhale more VOCs than the younger cohort. The mass of aerosol-phase VOCs inhaled for 24 h is < 200 pg which mimic a worst-case scenario. Using experimental K_p may inform inhalation toxicology, thus developing quantitative risk assessment to improve our understanding of the health impacts of VOCs in aerosols. Depending on the class of VOC, polar and nonpolar aromatics may be a significant additional burden to chronic VOC exposure. Adults, particularly those in occupational settings that uses VOCs, are vulnerable due to chronic VOC exposure. We call for more studies to understand the adverse impact of VOCs using more complex aerosols and assess their impact on human health, which to date remain scant.

REFERENCES

Abraham, M. H., Andonian-Haftvan, J., S. Whiting, G., Leo, A., & S. Taft, R. (1994). Hydrogen bonding. Part 34. The factors that influence the solubility of gases and vapours in water at 298 K, and a new method for its determination. *Journal of the Chemical Society, Perkin Transactions 2*, *0*(8), 1777–1791.

Abraham, M. H., Chadha, H. S., Whiting, G. S., & Mitchell, R. C. (1994). Hydrogen bonding. 32. An analysis of water-octanol and water-alkane partitioning and the Δlog p parameter of seiler. *Journal of Pharmaceutical Sciences*, *83*(8), 1085–1100.

Ahlberg, E., Falk, J., Eriksson, A., Holst, T., Brune, W. H., Kristensson, A., Roldin, P., & Svenningsson, B. (2017). Secondary organic aerosol from VOC mixtures in an oxidation flow reactor. *Atmospheric Environment*, *161*, 210–220.

Ahn, J., Rao, G., & Vejerano, E. (2021a). Partitioning of 1,2-dichlorobenzene onto organic and inorganic aerosols. *Environmental Chemistry*.

Ahn, J., Rao, G., & Vejerano, E. (2021b). Temperature dependence of the gas-particle partitioning of selected VOCs. *Environmental Science: Processes & Impacts*, *23*(7), 947–955.

Ahn, J., Rao, G., Vejerano, E., Ahn, J., Rao, G., & Vejerano, E. (2021). Partitioning of 1,2-dichlorobenzene onto organic and inorganic aerosols. *Environmental Chemistry*, *18*(2), 61–70.

Ansari, A. S., & Pandis, S. N. (2000). The effect of metastable equilibrium states on the partitioning of nitrate between the gas and aerosol phases. *Atmospheric Environment*, *34*(1), 157–168.

Arak Freedman, M. (2017). Phase separation in organic aerosol. *Chemical Society Reviews*, *46*(24), 7694–7705.

Arp, H. P. H., Schwarzenbach, R. P., & Goss, K.-U. (2008a). Ambient gas/particle partitioning. 1. Sorption mechanisms of apolar, polar, and ionizable organic compounds. *Environmental Science & Technology*, *42*(15), 5541–5547.

Arp, H. P. H., Schwarzenbach, R. P., & Goss, K.-U. (2008b). Ambient gas/particle partitioning. 2: The influence of particle source and temperature on sorption to dry terrestrial aerosols. *Environmental Science & Technology*, *42*(16), 5951–5957.

Asensio, D., Peñuelas, J., Filella, I., & Llusià, J. (2007). On-line screening of soil VOCs exchange responses to moisture, temperature and root presence. *Plant and Soil*, *291*(1–2), 249–261.

Baek, S.-O., & Jeon, C.-G. (2014). Distributional Characteristics of Volatile Organic Compounds in the Indoor Air of Various Office Environments. *Journal of Korean Society for Atmospheric Environment*, *30*(5), 477–491.

Bakke, B., Stewart, P. A., & Waters, M. A. (2007). Uses of and Exposure to Trichloroethylene in U.S. Industry: A Systematic Literature Review. *Journal of Occupational and Environmental Hygiene*, *4*(5), 375–390.

Batterman, S., Kulshrestha, A., & Cheng, H.-Y. (1995). Hydrocarbon vapor transport in low moisture soils. *Environmental Science & Technology*, *29*(1), 171–180.

Bernstein, J. A., Alexis, N., Bacchus, H., Bernstein, I. L., Fritz, P., Horner, E., Li, N., Mason, S., Nel, A., Oullette, J., Reijula, K., Reponen, T., Seltzer, J., Smith, A., & Tarlo, S. M. (2008). The health effects of nonindustrial indoor air pollution. *Journal of Allergy and Clinical Immunology*, *121*(3), 585–591.

Bilde, M., & Svenningsson, B. (2004). CCN activation of slightly soluble organics: The importance of small amounts of inorganic salt and particle phase. *Tellus B: Chemical and Physical Meteorology, 56*(2), 128–134.

Breus, I. P., & Mishchenko, A. A. (2006). Sorption of volatile organic contaminants by soils (a review). *Eurasian Soil Science*, *39*(12), 1271–1283.

Brooks, S. D., Wise, M. E., Cushing, M., & Tolbert, M. A. (2002). Deliquescence behavior of organic/ammonium sulfate aerosol. *Geophysical Research Letters*, *29*(19), 23-1-23–24.

Brown, D. R., Lewis, C., & Weinberger, B. I. (2015). Human exposure to unconventional natural gas development: A public health demonstration of periodic high exposure to chemical mixtures in ambient air. *Journal of Environmental Science and Health, Part A*, *50*(5), 460–472.

Brown, K., & Wherrett, A. (2018). *Bulk Density—Measurement*.

Cabbar, H. C. (1999). Effects of humidity and soil organic matter on the sorption of chlorinated methanes in synthetic humic-clay complexes. *Journal of Hazardous Materials*, *68*(3), 217–226.

Cakmak, S., Dales, R. E., Liu, L., Kauri, L. M., Lemieux, C. L., Hebbern, C., & Zhu, J. (2014). Residential exposure to volatile organic compounds and lung function:

Results from a population-based cross-sectional survey. *Environmental Pollution*, *194*, 145–151.

Cerón Bretón, J. G., Cerón Bretón, R. M., Martínez Morales, S., Kahl, J. D. W., Guarnaccia, C., Lara Severino, R. del C., Rangel Marrón, M., Ramírez Lara, E., Espinosa Fuentes, M. de la L., Uc Chi, M. P., & Sánchez, G. L. (2020). Health Risk Assessment of the Levels of BTEX in Ambient Air of One Urban Site Located in Leon, Guanajuato, Mexico during Two Climatic Seasons. *Atmosphere*, *11*(2), 165.

Chang, M., Park, H., Ha, M., Hong, Y.-C., Lim, Y.-H., Kim, Y., Kim, Y. J., Lee, D., & Ha, E.-H. (2017). The effect of prenatal TVOC exposure on birth and infantile weight: The Mothers and Children's Environmental Health study. *Pediatric Research*, *82*(3), 423.

Chemical Name Search. National Institute of Standards and Technology. Retrieved January 21, 2021, from https://webbook.nist.gov/chemistry/name-ser/

Cheng, H., Hu, E., & Hu, Y. (2012). Impact of mineral micropores on transport and fate of organic contaminants: A review. *Journal of Contaminant Hydrology*, *129*, 80–90.

Chin, J.-Y., Godwin, C., Jia, C., Robins, T., Lewis, T., Parker, E., Max, P., & Batterman, S. (2013). Concentrations and Risks of p-Dichlorobenzene in Indoor and Outdoor Air. *Indoor Air*, *23*(1), 40–49.

Chiou, C. T. (2003). *Partition and adsorption of organic contaminants in environmental systems*. John Wiley & Sons.

Choi, M. Y., & Chan, C. K. (2002). The effects of organic species on the hygroscopic behaviors of inorganic aerosols. *Environmental Science & Technology*, *36*(11), 2422–2428.

Ciobanu, V. G., Marcolli, C., Krieger, U. K., Zuend, A., & Peter, T. (2010). Efflorescence of ammonium sulfate and coated ammonium sulfate particles: Evidence for surface nucleation. *The Journal of Physical Chemistry A*, *114*(35), 9486–9495.

Costanza, M. S., & Brusseau, M. L. (2000). Contaminant vapor adsorption at the gas−water interface in soils. *Environmental Science & Technology*, *34*(1), 1–11.

Cotham, W. E., & Bidleman, T. F. (1992a). Laboratory investigations of the partitioning of organochlorine compounds between the gas phase and atmospheric aerosols on glass fiber filters. *Environmental Science & Technology*, *26*(3), 469–478.

Cotham, W. E., & Bidleman, T. F. (1992b). Laboratory investigations of the partitioning of organochlorine compounds between the gas phase and atmospheric aerosols on glass fiber filters. *Environmental Science & Technology*, *26*(3), 469–478.

Dallemagne, M. A., Huang, X. Y., & Eddingsaas, N. C. (2016). Variation in pH of model secondary organic aerosol during liquid–liquid phase separation. *The Journal of Physical Chemistry A*, *120*(18), 2868–2876.

Decesari, S., Facchini, M. C., Fuzzi, S., McFiggans, G. B., Coe, H., & Bower, K. N. (2005). The water-soluble organic component of size-segregated aerosol, cloud water and wet depositions from Jeju Island during ACE-Asia. *Atmospheric Environment*, *39*(2), 211–222.

DeJaco, R. F., Bai, P., Tsapatsis, M., & Siepmann, J. I. (2016). Adsorptive separation of 1-butanol from aqueous solutions using MFI- and FER-type zeolite frameworks: A monte carlo study. *Langmuir*, *32*(8), 2093–2101.

Ding, J., Dai, Q., Zhang, Y., Xu, J., Huangfu, Y., & Feng, Y. (2021). Air humidity affects secondary aerosol formation in different pathways. *Science of The Total Environment*, *759*, 143540.

Dockery, D. W., Pope, C. A., Xu, X., Spengler, J. D., Ware, J. H., Fay, M. E., Ferris, B. G., & Speizer, F. E. (1993). An association between air pollution and mortality in six U.S. cities. *New England Journal of Medicine*, *329*(24), 1753–1759.

Donahue, N. M., Robinson, A. L., & Pandis, S. N. (2009). Atmospheric organic particulate matter: From smoke to secondary organic aerosol. *Atmospheric Environment*, *43*(1), 94–106.

Donaldson, D. J., & Valsaraj, K. T. (2010). Adsorption and reaction of trace gas-phase organic compounds on atmospheric water film surfaces: A critical review. *Environmental Science & Technology*, *44*(3), 865–873.

Du, L., Batterman, S., Godwin, C., Rowe, Z., & Chin, J.-Y. (2015). Air exchange rates and migration of VOCs in basements and residences. *Indoor Air*, *25*(6), 598–609.

Dumanoglu, Y., Kara, M., Altiok, H., Odabasi, M., Elbir, T., & Bayram, A. (2014). Spatial and seasonal variation and source apportionment of volatile organic compounds (VOCs) in a heavily industrialized region. *Atmospheric Environment*, *98*, 168–178.

Ebersviller, S., Lichtveld, K., Sexton, K. G., Zavala, J., Lin, Y.-H., Jaspers, I., & Jeffries, H. E. (2012a). Gaseous VOCs rapidly modify particulate matter and its biological effects–Part 1: Simple VOCs and model PM. *Atmospheric Chemistry and Physics*, *12*(24), 12277–12292.

Ebersviller, S., Lichtveld, K., Sexton, K. G., Zavala, J., Lin, Y.-H., Jaspers, I., & Jeffries, H. E. (2012b). Gaseous VOCs rapidly modify particulate matter and its biological

effects – Part 2: Complex urban VOCs and model PM. *Atmos. Chem. Phys.*, *12*(24), 12293–12312.

Efstathiou, C. I., Matejovicová, J., Bieser, J., & Lammel, G. (2016). Evaluation of gas-particle partitioning in a regional air quality model for organic pollutants. *Atmospheric Chemistry and Physics; Katlenburg-Lindau*, *16*(23), 15327–15345.

Esplugues, A., Ballester, F., Estarlich, M., Llop, S., Fuentes-Leonarte, V., Mantilla, E., & Iñiguez, C. (2010). Indoor and outdoor air concentrations of BTEX and determinants in a cohort of one-year old children in Valencia, Spain. *The Science of the Total Environment*, *409*(1), 63–69.

Eum, Y., Song, I., Kim, H.-C., Leem, J.-H., & Kim, S.-Y. (2015). Computation of geographic variables for air pollution prediction models in South Korea. *Environmental Health and Toxicology*, *30*.

Finizio, A., Mackay, D., Bidleman, T., & Harner, T. (1997). Octanol-air partition coefficient as a predictor of partitioning of semi-volatile organic chemicals to aerosols. *Atmospheric Environment*, *31*(15), 2289–2296.

Fram, M. S., & Belitz, K. (2011). Occurrence and concentrations of pharmaceutical compounds in groundwater used for public drinking-water supply in California. *Science of the Total Environment*, *409*(18), 3409–3417.

Freedman, M. A. (2017). Phase separation in organic aerosol. *Chemical Society Reviews*, *46*(24), 7694–7705.

Freedman, M. A. (2020). Liquid–Liquid Phase Separation in Supermicrometer and Submicrometer Aerosol Particles. *Accounts of Chemical Research*, *53*(6), 1102–1110.

Galaon, T., & David, V. (2011). Deviation from van't Hoff dependence in RP-LC induced by tautomeric interconversion observed for four compounds. *Journal of Separation Science*, *34*(12), 1423–1428.

Gao, Y., Zhang, Y., Kamijima, M., Sakai, K., Khalequzzaman, M., Nakajima, T., Shi, R., Wang, X., Chen, D., Ji, X., Han, K., & Tian, Y. (2014). Quantitative assessments of indoor air pollution and the risk of childhood acute leukemia in Shanghai. *Environmental Pollution*, *187*, 81–89.

Goss, K. U. (1992). Effects of temperature and relative humidity on the sorption of organic vapors on quartz sand. *Environmental Science & Technology*, *26*(11), 2287–2294.

Goss, K. U. (1993a). Adsorption of organic vapors on ice and quartz sand at temperatures below 0.degree.C. *Environmental Science & Technology*, *27*(13), 2826–2830.

Goss, K.-U. (1993b). Effects of temperature and relative humidity on the sorption of organic vapors on clay minerals. *Environmental Science & Technology*, *27*(10), 2127–2132.

Goss, K.-U., & Eisenreich, S. J. (1996). Adsorption of VOCs from the gas phase to different minerals and a mineral mixture. *Environmental Science & Technology*, *30*(7), 2135–2142.

Goss, K.-U., & Eisenreich, S. J. (1997). Sorption of volatile organic compounds to particles from a combustion source at different temperatures and relative humidities. *Atmospheric Environment*, *31*(17), 2827–2834.

Goss, K.-U., & Schwarzenbach, R. P. (1998). Gas/solid and gas/liquid partitioning of organic compounds: Critical evaluation of the interpretation of equilibrium constants. *Environmental Science & Technology*, *32*(14), 2025–2032.

Goss, K.-U., & Schwarzenbach, R. P. (1999a). Quantification of the effect of humidity on the gas/mineral oxide and gas/salt adsorption of organic compounds. *Environmental Science & Technology*, *33*(22), 4073–4078.

Goss, K.-U., & Schwarzenbach, R. P. (1999b). Quantification of the effect of humidity on the gas/mineral oxide and gas/salt adsorption of organic compounds. *Environmental Science & Technology*, *33*(22), 4073–4078.

Goss, K.-U. (2004). The air/surface adsorption equilibrium of organic compounds under ambient conditions. *Critical Reviews in Environmental Science and Technology*, *34*(4), 339–389.

Gysel, M., Weingartner, E., Nyeki, S., Paulsen, D., Baltensperger, U., Galambos, I., & Kiss, G. (2004). Hygroscopic properties of water-soluble matter and humic-like organics in atmospheric fine aerosol. *Atmospheric Chemistry and Physics*, *4*(1), 35–50.

Hämeri, K., Väkevä, M., Hansson, H.-C., & Laaksonen, A. (2000). Hygroscopic growth of ultrafine ammonium sulphate aerosol measured using an ultrafine tandem differential mobility analyzer. *Journal of Geophysical Research: Atmospheres*, *105*(D17), 22231–22242.

Hamilton, J. F., Webb, P. J., Lewis, A. C., Hopkins, J. R., Smith, S., & Davy, P. (2004). Partially oxidised organic components in urban aerosol using GCXGC-TOF/MS. *Atmospheric Chemistry and Physics*, *4*(5), 1279–1290.

Han, C., Zhang, H., Gu, Q., Guo, G., Li, Y., & Li, F. (2013). Toluene sorption behavior on soil organic matter and its composition using three typical soils in China. *Environmental Earth Sciences*, *68*(3), 741–747.

Han, W. S., & Burian, S. J. (2009). Determining effective impervious area for urban hydrologic modeling. *Journal of Hydrologic Engineering*, *14*(2), 111–120.

Harner, T., & Bidleman, T. F. (1998). Octanol−Air Partition Coefficient for Describing Particle/Gas Partitioning of Aromatic Compounds in Urban Air. *Environmental Science & Technology*, *32*(10), 1494–1502.

Hazrati, S., Rostami, R., Farjaminezhad, M., & Fazlzadeh, M. (2016). Preliminary assessment of BTEX concentrations in indoor air of residential buildings and atmospheric ambient air in Ardabil, Iran. *Atmospheric Environment*, *132*, 91–97.

He, Y., Jain, P., & Yalkowsky, S. H. (2010). *Handbook of aqueous solubility data*. CRC press.

Heath, A. A., & Valsaraj, K. T. (2015). Effects of Temperature, Oxygen Level, Ionic Strength, and pH on the Reaction of Benzene with Hydroxyl Radicals at the Air–Water Interface in Comparison to the Bulk Aqueous Phase. *The Journal of Physical Chemistry A*, *119*(31), 8527–8536.

Hennigan, C. J., Bergin, M. H., Dibb, J. E., & Weber, R. J. (2008). Enhanced secondary organic aerosol formation due to water uptake by fine particles. *Geophysical Research Letters*, *35*(18).

Hennigan, C. J., Bergin, M. H., Russell, A. G., Nenes, A., & Weber, R. J. (2009). Gas/particle partitioning of water-soluble organic aerosol in Atlanta. *Atmospheric Chemistry and Physics*, *9*(11), 3613–3628.

Hinds, W. C. (1999). *Aerosol Technology: Properties, Behavior, and Measurement of Airborne Particles* (2nd ed.). John Wiley & Sons. Inc.

Hippelein, M., & Mclachlan, M. S. (1998). Soil/air partitioning of semivolatile organic compounds. 1. Method development and influence of physical-chemical properties. *Environmental Science and Technology*, *32*(2), 310–316.

Hoff, J. T., Gillham, R., Mackay, D., & Shiu, W. Y. (1993). Sorption of organic vapors at the air-water interface in a sandy aquifer material. *Environmental Science & Technology*, *27*(13), 2789–2794.

Hofmann, W., & Sturm, R. (2004). Stochastic Model of Particle Clearance in Human Bronchial Airways. *Journal of Aerosol Medicine*, *17*(1), 73–89.

Huang, T., Yu, Y., Wei, Y., Wang, H., Huang, W., & Chen, X. (2018). Spatial–seasonal characteristics and critical impact factors of PM2.5 concentration in the Beijing–Tianjin–Hebei urban agglomeration. *PLOS ONE*, *13*(9), e0201364.

Hwang, H.-M., Fiala, M. J., Wade, T. L., & Park, D. (2018). Review of pollutants in urban road dust: Part II. Organic contaminants from vehicles and road management. *International Journal of Urban Sciences*, 1–19.

Jang, M., Czoschke, N. M., & Northcross, A. L. (2004). Atmospheric organic aerosol production by heterogeneous acid-catalyzed reactions. *ChemPhysChem*, *5*(11), 1646–1661.

Jathar, S. H., Mahmud, A., Barsanti, K. C., Asher, W. E., Pankow, J. F., & Kleeman, M. J. (2016). Water uptake by organic aerosol and its influence on gas/particle partitioning of secondary organic aerosol in the United States. *Atmospheric Environment*, *129*, 142–154.

Jing, B., Wang, Z., Tan, F., Guo, Y., Tong, S., Wang, W., Zhang, Y., & Ge, M. (2018). Hygroscopic behavior of atmospheric aerosols containing nitrate salts and water-soluble organic acids. *Atmospheric Chemistry and Physics*, *18*(7), 5115–5127.

Jochum, T., Michalzik, B., Bachmann, A., Popp, J., & Frosch, T. (2015). Microbial respiration and natural attenuation of benzene contaminated soils investigated by cavity enhanced Raman multi-gas spectroscopy. *Analyst*, *140*(9), 3143–3149.

John D. Spengler, P. D., Jonathan M. Samet, M. D., & John F. McCarthy, S. D. (2001). *Indoor Air Quality Handbook*. McGraw-Hill Education. https://www.accessengineeringlibrary.com/content/book/9780074455494

Kaden, D. A., Mandin, C., Nielsen, G. D., & Wolkoff, P. (2010). Formaldehyde. In *WHO Guidelines for Indoor Air Quality: Selected Pollutants*. World Health Organization. https://www.ncbi.nlm.nih.gov/books/NBK138711/

Kang, K., Kim, H., Kim, D. D., Lee, Y. G., & Kim, T. (2019). Characteristics of cooking-generated PM10 and PM2.5 in residential buildings with different cooking and ventilation types. *The Science of the Total Environment*, *668*, 56–66.

Kawamura, K., & Bikkina, S. (2016). A review of dicarboxylic acids and related compounds in atmospheric aerosols: Molecular distributions, sources and transformation. *Atmospheric Research*, *170*, 140–160.

Kehrer, J. P., & Biswal, S. S. (2000). The molecular effects of acrolein. *Toxicological Sciences*, *57*(1), 6-15.

Khanal, O., & Shooter, D. (2004). Qualitative analysis of organics in atmospheric particulates by headspace solid phase microextraction-GC/MS. *Atmospheric Environment*, *38*(40), 6917–6925.

Kim, H., Lee, S., Moon, J.-W., & Rao, P. S. C. (2005). Gas transport of volatile organic compounds in unsaturated soils. *Soil Science Society of America Journal*, *69*(4), 990–995.

Kim, J.-H., Gan, J., Farmer, W. J., Yates, S. R., Papiernik, S. K., & Dungan, R. S. (2003). Organic matter effects on phase partition of 1, 3-dichloropropene in soil. *Journal of Agricultural and Food Chemistry*, *51*(1), 165–169.

Kim, Y.-H., & Kim, K.-H. (2015). Test on the reliability of gastight syringes as transfer/storage media for gaseous VOC analysis: The extent of VOC sorption between the inner needle and a glass wall surface. *Analytical Chemistry*, *87*(5), 3056–3063.

Klippel, W., & Warneck, P. (1980). The formaldehyde content of the atmospheric aerosol. *Atmospheric Environment (1967)*, *14*(7), 809–818. https://doi.org/10.1016/0004-6981(80)90137-7

Korea Environment Corporation. (2019). *AirKorea*. http://www.airkorea.or.kr/web

Kramer, C., & Gleixner, G. (2008). Soil organic matter in soil depth profiles: Distinct carbon preferences of microbial groups during carbon transformation. *Soil Biology and Biochemistry*, *40*(2), 425–433.

Kremser, A., Jochmann, M. A., & Schmidt, T. C. (2016). Systematic comparison of static and dynamic headspace sampling techniques for gas chromatography. *Analytical and Bioanalytical Chemistry*, *408*(24), 6567–6579.

Krieger, U. K., Marcolli, C., & Reid, J. P. (2012). Exploring the complexity of aerosol particle properties and processes using single particle techniques. *Chemical Society Reviews*, *41*(19), 6631–6662.

Kristensen, K., Bilde, M., Aalto, P. P., Petäjä, T., & Glasius, M. (2016). Denuder/filter sampling of organic acids and organosulfates at urban and boreal forest sites: Gas/particle distribution and possible sampling artifacts. *Atmospheric Environment*, *130*, 36–53.

Laskina, O., Morris, H. S., Grandquist, J. R., Qin, Z., Stone, E. A., Tivanski, A. V., & Grassian, V. H. (2015). Size matters in the water uptake and hygroscopic growth of atmospherically relevant multicomponent aerosol particles. *The Journal of Physical Chemistry A*, *119*(19), 4489–4497.

Last, J. A., Dasgupta, P. K., & Etchison, J. R. (1980). Inhalation toxicology of sodium sulfite aerosols in rats. *Toxicology and Applied Pharmacology*, *55*(2), 229–234.

Lee, S.-C., & Wang, B. (2004). Characteristics of emissions of air pollutants from burning of incense in a large environmental chamber. *Atmospheric Environment*, *38*(7), 941–951.

Lightstone, J. M., Onasch, T. B., Imre, D., & Oatis, S. (2000). Deliquescence, efflorescence, and water activity in ammonium nitrate and mixed ammonium nitrate/succinic acid microparticles. *The Journal of Physical Chemistry A*, *104*(41), 9337–9346.

Lin, C.-H., Lai, C.-H., Peng, Y.-P., Wu, P.-C., Chuang, K.-Y., Yen, T.-Y., & Xiang, Y.-K. (2019). Comparative health risk of inhaled exposure to organic solvents, toxic

metals, and hexavalent chromium from the use of spray paints in Taiwan. *Environmental Science and Pollution Research*, *26*(33), 33906–33916.

Lin, F.-Y., & MacKerell, A. D. (2017). Do halogen–hydrogen bond donor interactions dominate the favorable contribution of halogens to ligand–protein binding? *The Journal of Physical Chemistry B*, *121*(28), 6813–6821.

Liu, Q., Jing, B., Peng, C., Tong, S., Wang, W., & Ge, M. (2016). Hygroscopicity of internally mixed multi-component aerosol particles of atmospheric relevance. *Atmospheric Environment*, *125*, 69–77.

Liu, Y., Zhou, X., Wang, D., Song, C., & Liu, J. (2015). A prediction model of VOC partition coefficient in porous building materials based on adsorption potential theory. *Building and Environment*, *93*, 221–233.

Logue, J. M., McKone, T. E., Sherman, M. H., & Singer, B. C. (2011). Hazard assessment of chemical air contaminants measured in residences. *Indoor Air*, *21*(2), 92–109.

Lohmann, R., & Lammel, G. (2004). Adsorptive and absorptive contributions to the gas-particle partitioning of polycyclic aromatic hydrocarbons: State of knowledge and recommended parametrization for modeling. *Environmental Science & Technology*, *38*(14), 3793–3803.

Mai, H., Shiraiwa, M., Flagan, R. C., & Seinfeld, J. H. (2015). Under what conditions can equilibrium gas–particle partitioning be expected to hold in the atmosphere? *Environmental Science & Technology*, *49*(19), 11485–11491.

Martin, S. T. (2000). Phase transitions of aqueous atmospheric particles. *Chemical Reviews*, *100*(9), 3403–3454.

Matsumoto, K., Matsumoto, K., Mizuno, R., & Igawa, M. (2010). Volatile organic compounds in ambient aerosols. *Atmospheric Research*, *97*(1), 124–128.

Matubayasi, N., Morooka, S., Nakahara, M., & Takahashi, H. (2007). Chemical equilibrium of formaldehyde and methanediol in hot water: Free-energy analysis of the solvent effect. *Journal of Molecular Liquids*, *134*(1-3), 58-63.

McDonald, B. C., de Gouw, J. A., Gilman, J. B., Jathar, S. H., Akherati, A., Cappa, C. D., Jimenez, J. L., Lee-Taylor, J., Hayes, P. L., McKeen, S. A., Cui, Y. Y., Kim, S.-W., Gentner, D. R., Isaacman-VanWertz, G., Goldstein, A. H., Harley, R. A., Frost, G. J., Roberts, J. M., Ryerson, T. B., & Trainer, M. (2018). Volatile chemical products emerging as largest petrochemical source of urban organic emissions. *Science*, *359*(6377), 760–764.

Mead, R. N., Cala, J. M., Felix, J. D., Shimizu, M. S., Casas, M. S., Lathrope, T., Avery, G. B., Kieber, R. J., & Willey, J. D. (2017). A static headspace GC-MS/MS method for the determination of ethanol, iso-butanol, and n-butanol at nanomolar concentrations in aqueous environmental samples. *Limnology and Oceanography: Methods*, *15*(12), 1007–1014.

Miles, J. (2005). R-Squared, Adjusted R-Squared. In *Statistics in Behavioral Science*.

Misuri, A., Moreno, V. C., Quddus, N., & Cozzani, V. (2019). Lessons learnt from the impact of hurricane Harvey on the chemical and process industry. *Reliability Engineering & System Safety*, *190*, 106521.

Mo, Z., Shao, M., Lu, S., Qu, H., Zhou, M., Sun, J., & Gou, B. (2015). Process-specific emission characteristics of volatile organic compounds (VOCs) from petrochemical

facilities in the Yangtze River Delta, China. *Science of The Total Environment*, *533*(15), 422–431.

Moran, M. J., Zogorski, J. S., & Squillace, P. J. (2007). Chlorinated solvents in groundwater of the United States. *Environmental Science & Technology*, *41*(1), 74–81.

National Research Council (US) Committee on Contaminated Drinking Water at Camp Lejeune. (2009). Systemic Exposures to Volatile Organic Compounds and Factors Influencing Susceptibility to Their Effects. In *Contaminated Water Supplies at Camp Lejeune: Assessing Potential Health Effects*. National Academies Press (US). https://www.ncbi.nlm.nih.gov/books/NBK215288/

Nicole, W. (2018). Wristbands for research: Using wearable sensors to collect exposure data after Hurricane Harvey. *Environmental Health Perspectives*, *126*(4), 042001.

Nofziger, D. L. (2003). *Soil temperature changes with time and depth: Theory*. Department of Plant and Soil Sciences, Oklahoma State University, Oklahoma, USA.

Odabasi, M., Ongan, O., & Cetin, E. (2005). Quantitative analysis of volatile organic compounds (VOCs) in atmospheric particles. *Atmospheric Environment*, *39*(20), 3763–3770.

Ong, S. K., & Lion, L. W. (1991a). Effects of soil properties and moisture on the sorption of trichloroethylene vapor. *Water Research*, *25*(1), 29–36.

Ong, S. K., & Lion, L. W. (1991b). Mechanisms for trichloroethylene vapor sorption onto soil minerals. *Journal of Environmental Quality*, *20*(1), 180–188.

OSHA Fact Sheet: Formaldehyde | Occupational Safety and Health Administration. (n.d.). Retrieved May 4, 2021, from https://www.osha.gov/OshDoc/data_General_Facts/formaldehyde-factsheet.html

Pankow, J. F. (1987). Review and comparative analysis of the theories on partitioning between the gas and aerosol particulate phases in the atmosphere. *Atmospheric Environment*, *21*(11), 2275–2283.

Pankow, J. F., & Bidleman, T. F. (1991). Effects of temperature, TSP and per cent non-exchangeable material in determining the gas-particle partitioning of organic compounds. *Atmospheric Environment. Part A. General Topics*, *25*(10), 2241–2249.

Pankow, J. F. (1994). An absorption model of the gas/aerosol partitioning involved in the formation of secondary organic aerosol. *Atmospheric Environment*, *28*(2), 189–193.

Pankow, J. F. (1998). Further discussion of the octanol/air partition coefficient Koa as a correlating parameter for gas/particle partitioning coefficients. *Atmospheric Environment*, *32*(9), 1493–1497.

Patel, S., Sankhyan, S., Boedicker, E. K., DeCarlo, P. F., Farmer, D. K., Goldstein, A. H., Katz, E. F., Nazaroff, W. W., Tian, Y., Vanhanen, J., & Vance, M. E. (2020). Indoor Particulate Matter during HOMEChem: Concentrations, Size Distributions, and Exposures. *Environmental Science & Technology*, *54*(12), 7107–7116.

Peng, C., Chan, M. N., & Chan, C. K. (2001). The hygroscopic properties of dicarboxylic and multifunctional acids: Measurements and UNIFAC predictions. *Environmental Science & Technology*, *35*(22), 4495–4501.

Petersen, L. W., Moldrup, P., El-Farhan, Y. H., Jacobsen, O. H., Yamaguchi, T., & Rolston, D. E. (1995). The effect of moisture and soil texture on the adsorption of organic vapors. *Journal of Environmental Quality*, *24*(4), 752–759.

Pierce, R. H., Olney, C. E., & Felbeck, G. T. (1974). Pp′-DDT adsorption to suspended particulate matter in sea water. *Geochimica et Cosmochimica Acta*, *38*(7), 1061–1073.

Pilinis, C., Seinfeld, J. H., & Grosjean, D. (1989). Water content of atmospheric aerosols. *Atmospheric Environment (1967)*, *23*(7), 1601–1606.

Pope, C. A., Thun, M. J., Namboodiri, M. M., Dockery, D. W., Evans, J. S., Speizer, F. E., & Heath, C. W. (1995). Particulate air pollution as a predictor of mortality in a prospective study of U.S. adults. *American Journal of Respiratory and Critical Care Medicine*, *151*(3_pt_1), 669–674.

Pöschl, U. (2005). Atmospheric aerosols: Composition, transformation, climate and health effects. *Angewandte Chemie International Edition*, *44*(46), 7520–7540.

Post, E., & Henderson, J. B. (2012). *Characterization of two different clay materials by thermogravimetry (TG), differential scanning calorimetry (DSC), dilatometry (DIL) and mass Spectrometry (MS)-12215*.

Prenni, A. J., DeMott, P. J., & Kreidenweis, S. M. (2003). Water uptake of internally mixed particles containing ammonium sulfate and dicarboxylic acids. *Atmospheric Environment*, *37*(30), 4243–4251.

Qin, R., Khakzad, N., & Zhu, J. (2020). An overview of the impact of Hurricane Harvey on chemical and process facilities in Texas. *International Journal of Disaster Risk Reduction*, *45*, 101453.

Ramelot, T. A., Hu, C., Fowler, J. E., DeLeeuw, B. J., & Schaefer, H. F. (1994). Carbonyl–water hydrogen bonding: The H2CO–H2O prototype. *The Journal of Chemical Physics*, *100*(6), 4347–4354.

Ranjan, M., Presto, A. A., May, A. A., & Robinson, A. L. (2012). Temperature dependence of gasparticle partitioningof primary organic aerosol emissions from a small diesel engine. *Aerosol Science and Technology*, *46*(1), 13–21.

Rao, G., & Vejerano, E. P. (2018). Partitioning of volatile organic compounds to aerosols: A review. *Chemosphere*, *212*, 282–296.

Rivett, M. O., Wealthall, G. P., Dearden, R. A., & McAlary, T. A. (2011). Review of unsaturated-zone transport and attenuation of volatile organic compound (VOC) plumes leached from shallow source zones. *Journal of Contaminant Hydrology*, *123*(3–4), 130–156.

Rogers, R. D., McFarlane, J. C., & Cross, A. J. (1980). Adsorption and desorption of benzene in two soils and montmorillonite clay. *Environmental Science & Technology*, *14*(4), 457–460.

Rossabi, S., Choudoir, M., Helmig, D., Hueber, J., & Fierer, N. (2018). Volatile organic compound emissions from soil following wetting events. *Journal of Geophysical Research: Biogeosciences*, *123*(6), 1988–2001.

Ruzmaikin, A., Aumann, H. H., & Manning, E. M. (2014). Relative humidity in the troposphere with AIRS. *Journal of the Atmospheric Sciences*, *71*(7), 2516–2533.

Salthammer, T. (2014). Release of organic compounds and particulate matter from products, materials, and electrical devices in the indoor environment. In *Indoor Air Pollution* (pp. 1–35). Springer.

Salthammer, T. (2016). Very volatile organic compounds: An understudied class of indoor air pollutants. *Indoor Air*, *26*(1), 25–38. https://doi.org/10.1111/ina.12173

Salthammer, T., Mentese, S., & Marutzky, R. (2010). Formaldehyde in the Indoor Environment. *Chemical Reviews*, *110*(4), 2536–2572.

Sanscartier, D., Zeeb, B., Koch, I., & Reimer, K. (2009). Bioremediation of diesel-contaminated soil by heated and humidified biopile system in cold climates. *Cold Regions Science and Technology*, *55*(1), 167–173.

Saxena, P., & Hildemann, L. M. (1996). Water-soluble organics in atmospheric particles: A critical review of the literature and application of thermodynamics to identify candidate compounds. *Journal of Atmospheric Chemistry*, *24*(1), 57–109.

Schwarzenbach, R. P., Gschwend, P. M., & Imboden, D. M. (2016). *Environmental organic chemistry*. John Wiley & Sons.

Seitz, H. K., & Stickel, F. (2010). Acetaldehyde as an underestimated risk factor for cancer development: Role of genetics in ethanol metabolism. *Genes & Nutrition*, *5*(2), 121–128.

Seneviratne, S. I., Corti, T., Davin, E. L., Hirschi, M., Jaeger, E. B., Lehner, I., Orlowsky, B., & Teuling, A. J. (2010). Investigating soil moisture–climate interactions in a changing climate: A review. *Earth-Science Reviews*, *99*(3–4), 125–161.

Shih, Y., & Wu, S. (2005). Distinctive sorption mechanisms of soil organic matter and mineral components as elucidated by organic vapor uptake kinetics. *Environmental Toxicology and Chemistry: An International Journal*, *24*(11), 2827–2832.

Shiraiwa, M., & Seinfeld, J. H. (2012). Equilibration timescale of atmospheric secondary organic aerosol partitioning. *Geophysical Research Letters*, *39*(24).

Shimizu, Y., Takei, N., & Terashima, Y. (1992). Sorption of organic pollutants from vapor phase: The effects of natural solid characteristics and moisture content. *Water Science and Technology*, *26*(1–2), 79–87.

Sobanska, S., Barbillat, J., Moreau, M., Nuns, N., De Waele, I., Petitprez, D., Tobon, Y., & Bremard, C. (2015). Influence of stearic acid coating of the NaCl surface on the reactivity with NO 2 under humidity. *Physical Chemistry Chemical Physics*, *17*(16), 10963–10977.

Song, M., Marcolli, C., Krieger, U. K., Zuend, A., & Peter, T. (2012). Liquid-liquid phase separation and morphology of internally mixed dicarboxylic acids/ammonium sulfate/water particles. *Atmospheric Chemistry and Physics*, *12*(5), 2691–2712.

Sriram, K., Jefferson, A. M., Lin, G. X., Afshari, A., Zeidler-Erdely, P. C., Meighan, T. G., McKinney, W., Jackson, M., Cumpston, A., Cumpston, J. L., Leonard, H. D., Frazer, D. G., & Antonini, J. M. (2014). Neurotoxicity following acute inhalation of aerosols generated during resistance spot weld-bonding of carbon steel. *Inhalation Toxicology*, *26*(12), 720–732.

Statista. (2018). *Volume of volatile organic compounds (VOC) emissions in the U.S. from 1970 to 2016 (in 1,000 tons)*.

St.Helen, G., Jacob, P., Peng, M., Dempsey, D. A., Hammond, S. K., & Benowitz, N. L. (2014). Intake of toxic and carcinogenic volatile organic compounds from secondhand smoke in motor vehicles. *Cancer Epidemiology and Prevention Biomarkers*, *23*(12), 2774–2782.

Sturm, R. (2011). Theoretical and experimental approaches to the deposition and clearance of ultrafine carcinogens in the human respiratory tract. *Thoracic Cancer*, *2*(2), 61–68.

Sturm, R. (2012). Theoretical models of carcinogenic particle deposition and clearance in children's lungs. *Journal of Thoracic Disease*, *4*(4), 368–376.

Sturm, R. (2020). Modelling the deposition of fine particulate matter (PM2.5) in the human respiratory tract. *AME Medical Journal*, *5*(0), Article 0.

SU, S. L., Singh, D. N., & Baghini, M. S. (2014). A critical review of soil moisture measurement. *Measurement*, *54*, 92–105.

Sun, Y., Wang, Z., Fu, P., Jiang, Q., Yang, T., Li, J., & Ge, X. (2013). The impact of relative humidity on aerosol composition and evolution processes during wintertime in Beijing, China. *Atmospheric Environment*, *77*, 927–934.

Svenningsson, B., Rissler, J., Swietlicki, E., Mircea, M., Bilde, M., Facchini, M. C., Decesari, S., Fuzzi, S., Zhou, J., Mønster, J., & Rosenørn, T. (2006). Hygroscopic growth and critical supersaturations for mixed aerosol particles of inorganic and organic compounds of atmospheric relevance. *Atmospheric Chemistry and Physics*, *6*(7), 1937–1952.

Tabuchi, H. (2017, September 6). High levels of carcinogen found in Houston area after Harvey. *The New York Times*. https://www.nytimes.com/2017/09/06/us/harvey-houston-valero-benzene.html

Taheri, P., Hauffman, T., Mol, J. M. C., Flores, J. R., Hannour, F., de Wit, J. H. W., & Terryn, H. (2011). Molecular interactions of electroadsorbed carboxylic acid and

succinic anhydride monomers on zinc surfaces. *The Journal of Physical Chemistry C*, *115*(34), 17054–17067.

Tanase, M., Soare, A., David, V., & Moldoveanu, S. C. (2019). Sources of nonlinear van't Hoff temperature dependence in high-performance liquid chromatography. *ACS Omega*, *4*(22), 19808–19817.

Tang, I. N., & Munkelwitz, H. R. (1993). Composition and temperature dependence of the deliquescence properties of hygroscopic aerosols. *Atmospheric Environment. Part A. General Topics*, *27*(4), 467–473.

Tekrony, M. C., & Ahlert, R. C. (2001). Adsorption of chlorinated hydrocarbon vapors onto soil in the presence of water. *Journal of Hazardous Materials*, *84*(2–3), 135–146.

Thevenet, F., Debono, O., Rizk, M., Caron, F., Verriele, M., & Locoge, N. (2018). VOC uptakes on gypsum boards: Sorption performances and impact on indoor air quality. *Building and Environment*, *137*, 138–146.

Thibodeaux, L. J., Nadler, K. C., Valsaraj, K. T., & Reible, D. D. (1991). The effect of moisture on volatile organic chemical gas-to-particle partitioning with atmospheric aerosols—Competitive adsorption theory predictions. *Atmospheric Environment. Part A. General Topics*, *25*(8), 1649–1656.

Toda, K., Yunoki, S., Yanaga, A., Takeuchi, M., Ohira, S.-I., & Dasgupta, P. K. (2014). Formaldehyde Content of Atmospheric Aerosol. *Environmental Science & Technology*, *48*(12), 6636–6643.

US EPA. (2014a, August 18). *Volatile organic compounds' impact on indoor air quality* [Overviews and Factsheets]. US EPA. https://www.epa.gov/indoor-air-quality-iaq/volatile-organic-compounds-impact-indoor-air-quality

US EPA. (2014b, August 18). *Technical overview of volatile organic compounds* [Overviews and Factsheets]. US EPA. https://www.epa.gov/indoor-air-quality-iaq/technical-overview-volatile-organic-compounds

US EPA, O. (2016, July 19). *Particulate Matter (PM2.5) Trends* [Data and Tools]. US EPA. https://www.epa.gov/air-trends/particulate-matter-pm25-trends

USDA. (2019). *Web Soil Survey*. https://websoilsurvey.nrcs.usda.gov/app/

Vijayaraghavan, K., DenBleyker, A., Ma, L., Lindhjem, C., & Yarwood, G. (2014). Trends in on-road vehicle emissions and ambient air quality in Atlanta, Georgia, USA, from the late 1990s through 2009. *Journal of the Air & Waste Management Association*, *64*(7), 808–816.

Volkamer, R., Martini, F. S., Molina, L. T., Salcedo, D., Jimenez, J. L., & Molina, M. J. (2007). A missing sink for gas-phase glyoxal in Mexico City: Formation of secondary organic aerosol. *Geophysical Research Letters*, *34*(19).

Wang, X., Jing, B., Tan, F., Ma, J., Zhang, Y., & Ge, M. (2017). Hygroscopic behavior and chemical composition evolution of internally mixed aerosols composed of oxalic acid and ammonium sulfate. *Atmospheric Chemistry and Physics*, *17*(20), 12797–12812.

Wang, Z., Xie, Z., Möller, A., Mi, W., Wolschke, H., & Ebinghaus, R. (2014). Atmospheric concentrations and gas/particle partitioning of neutral poly- and perfluoroalkyl substances in northern German coast. *Atmospheric Environment*, *95*, 207–213.

Wei, W., Cheng, S., Li, G., Wang, G., & Wang, H. (2014). Characteristics of volatile organic compounds (VOCs) emitted from a petroleum refinery in Beijing, China. *Atmospheric Environment*, *89*, 358–366.

Wei, W., Mandin, C., Blanchard, O., Mercier, F., Pelletier, M., Le Bot, B., Glorennec, P., & Ramalho, O. (2016a). Temperature dependence of the particle/gas partition coefficient: An application to predict indoor gas-phase concentrations of semi-volatile organic compounds. *Science of the Total Environment*, *563*, 506–512.

Weschler, C. J., & Nazaroff, W. W. (2010). SVOC partitioning between the gas phase and settled dust indoors. *Atmospheric Environment*, *44*(30), 3609-3620.

Wex, H., Ziese, M., Kiselev, A., Henning, S., & Stratmann, F. (2007). Deliquescence and hygroscopic growth of succinic acid particles measured with LACIS. *Geophysical Research Letters*, *34*(17).

World Development Indicators. Retrieved January 15, 2021, from https://data.worldbank.org/indicator/EN.ATM.PM25.MC.M3?end=2017&most_recent_value_desc=true&start=2009&view=chart

World's Most Polluted Cities in 2020—PM2.5 Ranking | AirVisual. (n.d.). Retrieved March 25, 2021, from https://www.iqair.com/us/world-most-polluted-cities

Wu, L., Li, X., & Ro, C.-U. (2019). Hygroscopic behavior of ammonium sulfate, ammonium nitrate, and their mixture particles. *Asian Journal of Atmospheric Environment*, *13*(3), 196–211.

Yeoman, A. M., & Lewis, A. C. (2021). Global emissions of VOCs from compressed aerosol products. *Elementa: Science of the Anthropocene*, *9*(00177).

You, Y., Renbaum-Wolff, L., Carreras-Sospedra, M., Hanna, S. J., Hiranuma, N., Kamal, S., Smith, M. L., Zhang, X., Weber, R. J., Shilling, J. E., Dabdub, D., Martin, S. T., & Bertram, A. K. (2012). Images reveal that atmospheric particles can undergo liquid–liquid phase separations. *Proceedings of the National Academy of Sciences*, *109*(33), 13188–13193.

You, Y., Smith, M. L., Song, M., Martin, S. T., & Bertram, A. K. (2014). Liquid–liquid phase separation in atmospherically relevant particles consisting of organic species and inorganic salts. *International Reviews in Physical Chemistry*, *33*(1), 43–77.

Zannetti, P. (2013). *Air pollution modeling: Theories, computational methods and available software*. Springer Science & Business Media.

Zhang, X., Liu, J., Parker, E. T., Hayes, P. L., Jimenez, J. L., Gouw, J. A. de, Flynn, J. H., Grossberg, N., Lefer, B. L., & Weber, R. J. (2012). On the gas-particle partitioning of soluble organic aerosol in two urban atmospheres with contrasting emissions: 1. Bulk water-soluble organic carbon. *Journal of Geophysical Research: Atmospheres*, *117*(D21).

Zhu, Q., Zheng, M., Liu, G., Zhang, X., Dong, S., Gao, L., & Liang, Y. (2017). Particle size distribution and gas–particle partitioning of polychlorinated biphenyls in the atmosphere in Beijing, China. *Environmental Science and Pollution Research*, *24*(2), 1389-1396.

APPENDIX A

PRINTABLE AUTHORSHIP LICENSE

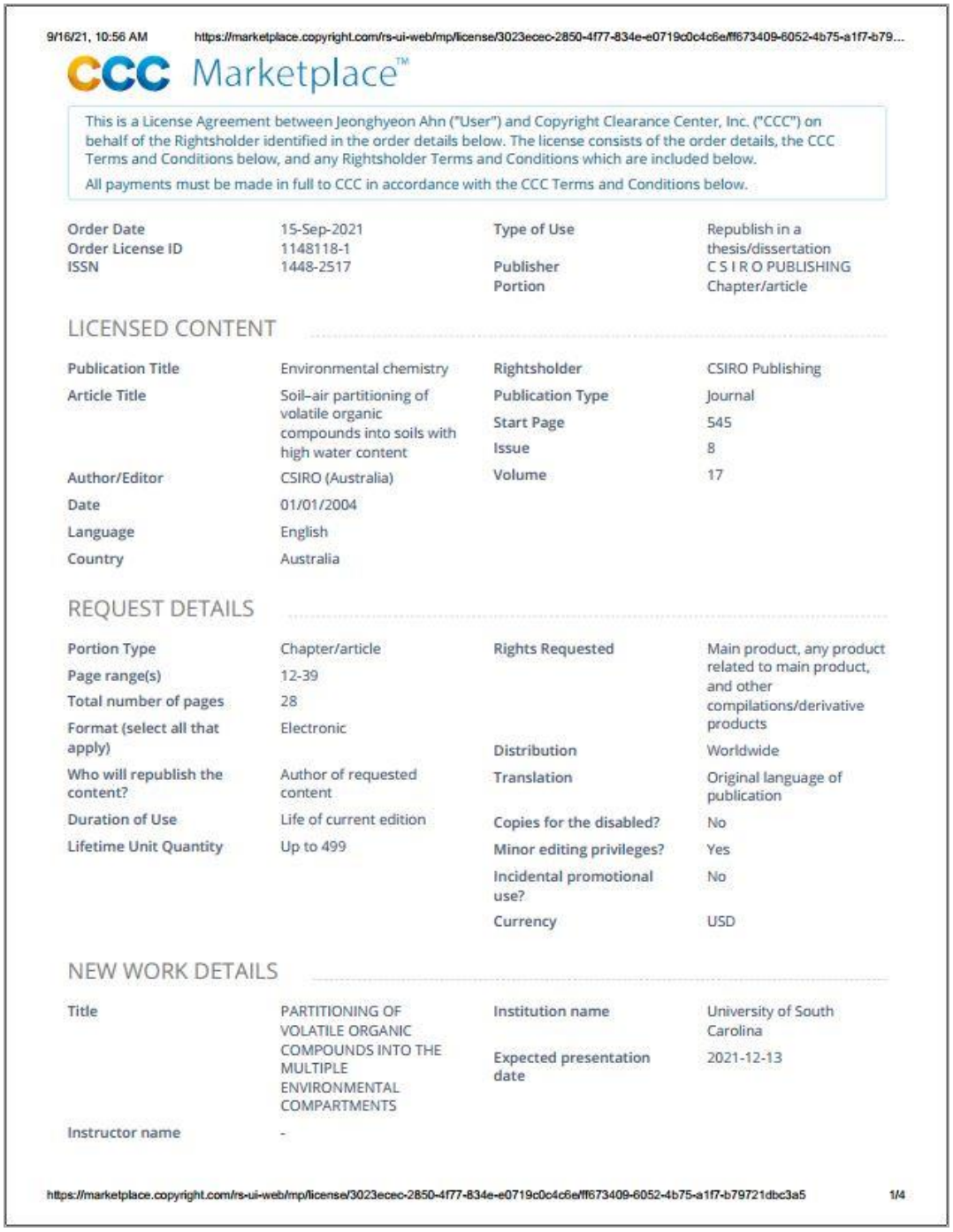

9/16/21, 10:56 AM https://marketplace.copyright.com/rs-ui-web/mp/license/3023ecec-2850-4f77-834e-e0719c0c4c6e/ff673409-6052-4b75-a1f7-b79...

CCC Marketplace™

This is a License Agreement between Jeonghyeon Ahn ("User") and Copyright Clearance Center, Inc. ("CCC") on behalf of the Rightsholder identified in the order details below. The license consists of the order details, the CCC Terms and Conditions below, and any Rightsholder Terms and Conditions which are included below.

All payments must be made in full to CCC in accordance with the CCC Terms and Conditions below.

Order Date	15-Sep-2021	Type of Use	Republish in a thesis/dissertation
Order License ID	1148118-1		
ISSN	1448-2517	Publisher	C S I R O PUBLISHING
		Portion	Chapter/article

LICENSED CONTENT

Publication Title	Environmental chemistry	Rightsholder	CSIRO Publishing
Article Title	Soil–air partitioning of volatile organic compounds into soils with high water content	Publication Type	Journal
		Start Page	545
		Issue	8
Author/Editor	CSIRO (Australia)	Volume	17
Date	01/01/2004		
Language	English		
Country	Australia		

REQUEST DETAILS

Portion Type	Chapter/article	Rights Requested	Main product, any product related to main product, and other compilations/derivative products
Page range(s)	12-39		
Total number of pages	28		
Format (select all that apply)	Electronic	Distribution	Worldwide
Who will republish the content?	Author of requested content	Translation	Original language of publication
Duration of Use	Life of current edition	Copies for the disabled?	No
Lifetime Unit Quantity	Up to 499	Minor editing privileges?	Yes
		Incidental promotional use?	No
		Currency	USD

NEW WORK DETAILS

Title	PARTITIONING OF VOLATILE ORGANIC COMPOUNDS INTO THE MULTIPLE ENVIRONMENTAL COMPARTMENTS	Institution name	University of South Carolina
		Expected presentation date	2021-12-13
Instructor name	-		

https://marketplace.copyright.com/rs-ui-web/mp/license/3023ecec-2850-4f77-834e-e0719c0c4c6e/ff673409-6052-4b75-a1f7-b79721dbc3a5 1/4

ADDITIONAL DETAILS

Order reference number	N/A	The requesting person / organization to appear on the license	Jeonghyeon Ahn

REUSE CONTENT DETAILS

Title, description or numeric reference of the portion(s)	PARTITIONING OF VOLATILE ORGANIC COMPOUNDS INTO THE MULTIPLE ENVIRONMENTAL COMPARTMENTS	Title of the article/chapter the portion is from	Soil–air partitioning of volatile organic compounds into soils with high water content
Editor of portion(s)	Ahn, Jeonghyeon; Rao, Guiying; Mamun, Mustafa; Vejerano, Eric P.	Author of portion(s)	Ahn, Jeonghyeon; Rao, Guiying; Mamun, Mustafa; Vejerano, Eric P.
Volume of serial or monograph	17	Issue, if republishing an article from a serial	8
Page or page range of portion	545	Publication date of portion	2020-01-01

CCC Terms and Conditions

1. Description of Service; Defined Terms. This Republication License enables the User to obtain licenses for republication of one or more copyrighted works as described in detail on the relevant Order Confirmation (the "Work(s)"). Copyright Clearance Center, Inc. ("CCC") grants licenses through the Service on behalf of the rightsholder identified on the Order Confirmation (the "Rightsholder"). "Republication", as used herein, generally means the inclusion of a Work, in whole or in part, in a new work or works, also as described on the Order Confirmation. "User", as used herein, means the person or entity making such republication.

2. The terms set forth in the relevant Order Confirmation, and any terms set by the Rightsholder with respect to a particular Work, govern the terms of use of Works in connection with the Service. By using the Service, the person transacting for a republication license on behalf of the User represents and warrants that he/she/it (a) has been duly authorized by the User to accept, and hereby does accept, all such terms and conditions on behalf of User, and (b) shall inform User of all such terms and conditions. In the event such person is a "freelancer" or other third party independent of User and CCC, such party shall be deemed jointly a "User" for purposes of these terms and conditions. In any event, User shall be deemed to have accepted and agreed to all such terms and conditions if User republishes the Work in any fashion.

3. Scope of License; Limitations and Obligations.

   3.1. All Works and all rights therein, including copyright rights, remain the sole and exclusive property of the Rightsholder. The license created by the exchange of an Order Confirmation (and/or any invoice) and payment by User of the full amount set forth on that document includes only those rights expressly set forth in the Order Confirmation and in these terms and conditions, and conveys no other rights in the Work(s) to User. All rights not expressly granted are hereby reserved.

   3.2. General Payment Terms: You may pay by credit card or through an account with us payable at the end of the month. If you and we agree that you may establish a standing account with CCC, then the following terms apply: Remit Payment to: Copyright Clearance Center, 29118 Network Place, Chicago, IL 60673-1291. Payments Due: Invoices are payable upon their delivery to you (or upon our notice to you that they are available to you for downloading). After 30 days, outstanding amounts will be subject to a service charge of 1-1/2% per month or, if less, the maximum rate allowed by applicable law. Unless otherwise specifically set forth in the Order Confirmation or in a separate written agreement signed by CCC, invoices are due

and payable on "net 30" terms. While User may exercise the rights licensed immediately upon issuance of the Order Confirmation, the license is automatically revoked and is null and void, as if it had never been issued, if complete payment for the license is not received on a timely basis either from User directly or through a payment agent, such as a credit card company.

3.3. Unless otherwise provided in the Order Confirmation, any grant of rights to User (i) is "one-time" (including the editions and product family specified in the license), (ii) is non-exclusive and non-transferable and (iii) is subject to any and all limitations and restrictions (such as, but not limited to, limitations on duration of use or circulation) included in the Order Confirmation or invoice and/or in these terms and conditions. Upon completion of the licensed use, User shall either secure a new permission for further use of the Work(s) or immediately cease any new use of the Work(s) and shall render inaccessible (such as by deleting or by removing or severing links or other locators) any further copies of the Work (except for copies printed on paper in accordance with this license and still in User's stock at the end of such period).

3.4. In the event that the material for which a republication license is sought includes third party materials (such as photographs, illustrations, graphs, inserts and similar materials) which are identified in such material as having been used by permission, User is responsible for identifying, and seeking separate licenses (under this Service or otherwise) for, any of such third party materials; without a separate license, such third party materials may not be used.

3.5. Use of proper copyright notice for a Work is required as a condition of any license granted under the Service. Unless otherwise provided in the Order Confirmation, a proper copyright notice will read substantially as follows: "Republished with permission of [Rightsholder's name], from [Work's title, author, volume, edition number and year of copyright]; permission conveyed through Copyright Clearance Center, Inc. " Such notice must be provided in a reasonably legible font size and must be placed either immediately adjacent to the Work as used (for example, as part of a by-line or footnote but not as a separate electronic link) or in the place where substantially all other credits or notices for the new work containing the republished Work are located. Failure to include the required notice results in loss to the Rightsholder and CCC, and the User shall be liable to pay liquidated damages for each such failure equal to twice the use fee specified in the Order Confirmation, in addition to the use fee itself and any other fees and charges specified.

3.6. User may only make alterations to the Work if and as expressly set forth in the Order Confirmation. No Work may be used in any way that is defamatory, violates the rights of third parties (including such third parties' rights of copyright, privacy, publicity, or other tangible or intangible property), or is otherwise illegal, sexually explicit or obscene. In addition, User may not conjoin a Work with any other material that may result in damage to the reputation of the Rightsholder. User agrees to inform CCC if it becomes aware of any infringement of any rights in a Work and to cooperate with any reasonable request of CCC or the Rightsholder in connection therewith.

4. Indemnity. User hereby indemnifies and agrees to defend the Rightsholder and CCC, and their respective employees and directors, against all claims, liability, damages, costs and expenses, including legal fees and expenses, arising out of any use of a Work beyond the scope of the rights granted herein, or any use of a Work which has been altered in any unauthorized way by User, including claims of defamation or infringement of rights of copyright, publicity, privacy or other tangible or intangible property.

5. Limitation of Liability. UNDER NO CIRCUMSTANCES WILL CCC OR THE RIGHTSHOLDER BE LIABLE FOR ANY DIRECT, INDIRECT, CONSEQUENTIAL OR INCIDENTAL DAMAGES (INCLUDING WITHOUT LIMITATION DAMAGES FOR LOSS OF BUSINESS PROFITS OR INFORMATION, OR FOR BUSINESS INTERRUPTION) ARISING OUT OF THE USE OR INABILITY TO USE A WORK, EVEN IF ONE OF THEM HAS BEEN ADVISED OF THE POSSIBILITY OF SUCH DAMAGES. In any event, the total liability of the Rightsholder and CCC (including their respective employees and directors) shall not exceed the total amount actually paid by User for this license. User assumes full liability for the actions and omissions of its principals, employees, agents, affiliates, successors and assigns.

6. Limited Warranties. THE WORK(S) AND RIGHT(S) ARE PROVIDED "AS IS". CCC HAS THE RIGHT TO GRANT TO USER

THE RIGHTS GRANTED IN THE ORDER CONFIRMATION DOCUMENT. CCC AND THE RIGHTSHOLDER DISCLAIM ALL OTHER WARRANTIES RELATING TO THE WORK(S) AND RIGHT(S), EITHER EXPRESS OR IMPLIED, INCLUDING WITHOUT LIMITATION IMPLIED WARRANTIES OF MERCHANTABILITY OR FITNESS FOR A PARTICULAR PURPOSE. ADDITIONAL RIGHTS MAY BE REQUIRED TO USE ILLUSTRATIONS, GRAPHS, PHOTOGRAPHS, ABSTRACTS, INSERTS OR OTHER PORTIONS OF THE WORK (AS OPPOSED TO THE ENTIRE WORK) IN A MANNER CONTEMPLATED BY USER; USER UNDERSTANDS AND AGREES THAT NEITHER CCC NOR THE RIGHTSHOLDER MAY HAVE SUCH ADDITIONAL RIGHTS TO GRANT.

7. Effect of Breach. Any failure by User to pay any amount when due, or any use by User of a Work beyond the scope of the license set forth in the Order Confirmation and/or these terms and conditions, shall be a material breach of the license created by the Order Confirmation and these terms and conditions. Any breach not cured within 30 days of written notice thereof shall result in immediate termination of such license without further notice. Any unauthorized (but licensable) use of a Work that is terminated immediately upon notice thereof may be liquidated by payment of the Rightsholder's ordinary license price therefor; any unauthorized (and unlicensable) use that is not terminated immediately for any reason (including, for example, because materials containing the Work cannot reasonably be recalled) will be subject to all remedies available at law or in equity, but in no event to a payment of less than three times the Rightsholder's ordinary license price for the most closely analogous licensable use plus Rightsholder's and/or CCC's costs and expenses incurred in collecting such payment.

8. Miscellaneous.

   8.1. User acknowledges that CCC may, from time to time, make changes or additions to the Service or to these terms and conditions, and CCC reserves the right to send notice to the User by electronic mail or otherwise for the purposes of notifying User of such changes or additions; provided that any such changes or additions shall not apply to permissions already secured and paid for.

   8.2. Use of User-related information collected through the Service is governed by CCC's privacy policy, available online here:**https://marketplace.copyright.com/rs-ui-web/mp/privacy-policy**

   8.3. The licensing transaction described in the Order Confirmation is personal to User. Therefore, User may not assign or transfer to any other person (whether a natural person or an organization of any kind) the license created by the Order Confirmation and these terms and conditions or any rights granted hereunder; provided, however, that User may assign such license in its entirety on written notice to CCC in the event of a transfer of all or substantially all of User's rights in the new material which includes the Work(s) licensed under this Service.

   8.4. No amendment or waiver of any terms is binding unless set forth in writing and signed by the parties. The Rightsholder and CCC hereby object to any terms contained in any writing prepared by the User or its principals, employees, agents or affiliates and purporting to govern or otherwise relate to the licensing transaction described in the Order Confirmation, which terms are in any way inconsistent with any terms set forth in the Order Confirmation and/or in these terms and conditions or CCC's standard operating procedures, whether such writing is prepared prior to, simultaneously with or subsequent to the Order Confirmation, and whether such writing appears on a copy of the Order Confirmation or in a separate instrument.

   8.5. The licensing transaction described in the Order Confirmation document shall be governed by and construed under the law of the State of New York, USA, without regard to the principles thereof of conflicts of law. Any case, controversy, suit, action, or proceeding arising out of, in connection with, or related to such licensing transaction shall be brought, at CCC's sole discretion, in any federal or state court located in the County of New York, State of New York, USA, or in any federal or state court whose geographical jurisdiction covers the location of the Rightsholder set forth in the Order Confirmation. The parties expressly submit to the personal jurisdiction and venue of each such federal or state court.If you have any comments or questions about the Service or Copyright Clearance Center, please contact us at 978-750-8400 or send an e-mail to **support@copyright.com**.

v 1.1

CCC Marketplace™

This is a License Agreement between Jeonghyeon Ahn ("User") and Copyright Clearance Center, Inc. ("CCC") on behalf of the Rightsholder identified in the order details below. The license consists of the order details, the CCC Terms and Conditions below, and any Rightsholder Terms and Conditions which are included below.

All payments must be made in full to CCC in accordance with the CCC Terms and Conditions below.

Order Date	15-Sep-2021	Type of Use	Republish in a thesis/dissertation
Order License ID	1148118-2		
ISSN	1448-2517	Publisher	C S I R O PUBLISHING
		Portion	Chapter/article

LICENSED CONTENT

Publication Title	Environmental chemistry	Rightsholder	CSIRO Publishing
Article Title	Partitioning of 1,2-dichlorobenzene onto organic and inorganic aerosols	Publication Type	Journal
		Start Page	61
		Issue	2
Author/Editor	CSIRO (Australia)	Volume	18
Date	01/01/2004		
Language	English		
Country	Australia		

REQUEST DETAILS

Portion Type	Chapter/article	Rights Requested	Main product, any product related to main product, and other compilations/derivative products
Page range(s)	40-63		
Total number of pages	24		
Format (select all that apply)	Electronic		
		Distribution	Worldwide
Who will republish the content?	Author of requested content	Translation	Original language of publication
Duration of Use	Life of current edition	Copies for the disabled?	No
Lifetime Unit Quantity	Up to 499	Minor editing privileges?	Yes
		Incidental promotional use?	No
		Currency	USD

NEW WORK DETAILS

Title	PARTITIONING OF VOLATILE ORGANIC COMPOUNDS INTO THE MULTIPLE ENVIRONMENTAL COMPARTMENTS	Institution name	University of South Carolina
		Expected presentation date	2021-12-13
Instructor name	-		

ADDITIONAL DETAILS

Order reference number	N/A	The requesting person / organization to appear on the license	Jeonghyeon Ahn

REUSE CONTENT DETAILS

Title, description or numeric reference of the portion(s)	PARTITIONING OF VOLATILE ORGANIC COMPOUNDS INTO THE MULTIPLE ENVIRONMENTAL COMPARTMENTS	Title of the article/chapter the portion is from	Partitioning of 1,2-dichlorobenzene onto organic and inorganic aerosols
		Author of portion(s)	Ahn, Jeonghyeon; Rao, Guiying; Vejerano, Eric
Editor of portion(s)	Ahn, Jeonghyeon; Rao, Guiying; Vejerano, Eric	Issue, if republishing an article from a serial	2
Volume of serial or monograph	18	Publication date of portion	2021-01-01
Page or page range of portion	61		

CCC Terms and Conditions

1. Description of Service; Defined Terms. This Republication License enables the User to obtain licenses for republication of one or more copyrighted works as described in detail on the relevant Order Confirmation (the "Work(s)"). Copyright Clearance Center, Inc. ("CCC") grants licenses through the Service on behalf of the rightsholder identified on the Order Confirmation (the "Rightsholder"). "Republication", as used herein, generally means the inclusion of a Work, in whole or in part, in a new work or works, also as described on the Order Confirmation. "User", as used herein, means the person or entity making such republication.

2. The terms set forth in the relevant Order Confirmation, and any terms set by the Rightsholder with respect to a particular Work, govern the terms of use of Works in connection with the Service. By using the Service, the person transacting for a republication license on behalf of the User represents and warrants that he/she/it (a) has been duly authorized by the User to accept, and hereby does accept, all such terms and conditions on behalf of User, and (b) shall inform User of all such terms and conditions. In the event such person is a "freelancer" or other third party independent of User and CCC, such party shall be deemed jointly a "User" for purposes of these terms and conditions. In any event, User shall be deemed to have accepted and agreed to all such terms and conditions if User republishes the Work in any fashion.

3. Scope of License; Limitations and Obligations.

   3.1. All Works and all rights therein, including copyright rights, remain the sole and exclusive property of the Rightsholder. The license created by the exchange of an Order Confirmation (and/or any invoice) and payment by User of the full amount set forth on that document includes only those rights expressly set forth in the Order Confirmation and in these terms and conditions, and conveys no other rights in the Work(s) to User. All rights not expressly granted are hereby reserved.

   3.2. General Payment Terms: You may pay by credit card or through an account with us payable at the end of the month. If you and we agree that you may establish a standing account with CCC, then the following terms apply: Remit Payment to: Copyright Clearance Center, 29118 Network Place, Chicago, IL 60673-1291. Payments Due: Invoices are payable upon their delivery to you (or upon our notice to you that they are available to you for downloading). After 30 days, outstanding amounts will be subject to a service charge of 1-1/2% per month or, if less, the maximum rate allowed by applicable law. Unless otherwise specifically set forth in the Order Confirmation or in a separate written agreement signed by CCC, invoices are due and payable on "net 30" terms. While User may exercise the rights licensed immediately upon issuance of

the Order Confirmation, the license is automatically revoked and is null and void, as if it had never been issued, if complete payment for the license is not received on a timely basis either from User directly or through a payment agent, such as a credit card company.

3.3. Unless otherwise provided in the Order Confirmation, any grant of rights to User (i) is "one-time" (including the editions and product family specified in the license), (ii) is non-exclusive and non-transferable and (iii) is subject to any and all limitations and restrictions (such as, but not limited to, limitations on duration of use or circulation) included in the Order Confirmation or invoice and/or in these terms and conditions. Upon completion of the licensed use, User shall either secure a new permission for further use of the Work(s) or immediately cease any new use of the Work(s) and shall render inaccessible (such as by deleting or by removing or severing links or other locators) any further copies of the Work (except for copies printed on paper in accordance with this license and still in User's stock at the end of such period).

3.4. In the event that the material for which a republication license is sought includes third party materials (such as photographs, illustrations, graphs, inserts and similar materials) which are identified in such material as having been used by permission, User is responsible for identifying, and seeking separate licenses (under this Service or otherwise) for, any of such third party materials; without a separate license, such third party materials may not be used.

3.5. Use of proper copyright notice for a Work is required as a condition of any license granted under the Service. Unless otherwise provided in the Order Confirmation, a proper copyright notice will read substantially as follows: "Republished with permission of [Rightsholder's name], from [Work's title, author, volume, edition number and year of copyright]; permission conveyed through Copyright Clearance Center, Inc. " Such notice must be provided in a reasonably legible font size and must be placed either immediately adjacent to the Work as used (for example, as part of a by-line or footnote but not as a separate electronic link) or in the place where substantially all other credits or notices for the new work containing the republished Work are located. Failure to include the required notice results in loss to the Rightsholder and CCC, and the User shall be liable to pay liquidated damages for each such failure equal to twice the use fee specified in the Order Confirmation, in addition to the use fee itself and any other fees and charges specified.

3.6. User may only make alterations to the Work if and as expressly set forth in the Order Confirmation. No Work may be used in any way that is defamatory, violates the rights of third parties (including such third parties' rights of copyright, privacy, publicity, or other tangible or intangible property), or is otherwise illegal, sexually explicit or obscene. In addition, User may not conjoin a Work with any other material that may result in damage to the reputation of the Rightsholder. User agrees to inform CCC if it becomes aware of any infringement of any rights in a Work and to cooperate with any reasonable request of CCC or the Rightsholder in connection therewith.

4. Indemnity. User hereby indemnifies and agrees to defend the Rightsholder and CCC, and their respective employees and directors, against all claims, liability, damages, costs and expenses, including legal fees and expenses, arising out of any use of a Work beyond the scope of the rights granted herein, or any use of a Work which has been altered in any unauthorized way by User, including claims of defamation or infringement of rights of copyright, publicity, privacy or other tangible or intangible property.

5. Limitation of Liability. UNDER NO CIRCUMSTANCES WILL CCC OR THE RIGHTSHOLDER BE LIABLE FOR ANY DIRECT, INDIRECT, CONSEQUENTIAL OR INCIDENTAL DAMAGES (INCLUDING WITHOUT LIMITATION DAMAGES FOR LOSS OF BUSINESS PROFITS OR INFORMATION, OR FOR BUSINESS INTERRUPTION) ARISING OUT OF THE USE OR INABILITY TO USE A WORK, EVEN IF ONE OF THEM HAS BEEN ADVISED OF THE POSSIBILITY OF SUCH DAMAGES. In any event, the total liability of the Rightsholder and CCC (including their respective employees and directors) shall not exceed the total amount actually paid by User for this license. User assumes full liability for the actions and omissions of its principals, employees, agents, affiliates, successors and assigns.

6. Limited Warranties. THE WORK(S) AND RIGHT(S) ARE PROVIDED "AS IS". CCC HAS THE RIGHT TO GRANT TO USER THE RIGHTS GRANTED IN THE ORDER CONFIRMATION DOCUMENT. CCC AND THE RIGHTSHOLDER DISCLAIM ALL

OTHER WARRANTIES RELATING TO THE WORK(S) AND RIGHT(S), EITHER EXPRESS OR IMPLIED, INCLUDING WITHOUT LIMITATION IMPLIED WARRANTIES OF MERCHANTABILITY OR FITNESS FOR A PARTICULAR PURPOSE. ADDITIONAL RIGHTS MAY BE REQUIRED TO USE ILLUSTRATIONS, GRAPHS, PHOTOGRAPHS, ABSTRACTS, INSERTS OR OTHER PORTIONS OF THE WORK (AS OPPOSED TO THE ENTIRE WORK) IN A MANNER CONTEMPLATED BY USER; USER UNDERSTANDS AND AGREES THAT NEITHER CCC NOR THE RIGHTSHOLDER MAY HAVE SUCH ADDITIONAL RIGHTS TO GRANT.

7. Effect of Breach. Any failure by User to pay any amount when due, or any use by User of a Work beyond the scope of the license set forth in the Order Confirmation and/or these terms and conditions, shall be a material breach of the license created by the Order Confirmation and these terms and conditions. Any breach not cured within 30 days of written notice thereof shall result in immediate termination of such license without further notice. Any unauthorized (but licensable) use of a Work that is terminated immediately upon notice thereof may be liquidated by payment of the Rightsholder's ordinary license price therefor; any unauthorized (and unlicensable) use that is not terminated immediately for any reason (including, for example, because materials containing the Work cannot reasonably be recalled) will be subject to all remedies available at law or in equity, but in no event to a payment of less than three times the Rightsholder's ordinary license price for the most closely analogous licensable use plus Rightsholder's and/or CCC's costs and expenses incurred in collecting such payment.

8. Miscellaneous.

   8.1. User acknowledges that CCC may, from time to time, make changes or additions to the Service or to these terms and conditions, and CCC reserves the right to send notice to the User by electronic mail or otherwise for the purposes of notifying User of such changes or additions; provided that any such changes or additions shall not apply to permissions already secured and paid for.

   8.2. Use of User-related information collected through the Service is governed by CCC's privacy policy, available online here:**https://marketplace.copyright.com/rs-ui-web/mp/privacy-policy**

   8.3. The licensing transaction described in the Order Confirmation is personal to User. Therefore, User may not assign or transfer to any other person (whether a natural person or an organization of any kind) the license created by the Order Confirmation and these terms and conditions or any rights granted hereunder; provided, however, that User may assign such license in its entirety on written notice to CCC in the event of a transfer of all or substantially all of User's rights in the new material which includes the Work(s) licensed under this Service.

   8.4. No amendment or waiver of any terms is binding unless set forth in writing and signed by the parties. The Rightsholder and CCC hereby object to any terms contained in any writing prepared by the User or its principals, employees, agents or affiliates and purporting to govern or otherwise relate to the licensing transaction described in the Order Confirmation, which terms are in any way inconsistent with any terms set forth in the Order Confirmation and/or in these terms and conditions or CCC's standard operating procedures, whether such writing is prepared prior to, simultaneously with or subsequent to the Order Confirmation, and whether such writing appears on a copy of the Order Confirmation or in a separate instrument.

   8.5. The licensing transaction described in the Order Confirmation document shall be governed by and construed under the law of the State of New York, USA, without regard to the principles thereof of conflicts of law. Any case, controversy, suit, action, or proceeding arising out of, in connection with, or related to such licensing transaction shall be brought, at CCC's sole discretion, in any federal or state court located in the County of New York, State of New York, USA, or in any federal or state court whose geographical jurisdiction covers the location of the Rightsholder set forth in the Order Confirmation. The parties expressly submit to the personal jurisdiction and venue of each such federal or state court.If you have any comments or questions about the Service or Copyright Clearance Center, please contact us at 978-750-8400 or send an e-mail to **support@copyright.com**.

v 1.1

CCC Marketplace™

This is a License Agreement between Jeonghyeon Ahn ("User") and Copyright Clearance Center, Inc. ("CCC") on behalf of the Rightsholder identified in the order details below. The license consists of the order details, the CCC Terms and Conditions below, and any Rightsholder Terms and Conditions which are included below.

All payments must be made in full to CCC in accordance with the CCC Terms and Conditions below.

Order Date	16-Sep-2021	Type of Use	Republish in a thesis/dissertation
Order License ID	1148229-1		
ISSN	2050-7887	Publisher	RSC Publishing
		Portion	Chapter/article

LICENSED CONTENT

Publication Title	Environmental science, processes & impacts	Rightsholder	Royal Society of Chemistry
		Publication Type	Journal
Article Title	Temperature dependence of the gas-particle partitioning of selected VOCs	Start Page	947
		End Page	955
		Issue	7
Author/Editor	Royal Society of Chemistry (Great Britain)	Volume	23
Date	01/01/2013		
Language	English		
Country	United Kingdom of Great Britain and Northern Ireland		

REQUEST DETAILS

Portion Type	Chapter/article	Rights Requested	Main product, any product related to main product, and other compilations/derivative products
Page range(s)	64-83		
Total number of pages	20		
Format (select all that apply)	Electronic	Distribution	Worldwide
Who will republish the content?	Author of requested content	Translation	Original language of publication
Duration of Use	Life of current edition	Copies for the disabled?	No
Lifetime Unit Quantity	Up to 499	Minor editing privileges?	Yes
		Incidental promotional use?	No
		Currency	USD

NEW WORK DETAILS

Title	PARTITIONING OF VOLATILE ORGANIC COMPOUNDS INTO THE MULTIPLE ENVIRONMENTAL COMPARTMENTS	Institution name	University of South Carolina
		Expected presentation date	2021-12-13
Instructor name	-		

ADDITIONAL DETAILS

Order reference number	N/A	The requesting person / organization to appear on the license	Jeonghyeon Ahn

REUSE CONTENT DETAILS

Title, description or numeric reference of the portion(s)	PARTITIONING OF VOLATILE ORGANIC COMPOUNDS INTO THE MULTIPLE ENVIRONMENTAL COMPARTMENTS	Title of the article/chapter the portion is from	Temperature dependence of the gas-particle partitioning of selected VOCs
		Author of portion(s)	Ahn, Jeonghyeon; Rao, Guiying; Vejerano, Eric
Editor of portion(s)	Ahn, Jeonghyeon; Rao, Guiying; Vejerano, Eric	Issue, if republishing an article from a serial	7
Volume of serial or monograph	23	Publication date of portion	2021-07-21
Page or page range of portion	947-955		

SPECIAL RIGHTSHOLDER TERMS AND CONDITIONS

The Royal Society of Chemistry (RSC) hereby grants permission for the use of your paper(s) specified below in the printed and microfilm version of your thesis. You may also make available the PDF version of your paper(s) that the RSC sent to the corresponding author(s) of your paper(s) upon publication of the paper(s) in the following ways: in your thesis via any website that your university may have for the deposition of theses, via your university's Intranet or via your own personal website. We are however unable to grant you permission to include the PDF version of the paper(s) on its own in your institutional repository. The Royal Society of Chemistry is a signatory to the STM Guidelines on Permissions (available on request). Please note that if the material specified below or any part of it appears with credit or acknowledgement to a third party then you must also secure permission from that third party before reproducing that material. Please ensure that the thesis includes the correct acknowledgement (see http://rsc.li/permissions for details) and a link is included to the paper on the Royal Society of Chemistry's website. Please also ensure that your co-authors are aware that you are including the paper in your thesis.

CCC Terms and Conditions

1. Description of Service; Defined Terms. This Republication License enables the User to obtain licenses for republication of one or more copyrighted works as described in detail on the relevant Order Confirmation (the "Work(s)"). Copyright Clearance Center, Inc. ("CCC") grants licenses through the Service on behalf of the rightsholder identified on the Order Confirmation (the "Rightsholder"). "Republication", as used herein, generally means the inclusion of a Work, in whole or in part, in a new work or works, also as described on the Order Confirmation. "User", as used herein, means the person or entity making such republication.

2. The terms set forth in the relevant Order Confirmation, and any terms set by the Rightsholder with respect to a particular Work, govern the terms of use of Works in connection with the Service. By using the Service, the person transacting for a republication license on behalf of the User represents and warrants that he/she/it (a) has been

duly authorized by the User to accept, and hereby does accept, all such terms and conditions on behalf of User, and (b) shall inform User of all such terms and conditions. In the event such person is a "freelancer" or other third party independent of User and CCC, such party shall be deemed jointly a "User" for purposes of these terms and conditions. In any event, User shall be deemed to have accepted and agreed to all such terms and conditions if User republishes the Work in any fashion.

3. Scope of License; Limitations and Obligations.

3.1. All Works and all rights therein, including copyright rights, remain the sole and exclusive property of the Rightsholder. The license created by the exchange of an Order Confirmation (and/or any invoice) and payment by User of the full amount set forth on that document includes only those rights expressly set forth in the Order Confirmation and in these terms and conditions, and conveys no other rights in the Work(s) to User. All rights not expressly granted are hereby reserved.

3.2. General Payment Terms: You may pay by credit card or through an account with us payable at the end of the month. If you and we agree that you may establish a standing account with CCC, then the following terms apply: Remit Payment to: Copyright Clearance Center, 29118 Network Place, Chicago, IL 60673-1291. Payments Due: Invoices are payable upon their delivery to you (or upon our notice to you that they are available to you for downloading). After 30 days, outstanding amounts will be subject to a service charge of 1-1/2% per month or, if less, the maximum rate allowed by applicable law. Unless otherwise specifically set forth in the Order Confirmation or in a separate written agreement signed by CCC, invoices are due and payable on "net 30" terms. While User may exercise the rights licensed immediately upon issuance of the Order Confirmation, the license is automatically revoked and is null and void, as if it had never been issued, if complete payment for the license is not received on a timely basis either from User directly or through a payment agent, such as a credit card company.

3.3. Unless otherwise provided in the Order Confirmation, any grant of rights to User (i) is "one-time" (including the editions and product family specified in the license), (ii) is non-exclusive and non-transferable and (iii) is subject to any and all limitations and restrictions (such as, but not limited to, limitations on duration of use or circulation) included in the Order Confirmation or invoice and/or in these terms and conditions. Upon completion of the licensed use, User shall either secure a new permission for further use of the Work(s) or immediately cease any new use of the Work(s) and shall render inaccessible (such as by deleting or by removing or severing links or other locators) any further copies of the Work (except for copies printed on paper in accordance with this license and still in User's stock at the end of such period).

3.4. In the event that the material for which a republication license is sought includes third party materials (such as photographs, illustrations, graphs, inserts and similar materials) which are identified in such material as having been used by permission, User is responsible for identifying, and seeking separate licenses (under this Service or otherwise) for, any of such third party materials; without a separate license, such third party materials may not be used.

3.5. Use of proper copyright notice for a Work is required as a condition of any license granted under the Service. Unless otherwise provided in the Order Confirmation, a proper copyright notice will read substantially as follows: "Republished with permission of [Rightsholder's name], from [Work's title, author, volume, edition number and year of copyright]; permission conveyed through Copyright Clearance Center, Inc. " Such notice must be provided in a reasonably legible font size and must be placed either immediately adjacent to the Work as used (for example, as part of a by-line or footnote but not as a separate electronic link) or in the place where substantially all other credits or notices for the new work containing the republished Work are located. Failure to include the required notice results in loss to the Rightsholder and CCC, and the User shall be liable to pay liquidated damages for each such failure equal to twice the use fee specified in the Order Confirmation, in addition to the use fee itself and any other fees and charges specified.

3.6. User may only make alterations to the Work if and as expressly set forth in the Order Confirmation. No Work may be used in any way that is defamatory, violates the rights of third parties (including such third parties' rights of copyright, privacy, publicity, or other tangible or intangible property), or is otherwise illegal, sexually explicit or obscene. In addition, User may not conjoin a Work with any other material that

may result in damage to the reputation of the Rightsholder. User agrees to inform CCC if it becomes aware of any infringement of any rights in a Work and to cooperate with any reasonable request of CCC or the Rightsholder in connection therewith.

4. Indemnity. User hereby indemnifies and agrees to defend the Rightsholder and CCC, and their respective employees and directors, against all claims, liability, damages, costs and expenses, including legal fees and expenses, arising out of any use of a Work beyond the scope of the rights granted herein, or any use of a Work which has been altered in any unauthorized way by User, including claims of defamation or infringement of rights of copyright, publicity, privacy or other tangible or intangible property.

5. Limitation of Liability. UNDER NO CIRCUMSTANCES WILL CCC OR THE RIGHTSHOLDER BE LIABLE FOR ANY DIRECT, INDIRECT, CONSEQUENTIAL OR INCIDENTAL DAMAGES (INCLUDING WITHOUT LIMITATION DAMAGES FOR LOSS OF BUSINESS PROFITS OR INFORMATION, OR FOR BUSINESS INTERRUPTION) ARISING OUT OF THE USE OR INABILITY TO USE A WORK, EVEN IF ONE OF THEM HAS BEEN ADVISED OF THE POSSIBILITY OF SUCH DAMAGES. In any event, the total liability of the Rightsholder and CCC (including their respective employees and directors) shall not exceed the total amount actually paid by User for this license. User assumes full liability for the actions and omissions of its principals, employees, agents, affiliates, successors and assigns.

6. Limited Warranties. THE WORK(S) AND RIGHT(S) ARE PROVIDED "AS IS". CCC HAS THE RIGHT TO GRANT TO USER THE RIGHTS GRANTED IN THE ORDER CONFIRMATION DOCUMENT. CCC AND THE RIGHTSHOLDER DISCLAIM ALL OTHER WARRANTIES RELATING TO THE WORK(S) AND RIGHT(S), EITHER EXPRESS OR IMPLIED, INCLUDING WITHOUT LIMITATION IMPLIED WARRANTIES OF MERCHANTABILITY OR FITNESS FOR A PARTICULAR PURPOSE. ADDITIONAL RIGHTS MAY BE REQUIRED TO USE ILLUSTRATIONS, GRAPHS, PHOTOGRAPHS, ABSTRACTS, INSERTS OR OTHER PORTIONS OF THE WORK (AS OPPOSED TO THE ENTIRE WORK) IN A MANNER CONTEMPLATED BY USER; USER UNDERSTANDS AND AGREES THAT NEITHER CCC NOR THE RIGHTSHOLDER MAY HAVE SUCH ADDITIONAL RIGHTS TO GRANT.

7. Effect of Breach. Any failure by User to pay any amount when due, or any use by User of a Work beyond the scope of the license set forth in the Order Confirmation and/or these terms and conditions, shall be a material breach of the license created by the Order Confirmation and these terms and conditions. Any breach not cured within 30 days of written notice thereof shall result in immediate termination of such license without further notice. Any unauthorized (but licensable) use of a Work that is terminated immediately upon notice thereof may be liquidated by payment of the Rightsholder's ordinary license price therefor; any unauthorized (and unlicensable) use that is not terminated immediately for any reason (including, for example, because materials containing the Work cannot reasonably be recalled) will be subject to all remedies available at law or in equity, but in no event to a payment of less than three times the Rightsholder's ordinary license price for the most closely analogous licensable use plus Rightsholder's and/or CCC's costs and expenses incurred in collecting such payment.

8. Miscellaneous.

   8.1. User acknowledges that CCC may, from time to time, make changes or additions to the Service or to these terms and conditions, and CCC reserves the right to send notice to the User by electronic mail or otherwise for the purposes of notifying User of such changes or additions; provided that any such changes or additions shall not apply to permissions already secured and paid for.

   8.2. Use of User-related information collected through the Service is governed by CCC's privacy policy, available online here:https://marketplace.copyright.com/rs-ui-web/mp/privacy-policy

   8.3. The licensing transaction described in the Order Confirmation is personal to User. Therefore, User may not assign or transfer to any other person (whether a natural person or an organization of any kind) the license created by the Order Confirmation and these terms and conditions or any rights granted hereunder; provided, however, that User may assign such license in its entirety on written notice to CCC in the event of a transfer of all or substantially all of User's rights in the new material which includes the Work(s) licensed under this Service.

   8.4.

No amendment or waiver of any terms is binding unless set forth in writing and signed by the parties. The Rightsholder and CCC hereby object to any terms contained in any writing prepared by the User or its principals, employees, agents or affiliates and purporting to govern or otherwise relate to the licensing transaction described in the Order Confirmation, which terms are in any way inconsistent with any terms set forth in the Order Confirmation and/or in these terms and conditions or CCC's standard operating procedures, whether such writing is prepared prior to, simultaneously with or subsequent to the Order Confirmation, and whether such writing appears on a copy of the Order Confirmation or in a separate instrument.

8.5. The licensing transaction described in the Order Confirmation document shall be governed by and construed under the law of the State of New York, USA, without regard to the principles thereof of conflicts of law. Any case, controversy, suit, action, or proceeding arising out of, in connection with, or related to such licensing transaction shall be brought, at CCC's sole discretion, in any federal or state court located in the County of New York, State of New York, USA, or in any federal or state court whose geographical jurisdiction covers the location of the Rightsholder set forth in the Order Confirmation. The parties expressly submit to the personal jurisdiction and venue of each such federal or state court.If you have any comments or questions about the Service or Copyright Clearance Center, please contact us at 978-750-8400 or send an e-mail to **support@copyright.com**.

v 1.1